A comparative study of molybdenum and iron phosphate-based catalysts in *n*-hexane activation

by

Zibuyile Mncwabe

Submitted in fulfilment of the academic requirements for the degree of Master of Science in the School of Chemistry, University of KwaZulu-Natal, Durban

2009

As the candidate's supervisor I have approved this dissertation for submission

Signed: _____ Name: H. B. Friedrich

Date: _____

Declaration - Plagiarism

I, Zibuyile Mncwabe, declare that

1. The research reported in this thesis, except where otherwise indicated, is my original research.
2. This thesis has not been submitted for any degree or examination at any other university.
3. This thesis does not contain other persons' data, pictures, graphs or other information, unless specifically acknowledged as being sourced from other persons.
4. This thesis does not contain other persons' writing, unless specifically acknowledged as being sourced from other researchers. Where other written sources have been quoted, then:
    a. Their words have been re-written but the general information attributed to them has been referenced
    b. Where their exact words have been used, then their writing has been placed in italics and inside quotation marks, and referenced.
5. This thesis does not contain text, graphics or tables copied and pasted from the Internet, unless specifically acknowledged, and the source being detailed in the thesis and in the References sections.

Signed

……

Acknowledgements

I thank my supervisor Professor H. B. Friedrich for allowing me to grow independently through advice and from stories of his past experiences.

I thank Sasol Technology and THRIP for financial assistance during the course of this work, the University of KwaZulu-Natal for providing the research facilities.

I thank M. Mathebula and B. Pillay for introducing me to the field of catalysis through the honours project and for helping me to build the reactor, especially Mathebula. I thank the Catalysis Research Group for assistance in the laboratories and inputs into my project.

I thank F. Prinsloo, N. Govender and A. Harilal from Sasol for their much appreciated inputs during the campus visits. I thank M. Mamo from Wits for running TGA and DSC samples for me. I thank the UKZN Electron Microscope Unit for running SEM and TEM analysis for us and for providing liquid nitrogen.

I thank uMa for loving me and I thank all my brothers and my sister for being there and understanding.

I would like to send a big “Thank You” to my friends: Xolelwa, Mathebula, Bavani, Neo, Janine, Mdu, Thanda, Samkelo, Jali and Ayanda for their support and the time they took out of their schedules to spend with me.

Last but not least, I thank God for He is with me at all times.

List of Abbreviations

HPCs	heteropoly compounds
HPA	Heteropoly acid or $H_3PMo_{12}O_{40}$
Fe doped HPA	Fe^{3+} doped $H_3PMo_{12}O_{40}$
ICP-OES	Inductively Coupled Plasma - Optical Emission Spectrometer
XRD	X-ray diffraction
IR	Infrared Spectroscopy
BET	Brunauer-Emmett-Teller
DSC	Differential Scanning Calorimeter
TGA	Thermogravimetric Analysis
NMR	Nuclear Magnetic Resonance spectroscopy
TEM	Transmission Electron Microscopy
SEM	Scanning Electron Microscopy
TPD	Temperature Programmed Desorption
GC-FID	Gas Chromatograph – Flame Ionisation Detector
GC-TCD	Gas Chromatograph –Thermal Conductivity Detector
GC-MS	Gas Chromatograph – Mass Spectroscopy

ct	contact time
id	inner diameter
Temp	temperature
% Conv	% conversion
% Selec	% selectivity

List of Figures

List of Tables

Abstract

A comparative study of the activation of *n*-hexane over the 12-molybdophopshoric acid ($H_3PMo_{12}O_{40}$ or HPA), its Fe^{3+} doped salt ($Fe_{0.69}H_{0.93}PMo_{12}O_{40}$ or Fe doped HPA) and the iron phosphate catalyst (P/Fe = 1.22) was carried out. It was found that the Fe doped HPA catalyst is thermally more stable and less acidic that the HPA catalyst. The HPA and the Fe doped HPA catalysts were more reactive that the iron phosphate catalyst. Both the HPA and Fe doped HPA catalytically produced 2,5-dimethyltetrahydrofuran and 2,5-hexadione (oxygenates), with the Fe doped HPA catalyst selectively producing more oxygenates than the HPA catalyst. This implied that the Fe^{3+} cation promoted the oxygen insertion reactions. The iron phosphate catalyst catalytically produced cis-2-hexene and 1-hexene but did not produce oxygenates, which means that the iron phosphate catalyst promotes oxidative dehydrogenation but does not promote oxygen insertion reactions. At 349 ^{o}C, the HPA catalyst played a role in initiating benzene formation. At isoconversion, the iron phosphate catalyst produced the highest yield of benzene (5.8 % at 8.1 % hexane conversion), which may have formed through both catalytic and non-catalytic reactions. The Fe doped HPA catalyst produced a lower benzene yield (1.4 % at 6 % hexane conversion) than the HPA catalyst (3.6 % at 8.3 % hexane conversion) at almost isoconversion and isothermal conditions.

Foreword

This dissertation contains seven chapters and two appendices. Chapter 1 gives an overview of the scientific problem, Chapter 2 is the background to the 12-molybdophosphoric acid and Chapter 3 gives the background to the iron phosphate catalyst. The experimental section is contained in Chapter 4, Chapter 5 discusses the catalyst characterisation results, Chapter 6 discusses the activation of *n*-hexane over the catalysts and Chapter 7 gives an overall conclusion to this project.

Table of Contents

Page No.

Chapter 1 : SCIENTIFIC PROBLEM OVERVIEW

1.1 Heterogeneous catalytic activation of alkanes

A lot of research has been dedicated to oxidative transformation of short-chain alkanes (light paraffins) using different classes of catalytic materials or catalytic-system designs. This interest in light paraffin activation has been driven by the possibility of developing new environmentally friendly and low cost chemical production processes to partially oxidised organic compounds. Furthermore, as the world production of medium-to-long chain paraffins increases, the need to convert them to useful products has increased.

Selective oxidation of paraffins is very difficult since paraffins are very inactive compounds and there is a lack in control of product selectivity. It is difficult to break the C-H bond since the hydrogen atom is not labile and the maximum valence electron shell for carbon is eight. This low reactivity of paraffins forces the operation of the reaction to occur at high temperatures and/or pressures and hence forces radical reactions to be the dominant transformation reactions. Radical reactions lack control in product selectivity, and the oxidation products are more reactive than paraffins. This means that at the paraffin activation conditions, the oxidation products would be reacted further to CO or CO_2, hence reducing desired product selectivity. Consequently, the need of designing suitable catalysts that can activate paraffins and selectively produce the desired products is realised.

1.2 Historical background of alkane oxidation

The general sequence of reactions in the oxidation of alkanes is shown in Figure 1.1. It goes *via* alcohols, aldehydes or ketones, carboxylic acids and then to the less desirable combustion products (water and carbon dioxide). The oxidation process in not difficult and it is exothermic, however selective oxidation is a much more difficult challenge because the oxidation reaction has to stop before the formation of the combustion products. Before the introduction of oxidation catalysis with small-molecule sources of oxygen like O_2, H_2O_2 or NaOCl; most historical oxidation reactions were stoichiometric. Historically, oxidation was done *via* metal-based oxidants like $KMnO_4$, $K_2Cr_2O_7$ and OsO_4 but these have been proved to be less economically and environmentally friendly than the latter catalytic oxidation (meaning catalysis by using small-molecule sources of oxygen).

1.3 Industrial alkane oxidation (petrochemical industry)

Oxidation catalysis is a very important process and one of the largest scaled processes in the chemical

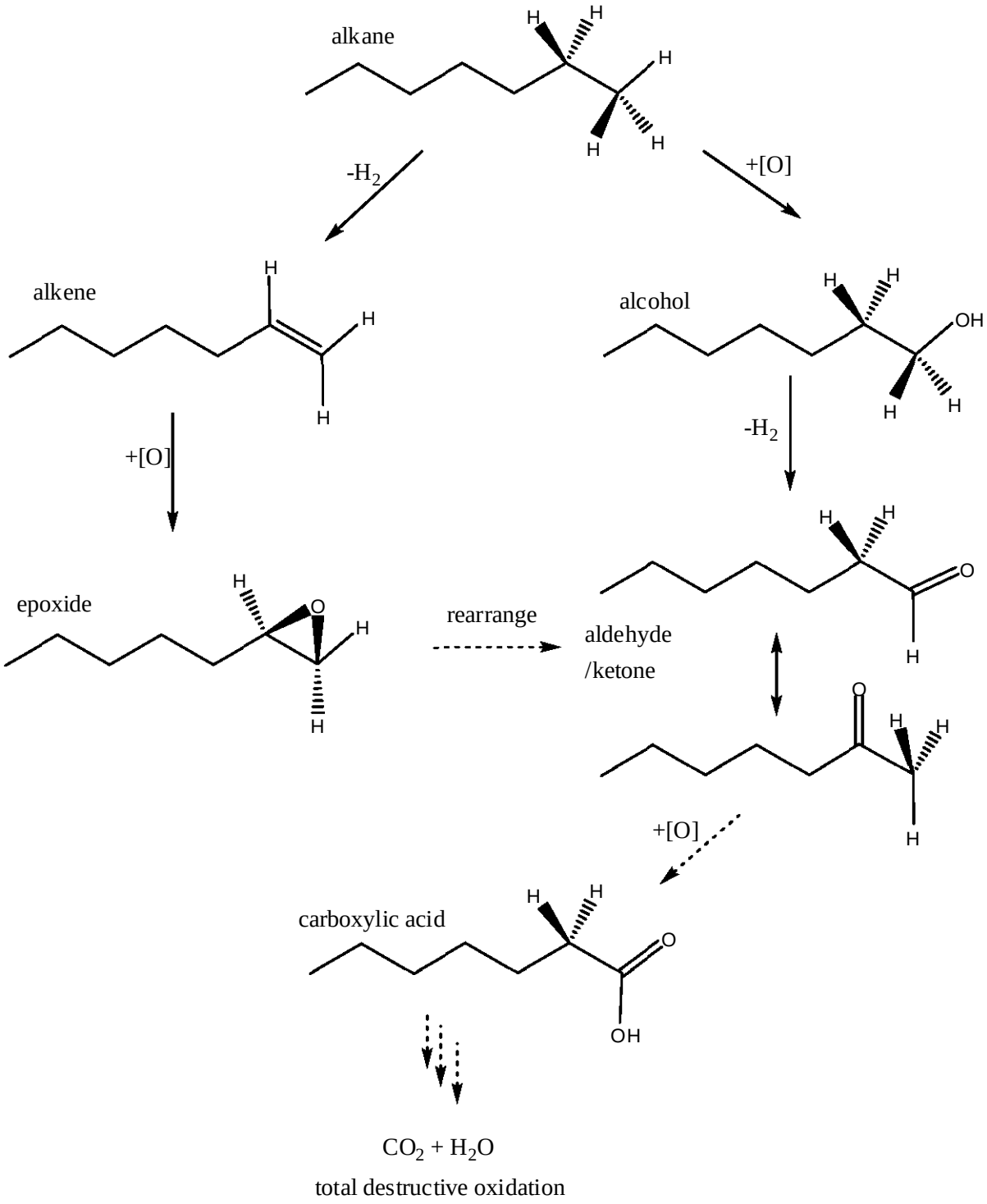

Figure 1.1: A general sequence of reactions for the oxidation of alkanes [1]

production industries, since a wide range of products and various functional groups can be derived from oxygenated compounds. Ketones and aldehydes can be used to form new C-C bonds *via* condensation; alcohols can be used to form esters, ethers and olefins *via* nucleophillic substitution and

halogenation reactions; carboxylic acids are used to produce amines, esters, acid anhydrides; and epoxides (*via* ring opening reactions) can be used in polymerisation reaction. World estimated scales of the production volumes of the oxygenated compounds were: world production of ethylene oxide was estimated to be 58 million tonnes, 2 million tonnes of adipic acid made mainly as a precursor for the synthesis of nylons and 8 million tonnes of terephthalic acid produced each year for the synthesis of poly(ethylene terephthalate)) [2].

The biggest challenge in obtaining these oxygenated compounds is that they are sourced or produced through costly production processes that are sometimes environmentally unfriendly. Hence activating or partially oxidizing less expensive feedstocks like alkanes through environmentally friendly processes became a reasonable solution. But then, of course, there are challenges associated with alkane oxidation, most of these challenges are mentioned in sections 1.1 and 1.4.

1.4 Determining factors in catalytic alkane oxidation

There are a number of factors that determine the selective oxidation of paraffins. This section will look at factors that are involved in the heterogeneous oxidation of paraffins when using molecular oxygen as an oxidant [3].

a) The activation of the substrate

It is believed that the initial step during hydrocarbon oxidation involves C-H activation or hydrogen abstraction. This process is governed mainly by the electronic potential (atomic charge) of the abstracted hydrogen. Literature has shown that a positively charged hydrogen is obtained from methane activation, a neutral hydrogen is obtained from ethane activation and a negatively charged hydrogen is obtained from the methylene groups of propane [4]. By assuming that the catalyst has a metal-oxygen double bond, it is then required that the oxygen ion becomes electrophillic ($M^{\delta-}=O^{\delta+}$) for the activation the methylene groups from propane, hence the catalyst should be acidic. On the other hand, positively charged hydrogens are obtained from methyl groups of unsaturated compounds (propene). Hence a nucleophilic oxygen ion ($M^{\delta+}=O^{\delta-}$, basic catalyst) is required to activate methane [4], C-H bonds at α-positions to the double bond and aromatic rings [5]. The opposite is true for the activation of a longer alkanes like propane.

The stability of carbocations is another determining factor for the susceptibility of the C-H bond breakage. The more stable the carbocation becomes, the easier it is to break the C-H

bond. The stability of carbocations decreases in the sequence: benzyl ~ allyl > tert-butyl > isopropyl > ethyl > methyl groups. Hence the activity of an oxidation catalyst is correlated to the Lewis acidity of the catalyst when assuming that the C-H bond breakage is the rate determining factor [4].

b) The effects from the catalyst structural properties

In most cases, catalytic oxidation reactions occur in a redox mechanism between the reactant molecule and the surface active sites by a mechanism that was suggested by Mars and van Krevelen in 1953 [5]. By definition a Mars and van Krevelen mechanism involves the oxidation of a substrate (hydrocarbon) by using lattice oxygen from the solid catalyst, thereby reducing the catalyst. The reduced catalyst is then reoxidised by activating molecular oxygen from the reaction stream to replaced the lattice oxygen [6] as shown in the schematic presentation in Figure 1.2. For a Mars and van Krevelen mechanism to occur, it is required that the catalyst must have a redox couple (like a transition metal ion), a character of high electrical conductivity and high lattice oxygen anion mobility within the material to allow for reoxidation of the reduced catalyst [5].

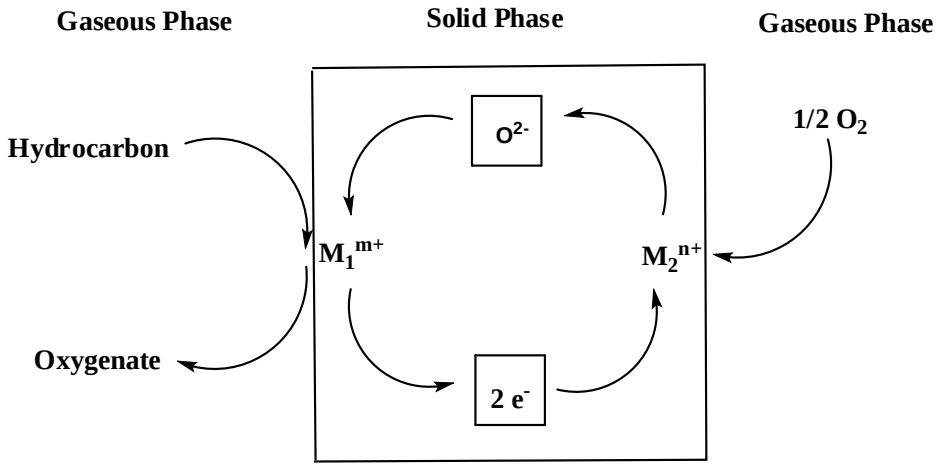

Figure 1.2: A Schematic representation of a Mars and van Krevelen mechanism [5]

c) The reactivity of products

The reactivity of the products controls or affects the selectivity of the catalyst to a great extent. It is required that the catalyst should desorb the desired products immediately after formation before further transformation to combustion products. An example is drawn from the partial oxidation of propene to acrolein, where acrolein, because of electron

delocalisation around the double bond, remains intact on the surface of less nucleophilic or basic MoO_3-TiO_2 and V_2O_5-TiO_2 surfaces, whereas acetone immediatetly forms enolates which directly go to total oxidation. But on a more nucleophillic CoO_3 surface, acrolein undergoes nucleophillic attack to form strongly bound acrylate which directly goes to total oxidation [4].

1.5 Catalyst design and strategies

Catalyst design and catalyst preparation is more of modifying existing catalysts or combining unique experience with already existing experiences to come up with a suitable material to perform a desired catalytic system. This has been noticed through the observation that most successful inventors have modified existing catalysts rather than developing a novel material, but this does not mean that novel materials cannot be converted into useful catalysts. When designing catalysts, there are strategic steps that are essential to follow. In order for these strategic steps to be applied properly, it is essential to define the target reaction. When the target reaction is known, then it becomes easier to design a catalyst that is going to favour the target reaction and at the same time suppress undesired side reactions, especially with the petroleum reactions that have many simultaneous reactions which lead to formation of undesired by-products.

The strategies involve proposing all possible chemical reaction equations, followed by thermodynamic analyses where the feasibilities of the proposed reactions are measured and at the same time non-feasible reactions and intermediates are eliminated. The third strategising step is to visualise the molecular events (propose the molecular mechanism), which means visualising the move from reactant to intermediates and finally to products. This is followed by proposing the surface mechanism. Surface mechanisms are more of a guess than a scientific observation but they become very useful in closing the gabs between what is expected and the apparent results, and they also give an idea of where further research needs to be done. The fifth and the sixth strategies involve identifying reaction paths and necessary catalyst properties; these are mainly determined by the desired target reaction. The last two strategies involved searching for the appropriate materials and proposing the catalyst. Searching for an appropriated material means coming-up with a list of materials that can perform the target reaction and proposing the catalyst means choosing a material that has an optimum performance out of the chosen list [1].

1.6 Justification of current study and choice of catalysts

In this project, two metal phosphate catalysts systems were chosen for comparison: the molybdenum

phosphate which is a 12-molybdophosphoric acid [$H_3PMo_{12}O_{40}$], a heteropoly compound, and iron phosphate [$FePO_4$], which has a tridymite-like structure. Both these catalysts have been intensely studied for various organic compound transformation reactions. The 12-molybdophosphoric acid, $H_3PMo_{12}O_{40}$, and its derivatives are commercial catalysts for the oxidation of methacrolein to methacrylic acid [7, 8]. On the other hand, iron phosphate, $FePO_4$, is known for the oxidative dehydrogenation of oxygenated compounds, like isobutyric acid to methacrylic acid [9]. The work done by Ai on the activation of *n*-butane has shown a 33 % selectivity to methacrylic acid (MAA) at 360 ^oC [7] over 12-molybdophosphoric acid and 32 % selectivity to maleic anhydride (MA) at 20 % conversion over vanadium promoted 12-molybdophosphoric acid [9]; on the other hand iron phosphate showed no selectivity to either MAA nor MA [7, 9].

The above shows that these catalysts have not been fully explored in the study of paraffin activation, especially the activation of *n*-hexane. *n*-Hexane serves as a good model for medium-to-long chain paraffins.

Hence the aim of this project was to synthesise solid 12-molybdophosphoric acid ($H_3PMo_{12}O_{40}\cdot 14 H_2O$), iron phosphate ($FePO_4$) and introduce a Fe^{3+} dopant into the 12-molybdophosphoric acid catalyst (Fe^{3+} is introduced for further comparison since iron is one metal promoter that might have desirable interactions with molybdenum in the HPA; refer to section 2.6.3 on page 20 for details). The catalysts were characterised and tested for *n*-hexane activation in a continuous gas flow reactor.

1.7 References

[1] D.L. Adams, P.J. Dyson, and S.J. Tavener, Chemistry in Alternative Reaction Media. John Wiley & Sons, 2004.

[2] J.T. Richardson, Principles of Catalytic Development. Plenum Press, New York, 1989.

[3] F. Cavani, and F. Trifiro, Catal. Today 51 (1999) 561-580.

[4] G. Busca, E. Finocchio, G. Ramis, and G. Ricchiardi, Catal. Today 32 (1996) 133 - 143.

[5] J.C. Vedrine, G. Coudurier, and J.-M.M. Millet, Catal. Today 33 (1997) 3 - 13.

[6] J.C. Vedrine, J.-M.M. Millet, and J.-C. Volta, Catal. Today 32 (1996) 115 - 123.

[7] M. Ai, J. Mol. Catal. A: Chem 114 (1996) 3 - 13.

[8] F. Cavani, Catal. Today 41 (1998) 73 - 86.

[9] M. Ai, Catal. Today 52 (1999) 65 - 69.

Chapter 2 : 12-MOLYBDOPHOSPHORIC ACID

2.1 Introduction

Heteropoly compounds (HPCs) became increasingly important in applied catalysis, through the studies done by the Japanese and the Russian researchers from the 1970s onwards [1]. Using these HPCs as acid and oxidation catalysts, a variety of selective transformation reactions of organic compounds have been performed. Some of these transformation reactions are commercialised while some are still under development. Keggin type HPCs (Figure 2.1) are commercially used to catalyse the oxidation of methacrolein to methacrylic acid and as co-catalysts in the oxidation of ethylene to acetic acid [2, 3]. They have also been studied for the hydration of olefins (propene and butenes), polymerisation of tetrahydrofuran [1], selective oxidation of propane to acrylic acid, selective oxidation of isobutane to methacrolein and methacrylic acid [2]. Most recently, Keggin type HPCs have been shown to produce maleic anhydride from *n*-butane better than the standard industrial vanadium phosphorus oxide catalyst [4] and selectively produce propylene from propane [5].

The main driving force in using HPCs is due to their versatility in composition and chemical-physical features. Furthermore, HPCs allow for tailoring the composition of the catalyst in order to achieve specific properties that favour a specific catalytic reaction [6].

Heteropoly compounds (sometimes referred to as polyoxometalates (POMs) or heteropolyanions) are polymeric compounds that are formed from the acidification of Mo^{6+} or W^{6+} oxoanions (refered to as addenda or peripharal) in the presence of other anions (referred to as heteroatoms). Heteropolyanions are formed as a result of the incorporation of the heteroatom into the centre of the polyanion of the addenda anions. Different type of ions can be heteroatoms in HPCs, these include Be, B, Al, Si, Ge, Sn, P, Te, and all the first row transition elements. The heteroatom can either have a tetrahedral or octahedral co-ordination. The atomic ratio of the addenda to the heteroatom can be 12, 11, 9, or 6. The addenda atoms, usually MO_6 octahedra but sometimes pentahedra or tetrahedra, organise themselves around the heteroatom. The most common HPCs are those that have octahedral coordination with one terminal M=O oxo group and five bridging oxo M-O-M groups (named type I octahedra). The less common HPCs are those with two terminal M=O oxo groups and four bridging oxo M-O-M groups (named type II octahedra) [6].

The 12-molybdophosphoric acid ($H_3PMo_{12}O_{40}$) is a heteropoly acid (HPA), which has a Keggin structure ($XM_{12}O_{40}$). There are a variety of other structures that HPCs can assume; like the Silverton ($XM_{12}O_{42}$), Dawson ($X_2M_{18}O_{62}$), Waugh (XM_9O_{32}) and Anderson (XM_6O_{24}) [7]. However, the Keggin

structure ($XM_{12}O_{40}$) is highly studied and mainly used in catalysis due to their relatively easily preparation, better thermal stability, and acid and redox properties when compared to other HPCs [6, 7]. Other heteropolyoxometalates like the Dawson structure, Keggin and Dawson lacunary[1] "defects" ($XM_{11}O_{39}$ and $X_2M_{17}O_{61}$) and transition metal complexes are also used in catalysis [8].

A lot of research has been carried out in order to understand the dependence of the structural stability on temperature and reaction atmosphere. Furthermore, the structural transformation during the catalytic activation of the catalyst has also been studied since it plays an important role in the understanding of the catalytic functionalities of the HPCs. These included studies that correlate the complexity of the transformation reaction to the complexity of the design of the HPC. The field that has been least explored is the use of these catalysts to activate inactive organic compounds like alkanes. The activation of alkanes requires the co-operation of different functional properties (acid and redox properties) and these properties can be obtained through proper catalyst design. In this project, a Keggin type, 12-molybdophosphoric acid, and its Fe^{3+} salt catalyst are used to catalytically activate *n*-hexane.

2.2 Historical Background of Keggin Heteropoly Compounds

It was 1826 when Berzelius reported the formation of a yellow precipitate when ammonium molybdate was added to phosphoric acid. This yellow precipitate (a heteropoly compound) is now known as ammonium 12-molybdophosphate $(NH_4)_3(PMo_{12}O_{40})\cdot xH_2O$. In 1854, the Struve postulation described the heteropoly molybdate of Cr^{3+} and Fe^{3+} as a double salt. However, the discovery of 12-tungstosilicic acid, by Marginac in 1862, showed that these compounds were in fact distinct classes rather than double salts. The structure of the 12-tungstosilicic acid was later correctly analysed as $SiO_2\cdot 12WO_3\cdot 2H_2O$. Werner's coordination theory was the first method that was used by Miolati to try and understand the composition of heteropolyanions; and structural determination was impossible before the X-Ray diffraction technique was introduced. In 1908, Moilati's hypothesis was then adopted and further developed by Rosenheim and co-workers [9]. Rosenheim became the most prominent researcher in the field of polyanion chemistry for the subsequent 25-30 years. The Miolita-Rosenheim (MR) theory described heteropoly acids as compounds having octahedral heteroatoms and MO_4^{2-} or $M_2O_7^{2-}$ anions as ligands or bridging groups. The validity of the MR theory was confirmed by the isolation of salts like $Cs_8[Si(W_2O_7)_6]$ and $(CN_3H_6)_7[P(W_2O_7)_6]\cdot 12H_2O$. In 1929, Pauling criticized the MR theory saying the Rosenheim structure of the 6:1 complex is possible but at the

[1] Derivatives that have vacancies resulting from the loss of M and O atoms (latin *lacunar* gap)

same time pointing out that the Mo^{6+} and W^{6+} had crystal radii appropriate to accommodate octahedral coordination by oxygen, hence proposed a 12:1 complex structure. Pauling's structure was based on twelve octahedra surrounding a central XO_4 tetrahedron. The structural formula became $H_4[SiO_4W_{12}(OH)_{36}]$, which predicted observed basicities but was later proved wrong since Pauling only considered corner sharing between MO_6 octahedra. Four years later (in 1933), using X-ray diffraction, Keggin solved the structure of $H_3[PW_{12}O_{40}]\cdot 5H_2O$ showing that the structure was based on WO_6 octahedra linked together by both shared edges and shared corners [10]. This anion structure was supported by Bradley and Illingworth's investigation of $H_3[PW_{12}O_{40}]\cdot 29H_2O$ [11].

2.3 Structural Features of Keggin Heteropoly Compounds

In the Keggin structure, there are twelve MO_6 octahedra surrounding one central XO_4 tetrahedron (refer to the primary structure in Figure 2.1). The M atom (poly or addenda atom) can be W^{6+}, Mo^{6+}, V^{5+} etc. and the X atom (central atom or heteroatom) can be P, B, Si, Ge, As, etc.

The solid HPA system is structurally subdivided into primary, secondary and tertiary structures. It is important to able to understand and distinguish the differences among these three classes since they influence the catalytic functioning of the heterogeneous catalyst [3].

2.3.1 Primary structure

In the solid state, HPAs are ionic crystals (sometimes amorphous) made up of large linked polyanions. The α-type and β-type polyanionic Keggin structure are the two Keggin isomers that are known to be stable. The α–type polyanionic Keggin structure has a T_d symmetry; it consists of a centrally located XO_4 tetrahedron (X referring to the heteroatom) surrounded by twelve edge and corner sharing MO_6 octahedra (M referring to the addenda atom). The octahedra are arranged in four M_3O_{13} groups. Each group is formed by three octahedra sharing edges and having a common oxygen atom, which is also shared with the central tetrahedron XO_4. In the β-type polyanionic Keggin structure, one of the M_3O_{13} groups from the α-Keggin is rotated by 60^o, hence reducing the overall symmetry from T_d symmetry to C_{3v}. This rotation results in the formation of new M-O-M bonds between the rotated groups and other changes to the rest of the anion like shortening of M-M distances and more acute M-O-M bond angles. As a result of coulombic repulsions and less favourable pπ-dπ interactions, the β-Keggin becomes less stable than the α-Keggin isomer. Baker and Figgis further proposed that rotation of the other M_3O_{13} groups results in the formation of even less stable γ-, δ- and ε- isomers [10].

The oxygen atoms in the Keggin structure are classified into four types of symmetric oxygen classes.

There is a chemical bond between the central XO_4 and MO_6 called the X-O_a bond. There are two other M-O-M bonds which are called M-O_b (bridges between two corner sharing MO_6) and M-O_c (bridges between two edge sharing MO_6 within the M_3O_{13} group) bonds [12]. The fourth group is the terminal M=O bond which is called the M-O_t bond. The POM cage of the primary structure of $PMo_{12}O_{40}^{3-}$, a Keggin-type anion, is shown in Figure 2.1.

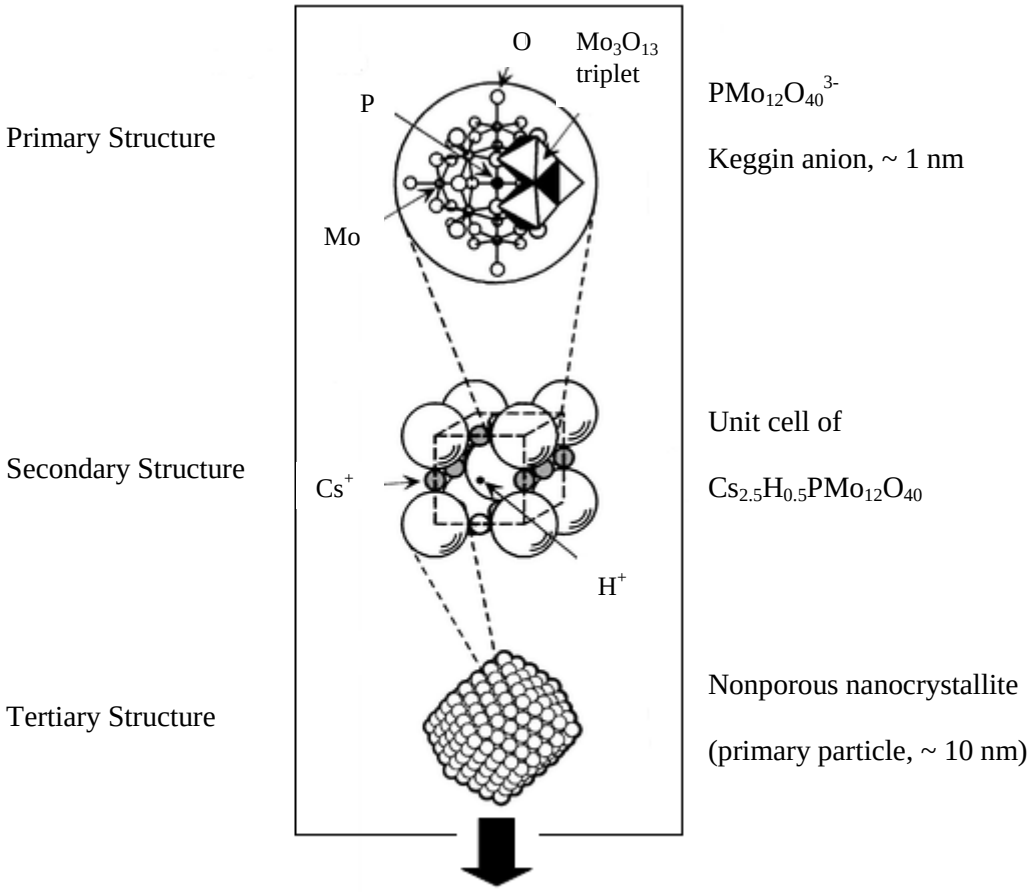

Figure 2.1: The primary, secondary and tertiary structure of a heteropoly compound in a solid state [13]

2.3.2 Secondary structure

A three-dimensional ionic crystal of the HPC secondary structure (refer to Figure 2.1) is made-up of large polyanions, water of crystallisation, cations and other molecules. The secondary structure consists of layers of crystal water between the Keggin anions and it results in various phase

transformations depending on the crystal water content [12].

Substituting cations (like Na^+, Cu^{2+}, Fe^{3+}), for protons, in the HPAs by salt-formation results in a change of the secondary crystallographic structure and also strongly affects the catalytic properties [12], since cations play an important role in linking adjacent heteropolyanions. Protons are incorporated into the $H_3PMo_{12}O_{40}\cdot 6H_2O$ crystal structure in a form of a $H_5O_2^+$ hydrated species. This hydrated species uses hydrogen bonding to link four polyanions by linking terminal oxygen atoms of the polyanions (Mo-O_t) with the two water molecules and one proton, to form a body centred cube structure of polyanion. Figure 2.2 shows the hydrogen bonding that is involved [1, 3, 8, 11]. The secondary structure can also accommodates organic compounds, e.g. a pair of pyridine molecules (Py) can form Py-H^+-Py cations in $[(Py)_2H]_3$-$PW_{12}O_{40}$ and a pair of dimethyl sulfoxide (DMSO) molecules can form DMSO-H^+-DMSO cation in $[(DMSO)_2$-$H]_4SiW_{12}O_{40}$. DMSO [3].

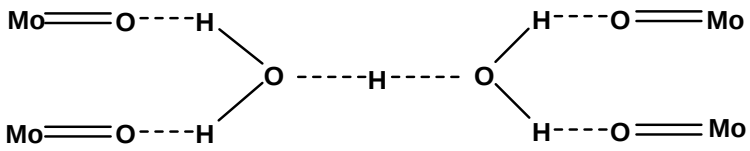

Figure 2.2: Hydrogen bonding between the hydrated proton with four polyanions [8]

2.3.3 Tertiary structure

The tertiary structure is defined by the way in which the secondary structures are assembled; it includes the variations in particle size, surface area, pore-structure and proton distribution in the particles (refer to Figure 2.1 above). The salts are classified by the size of counter-cation ions (group A for small cations like Na^+ or Cu^{2+} and group B for large cations like Cs^+ or NH_4^+). The tertiary structure is greatly influenced by the type of counter-cation [3].

In 1979 [7], it was reported that polar molecules, such as alcohols and amines, readily absorb into the solid bulk of HPAs and their group A (having small size counter cations) salts due to the flexibility of the secondary structure. The absorption occurs by replacing water molecules or by expanding the interdistance between polyanions; this resulted in a new phase called a “pseudoliquid phase”.

2.4 General Properties

Heteropoly compounds have a range of general properties that make them attractive in catalysis but they also have some drawbacks. They have gained popularity in catalysis because of their properties

such as strong Brønsted acidity and the ability to catalyse reversible redox reactions under mild conditions, high stability in water and oxygenated organic solvents, and fairly high stability in the solid state, a "pseudoliquid phase" [8]. The main drawback, however, is the low thermal stability during the catalytic reactions.

Generally, HPCs are heavy molecules, having ionic weights ranging from 1000 to 10 000 g mol^{-1}. Heteropoly molybdates and heteropoly tungstate anions are mostly hydrated compounds, of which the heteropoly molybdates having 30 water molecules of hydration per anion tend to form a series of isomorphous compounds [9, 10]. This water of hydration can gradually be removed in dry air and can be completely removed when the HPC is placed in a vacuum over sulphuric acid. HPCs are generally coloured compounds, with yellow crystals or solution as dominant colour. Partial substitution of addenda by other atoms can result in colour changes [9, 11].

2.4.1 Solubility

HPA and most heteropoly salts are very soluble in water and in polar organic solvents and these HPCs have a high dissociation constant (pK < 0) [10]. Heteropoly salts of small cations (heavy metal cations included) like Na^+, Cu^{2+} or Fe^{3+} are soluble in water, whereas salts of large size cations (large alkaline earth metal cations included) like Cs^+, Ag^+, NH_4^+, Rb^+ are either less soluble or completely insoluble in water [9]. The solubility of these salts in water is determined by the polyanion packing in the secondary structure. The small cations fit in between the large negative polyanions and thus allow solvation of the cations and also lowering the crystal lattice energy. On the other hand, large cations like Cs^+, because of their size, tend to occupy a large volumetric space in between the polyanions, thus forming stable packing, hence increasing the crystal lattice energy, which explains the low solubility [11].

2.4.2 Acidity

Heteropoly compounds are known to form very strongly acidic solutions (stronger than most mineral acids like H_2SO_4, HCl or HNO_3) and their acid properties are recorded in literature in terms of dissociation constants and Hammet acidity functions. Since these compounds are very soluble in polar solvents, the stability of HPAs towards hydrolysis in aqueous solutions has been shown to follow the order: $H_4SiW_{12}O_{40}{\cdot}xH_2O$ > $H_3PW_{12}O_{40}{\cdot}xH_2O$ > $H_4SiMo_{12}O_{40}{\cdot}xH_2O$ > $H_3PMo_{12}O_{40}{\cdot}xH_2O$ [1]. In aqueous solutions, the protons are completely dissociated and the excess negative charge is then delocalised over the large polyanions, hence the electrostatic interaction between the polyanion and

the protons is weak. In order words, it is easier to dissociate HPAs than mineral acids since heteropoly anions are more stable than the ions resulting from the dissociation of mineral acids, hence HPAs are more acidic than mineral acids.

Solid HPAs are considered to be very strong (approach the superacid region) Brønsted acids [1, 3]. Their Brønsted acidities are greater than those of the conventional solid acids like SiO_2-Al_2O_3, H_3PO_4/SiO_2, and HX and HY zeolites. The number and strength of acid sites can be controlled by the composition of the HPC and by its structure. Since HPAs have fairly low thermal stabilities, Keggin $H_3PMo_{12}O_{40}\cdot xH_2O$ starts decomposing at 375 ^oC [1] and the Keggin structure is completely lost at 450 ^oC [3], the decomposition results in loss of acidity. Acidity of partially decomposed molybdenum HPAs can be reconstructed when the HPA is exposed to water vapour [1]. In the case of metal salts, the variety of acid sites increases. These acidic sites include protons in the acidic salts, protons arising from partial hydrolysis during preparation, acid dissociation of coordinated water and Lewis acidity of metal ions [7].

Solid HPAs are capable of generating carbocations from adsorbed olefins and arenes. It has also been shown that crystalline solid HPAs behave like solutions during catalytic reactions of polar molecules. This is due to the mobile and discrete ionic structure, coupled with high proton mobility of the HPA, which easily allows absorption of polar molecules and for these to undergo catalytic reactions on the surface and in the bulk of the catalyst. This phenomenon is called the “pseudoliquid phase” [1].

2.4.3 Reduction and Oxidation

Most HPCs, especially the heteropoly molybdates are powerful oxidising agents (polyanions can accept as may as 32 electrons without major structural changes). These compounds get reduced easily to form deep blue mixed valence species known as “hereropoly blues”. The reduced compounds can also act as reducing agents when they are oxidised, hence restoring the original colour of the anions [9, 10]. This is one of the main attractive properties of HPCs in oxidation catalysis.

It is relatively easy to synthesise a wide range of HPCs and their derivatives by merely mixing salts, with their corresponding mineral acids, and by controlling the pH since HPCs are usually self-assembled structures. The incorporation of transition metals to HPCs results in changes of the electronic characteristics. Transition metals, because of the free movement of electrons in the d-orbitals, provide sources of weakly attached electrons, which can be transferred to other compounds or to the heteropoly atoms, hence favouring reduction. HPCs are also capable of withdrawing electrons from the substrate in oxidation reactions, hence lowering the activation energy. Furthermore,

HPCs are capable of transferring and accepting multiple electrons at the same time, hence preventing the formation of radical intermediates.

Mixed-addenda heteropoly compounds have been used industrially in controlling the redox properties of catalysts during oxidation catalysis. The effects of mixing different constituent elements in a HPC have been shown to perform a lot of redox catalytic reactions. A good example is where the rate of reduction of H_2 is slower and less reversible for the $PMo_{12-x}V_xO_{40}^{(3+x)-}$ than the solid $PMo_{12}O_{40}^{3-}$, although in solution the former catalyst system is a stronger oxidant than the latter [3]. Another great benefit of using HPCs in oxidation catalysis is because of their ability to promote green chemistry. They are capable of activating molecular oxygen (O_2) and hydrogen peroxide (H_2O_2), as opposed to using environmentally unfriendly metal oxides as oxidising agents.

2.4.4 Thermal stability

HPAs undergo dehydration by losing the water of crystallisation, when thermally treated at 100 ^oC. This is followed by a structural decomposition (loss of constitutional water), which occurs at 350 – 600 ^oC (*via* $PW_{12}O_{38.5}$ in the case of $H_3PW_{12}O_{40}$) [7]. In the case of the 12-molybdophosphoric acid catalyst, the Keggin structure is completely destroyed above 450 ^oC [3] and the decomposition leads to the formation of a less active molybdenum trioxide and phosphorous peroxide products (equation 1). The thermal stability of the HPAs depends on the heteroatom, polyanions and the polyanion structure. Compounds having phosphorus as a central atom are more thermally stable than those having silicon, and compounds having tungsten as an addenda atom are more stable than the molybdenum containing compounds [3]. The Keggin-type $H_3PW_{12}O_4 \cdot xH_2O$, $H_4SiW_{12}O_{40} \cdot xH_2O$, $H_3PMo_{12}O_{40} \cdot xH_2O$ and $H_4SiMo_{12}O_{40} \cdot xH_2O$ start decomposing at 456, 445, 375 and 350 ^oC respectively [1].

$$H_3PMo_{12}O_{40} \longrightarrow \tfrac{1}{2} P_2O_5 + 12\, MoO_3 + \tfrac{3}{2} H_2O \qquad \text{(eq 1)}$$

It is known that the less stable compounds start decomposing at lower temperature when heated. It was therefore claimed that at low temperature, before the formation of crystalline MoO_3, compounds like $H_3PMo_{12}O_{40}$ (PMo_{12}) and $H_5PV_2Mo_{10}O_{40}$ (PV_2Mo_{10}) start by partially disintegrating to form isopolymolybdates and PMo_{12-x} lacunary structures by expelling vanadyl and molybdenyl species from the Keggin stucture [12]. Mestl and co-workers [12] claimed that if the MoO_3 lattice formed from isolated molecules of HPA, then the rearrangement of Keggin anions, followed by the reorganisation and condensation of MoO_3 had to occur. Furthermore, if this argument is true, Keggin

anions are merely catalyst precursors and disintegration and recondensation leads to the formation of the catalyst (an "ill-defined" mixture of intermediates during catalytic conditions) [12]. The structural thermal instability of HPCs is still the major drawback of using HPCs, especially in high temperature heterogeneous catalysis. Although it may be argued that the defined HPC structure that is used in a catalytic reaction is merely a precursor, and the catalyst forms after thermal decomposition, there are still limits in terms of working conditions in which the catalyst can remained efficient and these conditions normally involve relatively low temperatures.

2.4.5 Degradation upon varying pH

Heteropolymolybdate and heteropolytungstates decompose in strong basic solutions to form molybdates and tungstates. Heteropolytungstates tend to be more stable in water and in acidic solutions than heteropolymolybdates. If the pH of a heteropoly anion solution is gradually raised, the polyanion structure is retained until the degradation pH is reached. Each heteropoly compound has its own pH range in which its corresponding anion retains its structure, before degradation as the pH of the solution is increased. Although there might be some minor changes that occur to the heteropoly anion as the pH is varied, it is generally assumed that the existing predominant species, in equilibrium with the solution, before the degradation pH, is similar (or closely related) in structure to the original anion in a solid state. The stability of the 12-heteropolymolybdates in water depend very much on the heteroatom, with silicon being the most stable; it followings this descending order: Si > (Zr, Ti) > Ge > P > As [9].

2.5 Preparation Methods

2.5.1 Synthesis of free acid

The synthesis methods of HPAs have become important due to their vast range of applications. Some of the HPAs are obtained as crystalline hydrates such as $H_3PMo_{12}O_{40}{\cdot}xH_2O$, $H_3PW_{12}O_{40}{\cdot}xH_2O$ and $H_4SiW_{12}O_{40}{\cdot}xH_2O$. The most common way of synthesising HPAs involves acidification of an aqueous solution containing the salt of the hetero-element and the alkali metal molybdate or tungstate as shown in equation 2 [8, 10].

$$12\ MoO_4^{2-} + HPO_4^{2-} + 23\ H^+ \longrightarrow \left[PMo_{12}O_{40}\right]^{3+} + 12\ H_2O \quad \text{(eq 2)}$$

Although the stoichiometry indicated by the formation equation (equation 2) is often a good guide in the design of the synthesis, in some instances excess of the heteroatom, or careful control of temperature or pH may be necessary. Common mineral acids are normally used to acidify. However, if the introduction of other anions is to be avoided, acidification can be achieved by electrolytic oxidation of the solvent or by addition of an appropriate anhydride [10].

Generally polyanions in solution are isolated by the addition of appropriate anions like ammonium, tetraalkyl ammonium or alkali metal. Lithium and sodium salts are soluble in water, while salts of larger cations like tetraalkyl ammonium are less soluble in water and so recrystallize in organic solvents like acetonitrile, acetone and nitromethane. If the HPA is stable enough to be crystallized in an aqueous solution, then it is isolated using a method called the "etherate" method (extracting with ether). This method involves shaking a highly acidified solution of the heteropolyanion with excess diethyl ether, where three phases separate. The upper layer is the diethyl ether, the middle layer is the aqueous layer and the lower layer is a heavy "etherate" layer. The "etherate" layer can be extracted with diethyl ether again, in order to remove entrained aqueous solution. Adding water to the "etherate" decomposes the "etherate" to form two layers, the ether is removed and the aqueous solution of the heteropoly acid is allowed to evaporate until crystallization. Although the nature of the etherate is not fully understood, it is reported that the etherate of $H_3PMo_{12}O_{40}$ is made up of approximately 20 mol ether and 50 mol water per mol of heteropoly acid. The main drawbacks of using the etherate method are the low yield of solid acid and the large amount of waste product formed [10].

2.5.2 General methods of preparation of transition metal substituted heteropoly compounds

HPAs can be converted into multicomponent systems by forming transition metal salts or by substituting transition metals into structures of the Keggin framework. In most cases, this modification of the Keggin structure helps in tuning the redox and acid-base properties of these HPCs so that they become suitable for specific catalytic applications. The transition metal cations can substitute the protons of the bulk HPA to forms transition metal salts. Transition metals can also be used to substitute the addenda atoms of the Keggin structure to transition metal substituted heteropoly anions. The most common transition metals introduced into the framework are the first-row transition metals. The transition metal fits into the lacunary vacancy that is created from the Keggin structure unit. The lacunary or "defects structure" is created by the loss of MO_6 octahedra (MO_6 is equavalent to the loss of a MO^{n+} unit, resulting in the formation of $XM_{11}O_{39}^{n-}$). Lacunary structures are obtained

by partial degradation of the Keggin structure by changing the pH of the solution by using appropriate buffer solutions [14]. The pH stability of the Keggin structure is dependent on the type of the heteropoly (central) atom and the addenda atoms (as mentioned section 2.4.5 above).

2.6 Gas phase oxidation catalyst

Application of HPC catalysts in paraffin activation has been limited by their low thermal stability during the catalytic conditions that are required to activate paraffins. Making use of mixed addenda Keggin-type HPCs has been shown to overcome some of these problems. Mixed addenda Keggin-type HPCs containing vanadium, and HPCs which have the alkali metal ions substituted in cationic positions and transition metal doping (normally called heteropoly acid salts or polyoxometalates) have been studied. These modifications have been claimed to improve structural stability and allow for better control in the oxidation properties on the HPCs [6]. The literature that is of interest to this project is light alkane gas phase catalytic oxidation.

2.6.1 Alkane oxidation

POMs have showed some promising results in the activation of *n*-butane and *n*-pentane, which is most relevant to the current study on the activation of *n*-hexane. The ability of 12-molybdovanadophosphoric acid ($H_{3+n}PV_nMo_{12-n}O_{40}.xH_2O$) to selectively transform *n*-butane [15-17] and *n*-pentane [18] to maleic anhydride has created an altenative catalytic system to the vanadium-phosphorus-oxide system for the selective transformation of *n*-butane to maleic anhydride. Centi found a similar turnover frequency of about 5 x 10^{-4} molecules of *n*-pentane transformed per vanadium atom per second over both the vanadyl pyrophosphate ($(VO)_2P_2O_7$), a V-P-O catalyst commercialized process for the transformation of *n*-butane to maleic anhydride, and the 12-molybdovanadophosphoric acid ($H_5PV_2Mo_{11}O_{40}\cdot xH_2O$) during the study of *n*-pentane selective oxidation. Furthermore, the oxidation of *n*-pentane over the heteropoly acid resulted in the formation of maleic anhydride, whereas the vanadyl anhydride resulted in the formation of maleic anhydride and phthalic anhydride. This observation favours the heteropoly acid since there is no need to develop a separation process in order to separate the two anhydrides [18].

In 1996, Mizuno and co-workers reported an improved catalytic activity where $Cs_{2.5}Fe_{0.08}H_{1.26}PVMo_{11}O_{40}$, during the oxidation of propane, gave an optimum acrylic acid yield of 13 %, which is higher than the 10.5 % yield obtained from V_2O_5-P_2O_5-TeO_2 [19]. Furthermore, Ni^{2+} substitution for H^+ also showed some enhancement in the catalytic activity during propane oxidation.

Another enhancement of the HPC catalyst performance was observed in the selective oxidation of light paraffins (isobutane, propane and ethane) by the introduction of di/trivalent transition metal ions (Cu^{2+}, Fe^{3+}, Ni^{2+}) in the secondary framework of the compound [20]. Iron was shown to improve the catalytic performance under both oxygen-rich and oxygen-poor conditions, whereas copper improved the performance under oxygen-poor conditions [21]. One of the effects resulting from the doping of HPA with transition metal ions is the change in the acidity. The partial hydrolysis of these cations (in the same way as it occurs in the zeolites) and the Lewis character of some of these ions contribute to the acidity of the HPC [6]. This affects the activity of the catalyst, since acidity plays a vital role in the C-H activation of paraffins [22]. The effect of acidity on selective oxidative dehydrogenation of propane is reported to produce a 9.3 % yield of propylene at 16 % conversion over the $Cs_{2.56}H_{0.44}PMo_{12}O_{40}$ catalyst [5].

2.6.2 Transition metal substitution

Literature has reported small structural changes on the HPCs upon transition metal substitution, but rather large changes in the catalytic properties during oxidation and oxidative dehydrogenation reactions, upon transition metal substitution [23]. In 1984, Ai reported that substitution of the Mo by V in the $H_3PMo_{12}O_{40}$ Keggin unit increased the oxidation activity, while substitution by W reduced the activity. Furthermore, the activity was improved by addition of Cu^{2+} cations with an optimum at 0.03 Cu^{2+} atoms per Keggin unit. Hence, it was understood that by combining cation and heteroatom substitution in the Keggin unit, the oxidation catalytic performance of the heteropoly compounds can be improved. This meant that catalytic performances can be controlled, since the oxidation function can be enhanced by vanadium compounds or other cations like Cu^{2+}; whereas the acidic function can be controlled by substitution of various cations [15].

It was further observed that thermally stability of the heteropoly acid decreased with increase in the number of vanadium atoms ($H_{3+n}PV_nMo_{12-n}O_{40}{\cdot}xH_2O$, n = 0 - 3); but selectivity and activity increased with increase in n, except for $H_6PV_3Mo_9O_{40}{\cdot}xH_2O$ which showed a drop in activity during the study of *n*-pentane catalytic oxidation [18].

Mizuno and co-workers substituted a range of transitions metal cations for H^+ in a heteropoly compound cesium salt ($M_{0.08n}Cs_{2.5}H_{0.5-0.08n}PMo_{12}O_{40}$ where M = Fe^{3+}, Ni^{2+}, Co^{2+}, Cu^{2+} and Mn^{2+}). With these catalysts, they found that Fe^{3+} and Ni^{2+} substitution resulted in an improved yield of acrylic acid from the oxidation of propane (both selectivity and conversion were increased). They also showed that substituting one Mo^{6+} with one V^{5+} atom per Keggin unit improved selectivity to acrylic

acid. Hence an optimum yield of 13 % to acrylic acid was obtained with the $Cs_{2.5}Fe_{0.08}H_{1.26}PVMo_{11}O_{40}$ catalyst [24]. A year later they reported that proton substitution by Fe^{3+}, Ni^{2+} and Mn^{2+} in the $Cs_{2.5}H_{0.5}PMo_{12}O_{40}$ catalyst resulted in an increased yield of methacrylic acid and methacrolein during the oxidation of isobutene, while substitution with Co^{2+}, Cu^{2+}, Hg^{2+}, Pt^{2+} and Pd^{2+} resulted in a reduced yield [25].

The most reasonable explanation for the observed changes of catalytic properties due to transition metal substitution is assigned to the contribution of these transition metal atoms to the redox system and also to the Lewis and Brønsted acidity of the system. It was shown in some comparative studies that Cu^{2+} increased the reducibility of both Cu^{2+} and Mo^{6+} to Cu^{+} and Mo^{5+} respectively, in the $Cs_2M_xH_{1-x}PMo_{12}O_{40}$ system ,where M = Fe^{3+} or Cu^{2+}. On the other hand, Fe^{3+} hindered the reducibility of Mo^{6+} atoms adjacent to the Fe atoms. Hence Cu^{2+} substituted catalyst showed higher activity but less selectivity to methacrylic acid (due to the increased acidity which has a negative effect on methacrylic acid selectivity) during the oxidation of isobutane. In contrast Fe^{3+} substituted catalyst showed higher selectivity, at a lower activity, to methacrylic acid. This observation was related to the fact that Fe^{3+} substitution reduces the number of protons, hence decreases the acidity (favours selectivity), but at the same time Fe^{3+} does not contribute to the redox system, hence indirectly decreases the activity of the catalyst [26]. However, Fe^{3+} substitution into the ammomium/potassium salt of 12-molybdophosphoric acid resulted in an increased activity but a decreased selectivity to methacrylic acid during the oxidation of isobutane. This observation was accounted for by the observed increased Brønsted and Lewis acidity of the surface of the catalyst with the increase in Fe^{3+} loading [27]. Another report showed the necessity of the acidic property during oxidation of propane with molecular oxygen, since the fully saturated $K_3PMo_{12}O_{40}$ heteropoly compound was catalytically inactive [28, 29].

2.6.3 Effects of the Fe counter-ion on the Keggin-type molybdophosphoric acid

The addition of iron counter-ions into molybdophosphoric acid has been shown to have various effects on the redox and catalytic properties of the heteropoly acid in the oxidation of isobutane into methacrylic acid [30]. These effects are determined by the form in which the iron metal is substituted into the acid; it could be substituted as a counter-cation in the bulk acid ($Fe_{0.85}H_{0.45}PMo_{12}O_{40}$), as an iron doped acid supported on the cesium salt ($Cs_2Fe_{0.2}H_{0.4}PMo_{12}O_{40}$) [30, 31] or it could be introduced into the Keggin ion by replacing one of the addenda atoms ($Cs_{1.5}(NH)_2H_{0.4}$ $Fe_{0.5}PMo_{11.5}O_{39.5}$) [32]. The addition of iron in the bulk acid showed an increase in both the activity of the acid and the selectivity to methacrylic acid and methacrolein. Whereas the cesium supported iron doped acid

showed only an increase in the selectivity [30]. This difference was explained by the existence of electron transfer between iron and molybdenum that occurs only in the bulk acid (when Fe^{3+} acts as a counter-ion), which is possible only when the solid acid is in a hydrated form [30, 33].

Other studies have shown an increased activity of the iron-doped potassium/ammonium salts of the 12-molybdophosphoric acid in isobutane oxidation related to the undoped catalyst [34]. This allows for the catalytic reaction to be operated under milder reaction conditions, which favour the usage of HPCs in paraffin activation. It was further shown that the amount of substituted Fe in place of the ammonium cation in $K_2(NH_4)_2PMo_{12}O_{40}$ led to a proportional increase in catalytic activity, but also led to a proportional decrease in selectivity to methacrylic acid [34]. The argument behind the increased activity is that the presence of Fe increases the acidity (Brønsted acidity is due to the presence of Fe cations, $Fe(HO)_n^{(3-n)}$, while Lewis acidity is due to the iron oxide dispersed on the surface of the polyoxometalate (POM) with an iron content greater than 0.5 Fe atoms per Keggin ion). The Lewis acidity may increase the ease of activation of the tertiary C-H bond and hence increase the activity. The argument behind the decrease in selectivity relates to the increased combustion reaction of methacrylic acid and methacrolein [34]. Various studies carried out by Mizuno and co-workers [20, 21, 25, 32] showed that the replacement of protons in polyoxometalates (POMs) by Fe cations improves the catalytic activity in propane oxidation to acrylic acid and in isobutane oxidation to methacrylic acid.

2.7 References

[1] I.V. Kozhevnikov, Chem. Rev. 98 (1998) 171 – 198.

[2] K. Song, J.E. Lyons, and M.A. Barteau, Catal. Today 81 (2003) 137 - 148.

[3] N. Mizuno, and M. Misono, Chem. Rev. 98 (1998) 199 – 217.

[4] J.H. Holles, C.J. Dillon, J.A. Labinger, and M.E. Davis, J. Catal. 218 (2003) 42 - 53.

[5] M. Sun, J. Zhang, C. Cao, Q. Zhang, Y. Wang, and H. Wan, Appl. Catal. A: Gen. 349 (2008) 212 - 221.

[6] F. Cavani, Catal. Today 41 (1998) 73 - 86.

[7] M. Misono, Catal. Rev.-Sci. Eng. 29 (1987) 269 – 321.

[8] I.V. Kozhevnikov, Catal. Rev.-Sci. Eng. 37 (1995) 311 – 352.

[9] G.A. Tsigdinos, Topics in Current Chemistry, Aspects of Molybdenum and Related Chemistry, 76. Spring-Verlag, Berlin Heidelberg New York, 1978.

[10] M.T. Pope, Heteropoly and Isopoly Oxometalates, Inorganic Chemistry Concepts 8. Springer-Verlag Berlin, Heidelberg, 1983.

[11] N. Alekar. 2000. Catalytic studies involving heteropoly acids and related compounds. In Inoganic and catalysis division. University of Pune, Pune, India.

[12] G. Mestl, T. Ilkenhans, D. Spielbauer, M. Dieterle, O. Timpe, J. Krohnert, F. Jentoft, H. Knozinger, and R. Schlogl, Appl. Catal. A: Gen. 210 (2001) 13- 34.

[13] P.I. Neel. Polyoxometalates - Why are they unique? Indian Institute of Technology Madras, http://203.199.213.48/697/1/Ph.D._semainar_finalindraneel.ppt#308,1,Slide1, accessed 11/01/09.

[14] R. Massart, R. Constant, J.-N. Fruchart, J.-P. Ciabrini, and M. Fournier, Inorg. Chem. 16 (1977) 2916 - 2921.

[15] M. Ai, Proc. 8th Inter. Congr. Catal. 5 (1984) 475-486.

[16] M. Ai, J. Catal. 85 (1984) 324.

[17] G. Centi, V. Lena, F. Trifiro, D. Ghoussoub, C.F. Aissl, M. Guelton, and J.P. Bonnelle, J. Chem. Soc. Faraday Trans. 86 (1990) 2775-2782.

[18] G. Centi, L. Lopez Nieto, C. Iapalucci, K. Bruckman, and E.M. Serwicka, Appl. Catal. 46 (1989) 197- 212.

[19] N. Mizuno, D.-J. Suh, W. Han, and T. Kudo, J. Mol. Catal. A: Chem 114 (1996) 309-317.

[20] J.-S. Min, and N. Mizuno, Catal. Today 71 (2001) 89 – 96.

[21] J.-S. Min, and N. Mizuno, Catal. Today 66 (2001) 47 – 52.

[22] Y. Moro-oka, Appl. Catal. A: Gen. 181 (1999) 323 - 329.

[23] Q. Huynh, and J.-M.M. Millet, J. Phys. Chem. Solids 66 (2005) 887 - 894.

[24] N. Mizuno, M. Tateishi, and M. Iwamoto, Appl. Catal. A: Gen. 128 (1995) L165-L170.

[25] N. Mizuno, M. Tateishi, and M. Iwamoto, J. Catal. 163 (1996) 87 – 94.

[26] M. Langpape, J.-M.M. Millet, U.S. Ozkan, and P. Dilichere, J. Catal. 182 (1999) 148 - 155.

[27] F. Cavani, E. Etienne, M. Favaro, A. Galli, F. Trifiro, and G. Hecquet, Catal. Lett. 32 (1995) 215 - 226.

[28] W. Ueda, and Y. Suzuki, Chem. Lett. 24 (1995) 541-542.

[29] W. Ueda, Y. Suzuki, W. Lee, and S. Imaoka, Stud. Surf. Sci. Catal. 101 (1996) 1065-1074.

[30] M. Langpape, and J.-M.M. Millet, Appl. Catal. A: Gen. 200 (2000) 89 – 101.

[31] M. Langpape, J.-M.M. Millet, U.S. Ozkan, and M. Boudeulle, J. Catal. 181 (1999) 80 - 90.

[32] C. Knapp, T. Ui, K. Nagai, and N. Mizuno, Catal. Today 71 (2001) 111 – 119.

[33] S.A. Borshch, H. Duclusaud, and J.-M.M. Millet, Appl. Catal. A: Gen. 200 (2000) 103 - 108.

[34] E. Etienne, F. Cavani, R. Mezzogori, F. Trifiro, G. Calestani, L. Gengembre, and M. Guelton, Appl. Catal. A: Gen. 256 (2003) 275 – 290.

Chapter 3 : IRON PHOSPHATE CATALYST

3.1 Introduction

The iron phosphate-based catalyst has been extensively studied as an oxidative dehydrogenation (ODH) catalyst for the transformation of isobutyric acid to methacyrlic acid and this has been reported in both the open and patent literature. A review by Millet gives a detailed summary regarding ODH reports; where the first patent for the preparation of the iron phosphate dates as early as 1971, which was then followed by the introduction of new preparation methods and/or catalyst formulations as the years progressed [1]. These catalytic formulations were patented, since it was noted that the catalytic performance is related to the catalyst preparation method [2].

Iron phosphate ($FePO_4$) has also been studied by Wang and Otsuka showing high selectivity during the oxidisation of methane to methanol with O_2 when co-fed with H_2 [3], and ethane to partially oxygenated products by O_2 in the presence of H_2 and N_2O [4]. Miller and co-workers reported that the iron phosphate-based catalyst is also active in the oxidative dehydrogenation of ethane to ethylene when using O_2 as an oxidant [5]. Furthermore, $FePO_4$ has been shown to be able to catalyse oxidative coupling of methane [6], oxidation of methanol to formaldehyde and ammoxidation of methyl pyrazine to cyanopyrazine [7].

A lot of work has been done in optimising the oxidative dehydrogenation capability of iron phosphate-based catalysts in reactions that involve transformation of acid compounds like isobutytric acid, lactic acid etc. But less attention has been paid in utilizing this catalyst in alkane activation. This project thus aims at using the tridymite-like iron phosphate catalyst to activate a medium-to-long chain alkane (*n*-hexane).

3.2 Historical background on the preparation methods on iron phosphate-based catalyst

Literature has reported three preparation methods, namely the precipitation method, ammonia gel method and the vivianite method. Some of these methods have been industrialised, while some are still under development.

3.2.1 Precipitation method

The precipitation method is the first method that was report (in 1956) and it is mostly used in the patent literature. In the precipitation method, ferric salt solution (mostly ferric nitrate) is mixed with

an aqueous solution of phosphoric acid or ammonium phosphate, in stoichiometric amounts. The mixture is then evaporated, dried and calcined in air at tempetatures ranging from 400 ^{o}C to 500 ^{o}C. Nitrates of alkaline metals and other metals can be added to the solution as promoters (the presence of Cs is known to favour the formation of the tridymite-like $FePO_4$ structure). Colloidal silica was also added to the mixture. As a result of the precipitation method of synthesis, $FePO_4$ crystallizing in a quartz-like structure (similar to SiO_2), where for every two (SiO_4) tetrahedra, an alternating substitution of one FeO_4 tetrahedron and one PO_4 tetrahedron was expected. But X-ray diffraction analysis of the catalyst obtained from the precipitation method (in 1991) showed the formation of an amorphous and a tridymite-like phase. It was further shown that when there was an excess of phosphorus (P/Fe greater than 1), then both tridymite and quartz-like structures were obtained and the tridymite-like phase was observed to increase with an increase in the P/Fe ratio. Mössbauer spectroscopy analysis showed that all iron atoms present were in a Fe^{3+} oxidation state [1].

3.2.2 Ammonia gel method

In 1993, Ai and co-workers [8] reported the ammonia gel method where a dilute solution of ammonia was mixed with iron nitrate to form an iron hydroxide gel. The gel was then reacted with an aqueous solution of orthophosphoric acid at approximately 100 ^{o}C. Colloidal silica can also be added to the solution during preparation. The paste-like compound was dried and the solids were calcined at a temperature ranging from 300 - 700 ^{o}C. The ammonia gel method showed the formation of an amorphous phase (sample calcined at a temperature less than 480 ^{o}C), a tridymite-like phase (samples calcined at 500 ^{o}C) at low crystalinity and quartz-like $FePO_4$ phase (from 550 ^{o}C and above calcination temperature) for samples with P/Fe = 1.0 - 1.2. In some cases, a minority of $NH_4FeP_2O_7$ phase was observed, with its proposed decomposition products ($FeH_2P_2O_7$ and $Fe(PO_3)_3$) occurring mainly at low temperatures. In this case, redox titration was used to determine the iron oxidation states and it also was shown to consist of only the Fe^{3+} oxidation state [1, 9].

3.2.3 Vivianite method

In 1996 Bonnet and co-workers developed another method of preparing the iron phosphate-based catalyst [10]. In this method, vivianite (a hydrated ferrous iron phosophate, $Fe_3(PO_4)_2.8H_2O$) was reacted with $H_4P_2O_7$ in acetone under reflux conditions. The P/Fe ratio in the reactant was 4.5 and the reaction took 15 hours. After completion, the solids were filtered, washed with acetone and dried at 313 K. It was shown through characterization that the obtained solids were amorphous. Mössbauer spectroscopy showed a $Fe^{3+}/(Fe^{2+} + Fe^{3+})$ ratio of 0.8 and the P/Fe composition ratio ranging from 1.8

to 2.3 [1, 10].

3.3 Structural Features of Iron Phosphate-based Catalyst

3.3.1 The tridymite-like phase

A tridymite-like iron phosphate has a similar structure to the tridymite structure of SiO_2 (silica). The only difference is that $FePO_4$ (iron phosphate) has alternating Fe-O and P-O tetrahedra [11] instead of SiO_4 tetrahedra. A typical tridymite structure is illustrated in Figure 3.1, where there are sheets of alternating tetrahedra facing up and down and arranged in a way that six sided ring channels are formed.

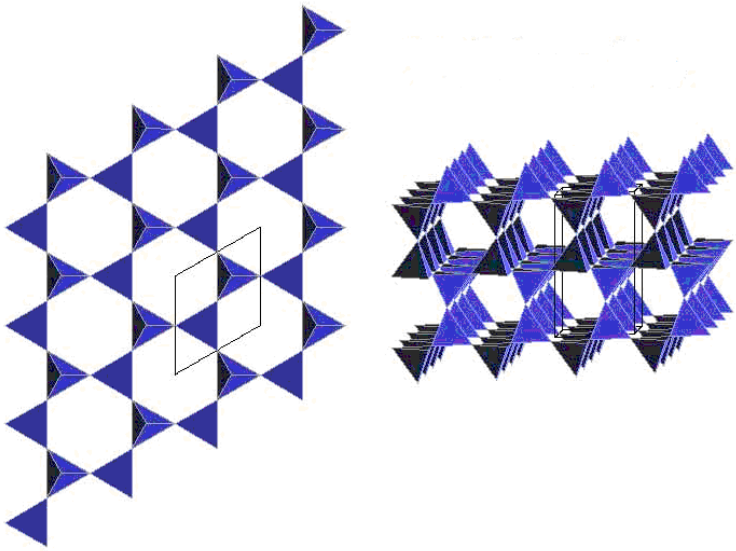

Figure 3.1: Schematic structure of tridymite [12]

The quartz structure is more stable than the tridymite structure of SiO_2, similarly the quartz-like structure is more stable than the tridymite-like structure of iron phosphate. However, studies have shown that when there is excess phosphorus compared to iron during the preparation of iron phosphate, the tridymite-like structure of iron phosphate is favoured over the more stable quartz-like structure [1, 13]. It is argued that when there is excess phosphorus, homopolyhedral linkages between two PO_4^{3-} corners occur to form $P_2O_7^{4-}$. In other words, one PO_4^{3-} and one Fe^{3+} is replaced by one $P_2O_7^{4-}$ in the structure. This results in excess negative charge, which is then compensated by protons or any other monovalent cations. These cations are located in the tridymite-like structure channels and

hence the structure is stabilised. This resultants in a solid solution ($Fe_{1-x}A_x(PO_4)_{1-2x}(P_2O_7)_x$) where A = H, Ag, Cu, Na, K, Rb or Cs. Bivalent and trivalent cations can also be used, with a substitution of Fe^{3+} by a smaller but more electronegative Al^{3+} being mostly reported in patented literature [1, 13].

3.2.2 The quartz-like phase

Just like the tridymite-like structure, $FePO_4$ also forms a quartz-like structure. The differences between the two polymorphs is the tilt of the tetrahedra but the topology is identical [14], refer to Figure 3.2. The quartz-like structure is favoured when there is 1:1 ratio between phosphorus and iron during preparation [13].

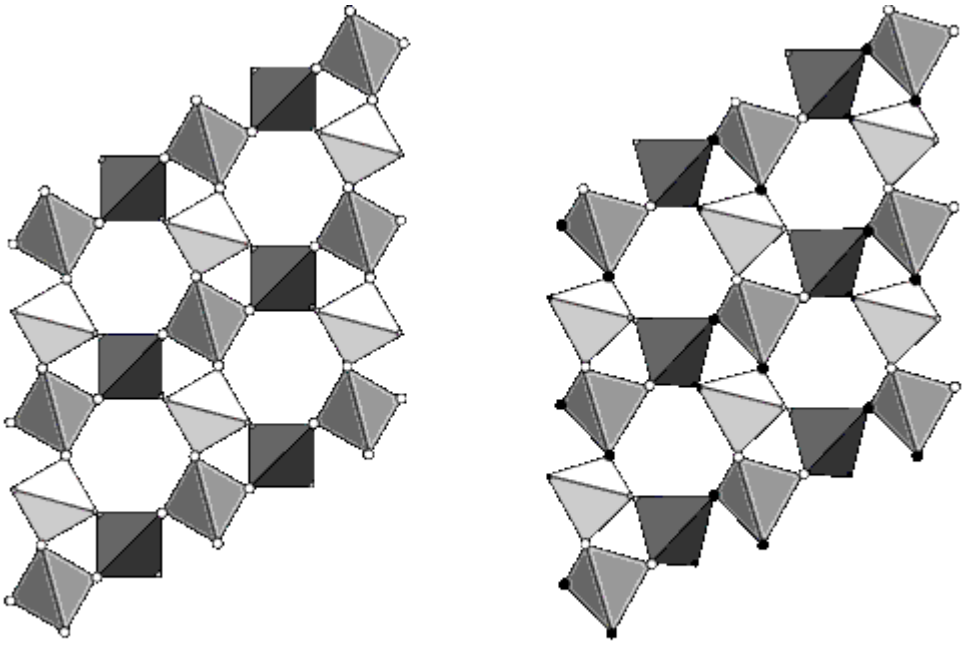

a b

Figure 3.2: Schematic structure of (a) β-quartz and (b) α-quartz [15]

3.3.3 Phases observed in catalytic reactions

It was found during catalytic reactions that the iron phosphate phases changed depending on the reaction conditions and on the method of catalyst preparation. During the oxidative dehydrogenation of isobutyric acid, phases like $Fe_2O_2P_7$, $FePO_4$ (low quartz), $CsFeP_2O_7$ and α-$Fe_3(P_2O_7)_2$ were identified from the Cs promoted industrial catalyst. α-$Fe_3(P_2O_7)_2$ was regarded as the active phase, while the other phases were regarded as inactive phases [1]. However, during the oxidative

dehydrogenation of ethane to ethene, Miller observed $FePO_4$ (low quartz) and β-$Fe_3(P_2O_7)_2$ phases in the post-reaction samples, with occasional evidence of α-$Fe_3(P_2O_7)_2$ and $Fe(PO_3)_3$ phases [5]. For the other reactions, less attention has been given to trying to identify the active phases. But a common observation was that a precursor that started with a Fe^{3+} oxidation state, ended, on post-reaction analysis, with both Fe^{3+} and Fe^{2+} oxidation states [1, 3, 5, 7].

3.4 General Properties

A catalyst that has a P/Fe ratio ranging from 1.0 to 1.3 consists of an amorphous phase, quartz-like phase and/or tridymite-like phase depending on the calcination temperature.

3.4.1 Acidity

The level of acidity in the iron phosphate catalyst is lower than that of heteropoly compounds. The acidity index[2] was reported to be 7.1 x 10^4 mol/g h over the $FePO_4$ catalyst, whereas 280 x 10^4 mol/g h was reported for the $H_5PV_2Mo_{12}O_{40}$ catalyst [16].

3.4.2 Reduction and reoxidation of iron phosphate

According to literature, freshly calcined iron phosphate catalyst that is prepared by the ammonia gel method contains only Fe^{3+} ions. The catalyst with a P/Fe ratio of 1.2 and above can be reduced by hydrogen (or isobutyric acid) in the absence of oxygen to $Fe_2P_2O_7$ *via* the β-$Fe_3(P_2O_7)_2$ phase containing both Fe^{2+} and Fe^{3+} ions. The catalyst with a P/Fe ratio of 1.0 can be reduced to $Fe_2P_2O_7$ without passing through the β-$Fe_3(P_2O_7)_2$ phase. $Fe_2P_2O_7$ is oxidised in air to form an α-$Fe_3(P_2O_7)_2$ phase called the Y-phase. The α-$Fe_3(P_2O_7)_2$ phase is reduced back to $Fe_2P_2O_7$ without passing through the β-$Fe_3(P_2O_7)_2$ phase, as shown in Figure 3.3 [17].

[2] Is a measure of 2-propanol conversion over that catalyst

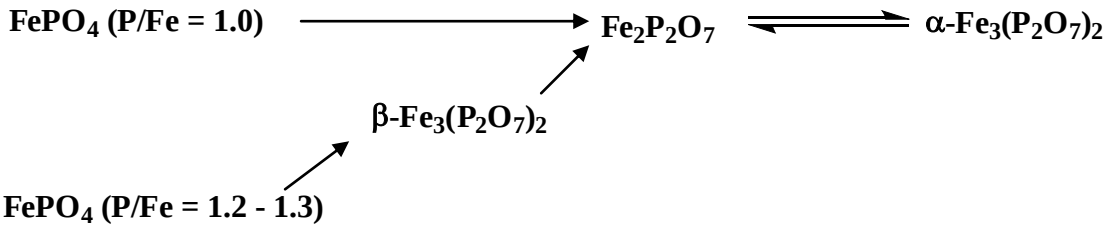

Figure 3.3: A schematic representation of the reduction and reoxidation of iron phosphate with P/Fe ratios of 1.0 to 1.3 prepared by the ammonia gel method [17]

3.4.3 Mechanistic studies

Kinetic studies of the oxydehydrogenation of isobuyric acid to methacrylic acid on various iron phosphate based phases were proposed to follow a Mars and Van Krevelen type mechanism (refer to section 1.4b, for the definition of a Mars and van Krevelen mechanism). It was also proposed that co-feeding water has an advantageous influence on the catalytic performance for this reaction [18].

3.5 Applications in gas phase oxidation

Literature has not only shown the iron phosphate-based catalyst as an excellent oxidative dehydrogenation catalyst for the transformation of isobutyric acid to methacyrlic acid, but it has also been reported to be active in other oxidative dehydrogenation reactions. These reactions include the formation of pyruvic acid from lactic acid or glyoxylic acid from glycolic acid [19] and the transformation of short chain paraffins as in the case of ethane to ethylene [5].

Wang and Otsuka shown that methanol can be selectively produced from methane over iron phosphate catalysts when using oxygen, co-fed with hydrogen, as an oxidant. The highest selectivity of 25.7 % methanol was obtained at 0.51 % methane conversion [20]. It was postulated that peroxide species adsorbed on the catalyst surface were responsible for the selective oxidation at relatively low temperature (300 – 500 ^{o}C); and that these peroxide species resulted from the reductive activation of oxygen by hydrogen.

Wang and Otsuka further applied the same oxidation conditions but eliminated the hydrogen co-feed and used ethane as a feed. In this case they found that only ethylene and carbon dioxide were formed. But when hydrogen was co-fed, the ethane conversion increased and new products like ethanol and acetaldehyde were formed. The highest yield of the C2-oxygenates[3] was 4.4 % (ethanol 1.4 % and

[3] Oxygenated organic products that have two carbon atoms

acetaldehyde 3.0 %) at a temperature of 400 ^{o}C [4]. It was also found that the conversion of C_2H_6 was about 7 - 8 times higher than that of CH_4 under similar conditions and that the selectivity to the corresponding alcohols was higher for CH_3OH (89 %) than for C_2H_5OH (22.5 %) at 350 ^{o}C. This might be due to the subsequent dehydrogenation of C_2H_5OH to C_2H_4 which is impossible for CH_3OH [4]. This work shows that co-feeding H_2 reduces the apparent activation energy of the reductant. A good example is the reduction of the methane activation from 205 kJ mol^{-1} in the absence of hydrogen to 145 kJ mol^{-1} in the presence of hydrogen [20]. Increased selectivity to oxygenates is also observed as a result of co-feeding hydrogen (formation of new products like ethanol and acetaldehyde [4]).

But what might be interesting is that about 60 % selectivity to C_2H_4 was observed during the oxidation of C_2H_6 in the absence of hydrogen at about 0.5 % conversion and approximately 680 K [4]. This has potential, especially when feeding a slightly more active paraffin like C_6H_{14} which requires even less activation energy.

In 2002, Miller and co-workers [5] reported an oxidation reaction of ethane over stoichiometric and non-stoichiometric iron phosphate catalysts. They found that the non-stoichiometric catalyst (P/Fe of 1.2 and 2) gave higher yields to ethylene than the stoichiometric (P/Fe of 1.0) catalyst. For the P/Fe = 1.2 catalyst, which was a mixture of the tridymite-like and amorphous phases, they found (for a non-optimised system) an ethane conversion of 41 % at 84 % selectivity to ethylene. This behaviour was observed only if the catalyst was activated from 450 to 650 ^{o}C at slow 25 ^{o}C increments in a flow of 10 % O_2, 10 % C_2H_2 and a balance of N_2, whereas non-activated catalyst showed only about 4.5 – 7 % ethane conversion under similar reaction conditions. It was also observed by analysis of the post-reaction catalyst that partially reduced iron (Fe^{2+}) was formed and that the Fe/P = 1.2 catalyst sample showed the presence of the $FePO_4$ quartz-like and the β-$Fe_3(P_2O_7)_2$ phases. Migration of phosphorus downstream of the reactor path was shown to play a role in increasing the activity of the catalyst. It was suggested that the high reaction temperatures may be the cause of the phosphorus migration which may also initiate homogeneous (gas phase) reactions.

3.6 References

[1] J.-M.M. Millet, Catal. Rev.-Sci. Eng. 40 (1998) 1 - 38.

[2] A.M. Beale, and G. Sankar, J. Mater. Chem. 12 (2002) 3064 - 3072.

[3] Y. Wang, and K. Otsuka, J. Catal. 155 (1995) 256 - 267.

[4] Y. Wang, and K. Otsuka, J. Catal. 171 (1997) 106 -114.

[5] J.E. Miller, M.M. Gonzales, L. Evans, A.G. Sault, C. Zhang, R. Rao, G. Whitwell, A. Maiti, and D. King-Smith, Appl. Catal. A: Gen. 231 (2002) 281 - 292.

[6] A.V. Annapragada, and E. Gulari, J. Catal. 123 (1990) 130 - 146.

[7] P. Nagaraju, C. Srilakshmi, N. Pasha, N. Lingaiah, I. Suryanarayana, and P.S.S. Prasad, Appl. Catal. A: Gen. 334 (2008) 10 - 19.

[8] M. Ai, E. Muneyama, A. Kunishige, and K. Ohdan, J. Catal. 144 (1993) 632 - 635.

[9] M. Ai, E. Muneyama, A. Kunishige, and K. Ohdan, Catal. Lett. 24 (1994) 355 - 362.

[10] P. Bonnet, J.-M.M. Millet, C. Leclercq, and J.C. Vedrine, J. Catal. 158 (1996) 128 - 141.

[11] G.O. Alptekin, A.M. Herring, D.L. Williamson, T.R. Ohno, and R.L. McCormick, J. Catal. 181 (1999) 104 - 112.

[12] Unknown,. Auburn education, http://www.auburn.edu/~hameswe/Tridy_Cristobpage.html, accessed 06/01/09.

[13] J.-M.M. Millet, and J.C. Vedrine, Appl. Catal. 76 (1991) 209 - 219.

[14] B.G. Hyde, and S. Andersson, Inoganic Crystal Structures. John Wiley & Sons, Inc., Canada, 1989.

[15] S.D. Guest. 2006. Simon Guest Symmetry. University of Cambridge, http://images.google.co.za/imgres?imgurl=http://www2.eng.cam.ac.uk/~sdg/symmetry/quartz.gif&imgrefurl=http://www2.eng.cam.ac.uk/~sdg/symmetry/&usg=__eVW4fDGcRS3ikRygVq0m3MYGKMQ=&h=341&w=480&sz=11&hl=en&start=13&um=1&tbnid=blPkShJiCZ6Q5M:&tbnh=92&tbnw=129&prev=/images%3Fq%3Dlow%2Band%2Bhigh%2Bquartz%2B%

2Bstructure%26um%3D1%26hl%3Den%26sa%3DG, accessed 11/01/09.

[16] M. Ai, E. Muneyama, A. Kunishige, and K. Ohdan, Appl. Catal. A: Gen. 109 (1994) 135 - 146.

[17] E. Muneyama, A. Kunishige, K. Ohdan, and M. Ai, J. Catal. 158 (1996) 378 - 384.

[18] D. Rouzies, J.-M.M. Millet, D.S.H. Sam, and J.C. Vedrine, Appl. Catal. A: Gen. 124 (1995) 189 - 203.

[19] M. Ai, J. Mol. Catal. A: Chem 159 (2000) 19 - 24.

[20] Y. Wang, and K. Otsuka, J. Chem. Soc. Chem. Commun. (1994) 2209 -2210.

Chapter 4 : EXPERIMENTAL

4.1 Introduction

The three catalysts that were prepared are the 12-molybdophosphoric acid, the iron doped salt of 12-molybdophosphoric acid and an iron phosphate catalyst. This chapter gives details of the methods that were used to prepare these compounds and instruments that were used to characterize them. It also gives details of the reactor that was used to test the catalytic performances during *n*-hexane activation; the reaction conditions and product characterisation techniques that were used to identify and quantify the products are also included. The reagents that were used during the preparation and testing are listed in Appendix 1: List of chemicals.

4.2 Catalyst preparation

4.2.1 Pure 12-molybdophosphoric acid preparation

The 12-molybdophosphoric acid, $H_3PMo_{12}O_{40}\cdot 14H_2O$, was prepared by modifying a method reported by Rocchiccioli-Deltcheff *et al.* [1]. An iron dopant was also introduced to the 12-molybdophosphoric acid by partially substituting the protons with iron(III) cations ($Fe_xH_{3-3x}PMo_{12}O_{40}$) [2].

(a) Preparation of $Na_2HPMo_{12}O_{40}\cdot 14H_2O$

Into 50 mL of 2.85 M warm (about 55 ^oC at pH 8.6) Na_2MoO_4 solution, 1.43 mL of 85 % H_3PO_4 solution was added dropwise, followed by 59.1 mL of 70 % $HClO_4$, while the solution was still hot. A yellow precipitate formed as the $HClO_4$ was added and as the mixture cooled. After cooling to room temperature, the yellow precipitate was filtered, re-crystallised in 5 mL $(C_2H_5)_2O$/ 25 mL H_2O and air-dried overnight.

(b) Preparation of $H_3PMo_{12}O_{40}\cdot 14H_2O$

About 21 g of $Na_2HPMo_{12}O_{40}\cdot 14H_2O$ was dissolved in 17.3 mL of H_2O and 4.21 mL of 37 % HCl was added. The mixture was then extracted using 40 mL $(C_2H_5)_2O$. The heavy "etherate" layer was collected; the middle water and the upper ether layers were discarded. The heavy etherate layer was re-extracted with 40 mL $(C_2H_5)_2O$ in order to isolate the anion from solution. The "etherate" heavy layer was then decomposed by mixing the heavy layer with water equal to half its volume, and then decanting the ether top layer. Yellow crystals form after oven (100 ^oC) drying the solution. The dry

solids were calcined at 380 and 400 ^{o}C in air flow for 5 hours.

(c) Doping of $H_3PMo_{12}O_{40}\cdot 14H_2O$ by exchanging H^+ for Fe^{3+} cations

Concentrated solutions of the 12-molybdophosphoric acid (3 g was dissolved in 1.5 mL H_2O) and ferric nitrate (0.58 g $Fe(NO_3)_3\cdot 9H_2O$ was dissolved in 1 mL H_2O) were mixed in a 1:1 stoichiometric ratio and yellow crystals started growing immediately upon mixing. These crystals were allowed to grow overnight, filtered off and dried in a desiccator. The dry solids were calcined at 380 and 400 ^{o}C in air flow for 5 hours.

All heteropoly compound based catalysts were stored in desiccators at ~ 4 ^{o}C.

4.2.2 Iron phosphate-based catalyst preparation

Iron phosphate, $FePO_4$, was prepared by using the well known Mamoru Ai method of synthesising silica supported iron phosphate [3-5].

Preparation of $FePO_4$ having a P/Fe ratio of 1.2

Ferric nitrate, $Fe(NO_3)_3\cdot 9H_2O$, (12.2 g) was dissolved in 500 mL of water and then 20 mL of dilute ammonium solution (25 % NH_4OH) was added to precipitate iron(III) hydroxide as a brown gel. The gel was filtered and while it was still wet, 4.16 g of 85 % orthophosphoric acid (H_3PO_4) was added while stirring the gel, followed by 0.45 g of 40 wt% silica solution. The stirred mixture was then heated up to above 90 ^{o}C using a water bath; it was then kept above 90 ^{o}C for 2 hours and covered to reduce the evaporation rate. Upon heating for an hour, the mixture completely changed from a brown to a cream white colour. After two hours, the mixture was heated directly to evaporate excess water until a cream white paste was obtained, which was then dried at 140 ^{o}C overnight. The dried solids were then calcined at a temperature ranging from 400 - 600 ^{o}C for 4 hours in air.

4.3 Catalyst characterization

4.3.1 Inductively Coupled Plasma - Optical Emission Spectrometer (ICP-OES)

The bulk composition of the precursor and catalyst were determined by Inductively Coupled Plasma (ICP) on a Perkin Elmer Precisely, Optical Emission Spectrometer, Optima 5300 DV.

(a) 12-Molybdophosphoric acid and its iron salt

Samples of ~ 0.05 g calcined and uncalcined catalyst were dissolved in 32 % HCl solution (separately) and diluted to 100 mL with distilled water. The instrument was calibrated by using standard solutions prepared from 1000 ppm phosphorus, iron and molybdenum standard solutions.

(b) Iron phosphate-based catalyst

Samples of ~ 0.05 g calcined and uncalcined catalyst were dissolved in 32 % HCl solution (separately) and diluted to 100 mL with distilled water. The instrument was calibrated by using standard solutions prepared from 1000 ppm phosphorus and iron standard solutions.

4.3.2 X-Ray Diffraction (XRD)

The X-ray diffraction (XRD) patterns were recorded at room temperature on two different instruments (see below) i.e. catalysts prior to catalytic reactions and post reaction catalysts, due to small sample size of post reaction catalysts (<0.5 mL), which could not be loaded in the PW 1710 instrument.

	Prior to reactions	**Post reactions**
Instrument	Philips PW 1710 Diffractometer	Philips PW 1050 Diffractometer
X-ray source	Cobalt (wavelength = 1.78897 Å)	Cobalt (wavelength = 1.78897 Å)
Generator tension	40 kV	40 kV
Current	30 mA	40 mA

4.3.3 Infrared Spectroscopy (IR)

(a) 12-Molybdophosphoric acid

Fourier-Transform Infrared Spectroscopy (FTIR) spectra were recorded by using an Impact 410, Nicolet FTIR. The samples were prepared by the KBr pellet method.

(b) Iron phosphate-based catalyst

A Perkin Elmer Precisely Universal Attenuated Total Reflectance (ATR) Sampling Accessory Infrared Spectroscopy (IR) was used.

4.3.4 Brunauer-Emmett-Teller (BET) surface analysis

The BET surface areas were obtained by using a Micromeritics Gemini instrument. The catalyst samples were de-gassed under a nitrogen flow at 200 ^{o}C overnight. Nitrogen gas was used, at 77 K (liquid nitrogen), as an adsorbing material to determine the surface area capacity of the catalyst. The instrument calculated the surface area as a function of mass of the de-gassed catalyst.

4.3.5 Differential Scanning Calorimeter (DSC) and Thermogravimetric Analysis (TGA)

The DSC data were obtained from a Mettler-Toledo DSC822e calorimeter; each pan was run in the temperature range of 25 – 400 ^{o}C under nitrogen atmosphere at a rate of 10 ^{o}C / min. TGA was performed using a Perkin Elmer Pyris 1 TG analyzer at a heating rate of 10 ^{o}C / min under air from 25 – 700 ^{o}C.

4.3.6 Nuclear Magnetic Resonance spectroscopy (NMR)

^{31}P NMR analysis was done on the 12-molybdophosphoric acid and its iron doped salt to test for its purity using D_2O as solvent and solid-state ^{31}P NMR analysis was also used to further elucidate the compounds. A Bruker Ultrashield 600 MHz instrument was used.

4.3.7 Transmission Electron Microscopy (TEM)

Transmission Electron Microscopy (TEM) images were obtained from a JEOL 1010 instrument.

4.3.8 Scanning Electron Microscopy (SEM)

The magnified images of the uncalcined and calcined samples were obtained by viewing carbon coated samples under a LEO 1450 Scanning Electron Microscope.

4.3.9 Temperature Programmed Desorption (TPD)

The Temperature Programmed Desorption was obtained through the use of a Micromeritics AutoChem II Chemisorption Analyser. The 4 NH_4-He (4.1 % ammonia, balance helium) gas was used for analysis.

TPD conditions: Flow He carrier at 20 ml/min for 30 min; Ramp to 150 ^{o}C at 5 ^{o}C/min and hold for 5 min; Flow 4 NH_4-He analysis gas at 20 ml/min for 60 min; Flow He carrier at 20 ml/min for 2 min; Ramp (cool) to 30 ^{o}C at 5 ^{o}C/min and hold for 2 min; Start recording: Ramp to 650 ^{o}C at 10 ^{o}C/min and hold for 10 min; Stop recording

4.4 Catalyst testing

4.4.1 Reactor configuration

A stainless steel, fixed-bed continuous-flow, reactor was built for the purpose of running catalytic reactions of gaseous hexane over a solid catalyst. Figure 4.1 shows a flow diagram, with all the necessary symbols labelled. The liquid feed (*n*-hexane) was pumped into the system, gasified at 150 ^{o}C, and then mixed with carrier gas (air). This gaseous mixture was then passed through a fixed-bed heated reactor tube packed with the catalyst and carborandum (SiC). The products from the reactor were then cooled in a sampling cylinder, keeping the temperature at approximately 0 ^{o}C, to form liquid samples. The liquid samples that were collected separated into two layers (the organic and the aqueous layer). Both the layers were injected separately into the Gas Chromatograph – Flame Ionisation Detector (GC-FID). The non-condensable gaseous products were passed to a gas-flow meter to measure the total flow rate of gaseous products. Gaseous samples are taken and injected into a GC-FID and Gas Chromatograph – Thermal Conductivity Detector (GC-TCD) for analysis. The carrier gas flow rates, the heating of the lines, the heating of the reactor tube and the exact temperature inside the reactor tube were controlled and monitored on a separate control panel. The temperature inside the reactor was monitored by using thermocouples and the pressure inside the reactor was monitored to determine any back-pressure. A pressure relief valve was used to relieve pressure inside the reactor, in cases where back pressure builds up inside the reactor, in order to avoid explosions.

4.4.2 Product characterisation techniques

An Agilent 6890 series GC system equipped with an Agilent 5973 Network Mass Selective detector (Mass Spectroscopy (MS) detector) was used to identify the hydrocarbons produced in the reaction. This Agilent GC-MS was fitted with a HP-5 (5%-phenyl)-methylpolysiloxane, HP 19091j-433, capillary column with 30.0 m x 250 µm x 0.25 µm nominal dimensions. All liquid products were analysed for the water content by using the 870 KF Titrino plus Metrohm Karl Fischer Titrator.

A Perkin Elmer Precisely, Clarus 400 Gas Chromatograph (GC), operated at room temperature and equipped with a thermal conductivity detector (TCD) was used to separate and quantify carbon oxides produced in the reaction. The Clarus 400 GC was fitted with a 50 m long Elite-Alumina (Aluminium oxide porous layer) open tubular capillary column with a 0.53 mm id. The detector was set at 250 ^{o}C, while the injector and TCD filament temperature was 150 ^{o}C. The helium carrier gas flowed through the column at a pressure of 60 kPa.

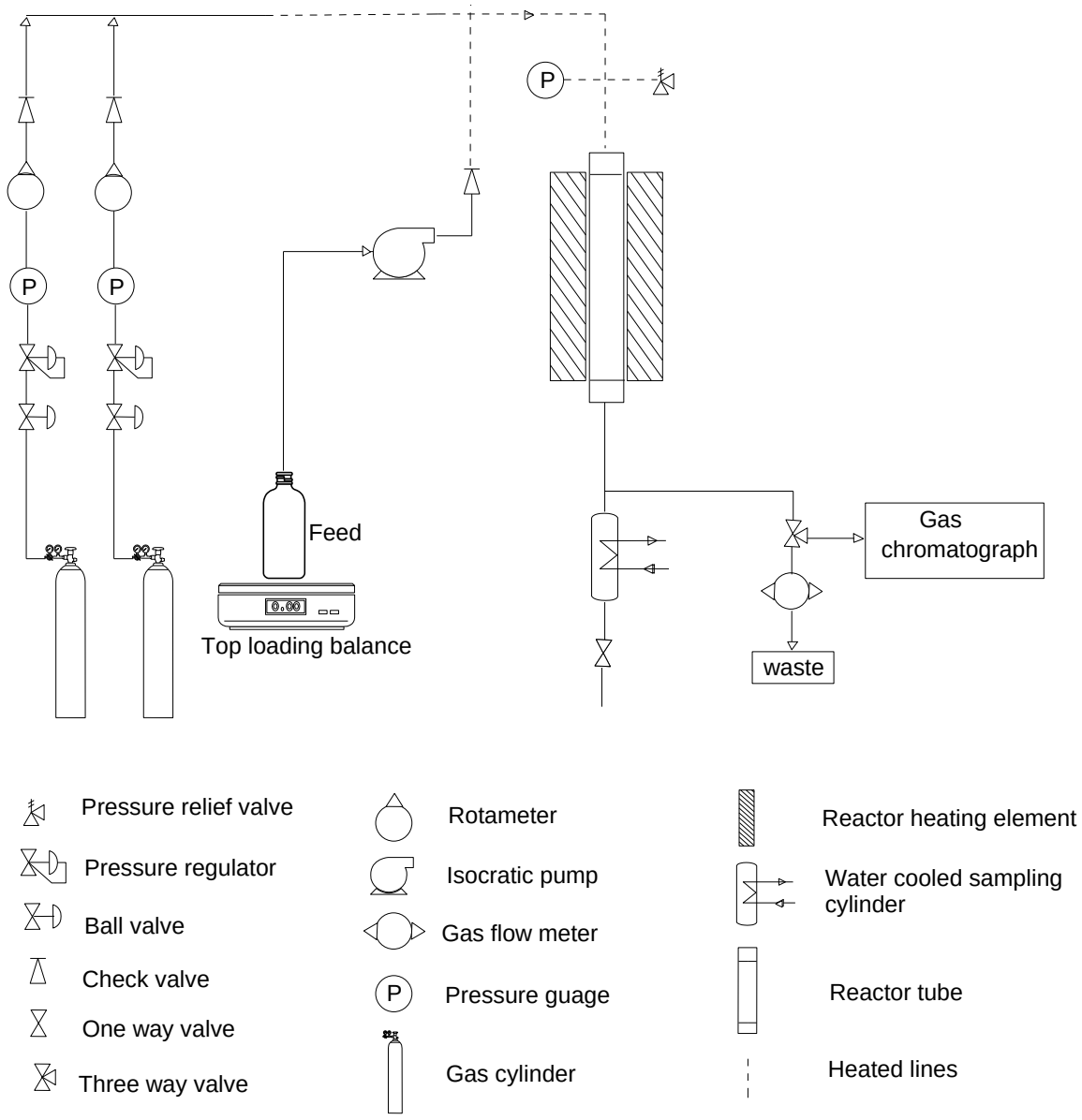

Figure 4.1: The flow diagram for a continuous-flow reactor

A Perkin Elmer Precisely, Clarus 500 GC equipped with a flame ionisation detector (FID) was used to separate and quantify hydrocarbons produced in the reaction. The Clarus 500 was fitted with a 50 m

long Elite-Petro capillary column with a 0.2 mm id. The detector was set at 250 ^{o}C and the injector at 220 ^{o}C. The hydrogen carrier gas flow was adjusted to give an inlet pressure of 206 kPa. As an exception, 3-hexene overlapped with hexane in the Elite column and so it was quantified using a Varian Capillary Column (CP – Sil 5 CB, 25 m long, 0.15 mm id, 2 μm nominal dimensions, #CP7692) fitted into a Perkin Elmer AutoSystem XL GC-FID.

The temperature programs used in the GC-MS, GC-TCD and GC-FID are shown in appendix 2.

4.4.3 Reaction conditions

The experiments were performed at atmospheric pressure using a 9 mm id x 34 cm long stainless steel fixed-bed continuous-flow reactor. A volume of 0.5 mL (approximately 0.5 g) catalyst, of particle size ranging from 300 – 600 μm, was loaded in the hottest spot of the reactor tube (the hottest spot was determined by probing different positions inside a heated reactor tube using a thermocouple). The catalyst was diluted with a coarse 24 gritt (14755/24 = 615 microns) SiC (carborandum) at a 1:4 volume ratio of catalyst:carborandum to avoid undesirable temperature rise on the catalyst surface during the catalytic oxidation reactions. The catalyst packing length was approximately 4 cm. Prior to the catalytic reactions; the catalyst packed reactor was heated for approximately 1 hour at 200 ^{o}C under a flow of air to remove absorbed water on the catalyst surface. General operation conditions included a temperature range from 250 - 500 ^{o}C. Each catalyst was kept on stream for approximately one week and online samples were taken every 4 hours after a steady state was reached. The C_6H_{14}/O_2 ratio of two was kept constant for all reactions and Table 4.1 gives the rest of the parameters that were changed across the catalytic testing process. The carbon balance of data points used was between 92 – 108 %.

An exception to the general catalyst loading protocol was carried out once, where the catalyst was loaded below the hottest spot of the reactor tube, to avoid polymerisation of the catalytic products (details are available in Chapter 6).

Refer to Appendix 2: Product quantification for calculation details

Table 4.1: The Reaction parameters that were used for catalytic testing

Catalyst Name	Catalyst mass / g	Loading position	*n*-Hexane gas flow / mL min^{-1}	Air flow / mL min^{-1}	Total flow/ mL min^{-1}	Contact time* / s
Carborandum	-	-	17.75	42.25	60	-
Carborandum	-	-	5.92	14.08	20	-
HPA	0.5470	hottest spot	17.75	42.25	60	0.5
HPA	0.5407	6.5 cm below hottest spot	17.75	42.25	60	0.5
Fe doped HPA	0.5243	hottest spot	17.75	42.25	60	0.5
$FePO_4$	0.4078	hottest spot	17.75	42.25	60	0.5
$FePO_4$	0.4119	hottest spot	11.83	28.17	40	1.0
$FePO_4$	0.4062	hottest spot	5.92	14.08	20	1.5

**Contact time =Volume of catalyst / Total gas flow (refer to Appendix 2 calculations)*

4.5 References

[1] C. Rocchiccioli-Deltcheff, M. Fournier, R. Franck, and R. Thouvent, Inorg. Chem. 22 (1983) 207-216.

[2] M. Langpape, and J.-M.M. Millet, Appl. Catal. A: Gen. 200 (2000) 89 – 101.

[3] M. Ai, E. Muneyama, A. Kunishige, and K. Ohdan, J. Catal. 144 (1993) 632 - 635.

[4] M. Ai, E. Muneyama, A. Kunishige, and K. Ohdan, Bull. Chem. Soc. Jpn. 67 (1994) 551 - 556.

[5] M. Ai, E. Muneyama, A. Kunishige, and K. Ohdan, Appl. Catal. A: Gen. 109 (1994) 135 - 146.

Chapter 5 : CHARACTERIZATION RESULTS AND DISCUSSION

5.1 The 12-Molybdophosphoric acid catalyst

This section will discuss the characterization results of 12-molybdophosphoric acid ($PMo_{12}O_{40}$) and its iron doped salt ($Fe_xH_{3-3x}PMo_{12}O_{40}$). The acid will be referred to as "HPA", whereas the salt will be referred to as "Fe doped HPA" to avoid repetition of these long names.

5.1.1 Inductively Coupled Plasma-Optical Emission Spectrometer (ICP-OES)

The ICP-OES results clearly show that the expected molybdenum to phosphorus ratio of twelve was obtained for the HPA ($H_3PMo_{12}O_{40}$), refer to Table 5.1. It was further observed that the Mo/P ratio increased with calcination temperature as a result of the loss of phosphorus. The lost phosphorus can be due to the loss of non-Keggin contaminant phosphorus atoms (^{31}P Solid-state NMR in section 5.1.4 supports this argument). On the other hand the iron doped HPA ($Fe_{0.69}H_{0.93}PMo_{12}O_{40}$) had a Mo/P phosphorus ratio which was slight greater than 12 (Table 5.1). The loss of phosphorus with increase in calcination temperature was also observed. The Fe^{3+} ion dopant was loaded at an iron to phosphorus ratio of 0.63 - 0.69, leaving behind 1.11 - 0.93 protons per Keggin unit.

Table 5.1: The bulk elemental composition of the HPA and the iron doped HPA obtained by ICP-OES analysis

Catalyst Formula	Mo/P ratio of uncalcined catalyst	Mo/P ratio of 380 ^oC calcined catalyst	Mo/P ratio of 400 ^oC calcined catalyst	Fe/P ratio
$H_3PMo_{12}O_{40}$	10.05	11.25	11.40	-
$Fe_{0.69}H_{0.93}PMo_{12}O_{40}$	12.17	13.16	14.01	0.69

5.1.2 Infrared Spectroscopy (IR)

The IR spectrum of an uncalcined 12-molybdophosphoric acid catalyst shown in Figure 5.1a shows typical Keggin structure characteristic IR peaks [1-4]. The peak at 1064 cm^{-1} corresponds to ν_{as} P-O_a, 961 cm^{-1} corresponds to ν_{as} Mo-O_t, 869 cm^{-1} corresponds to ν_{as} Mo-O_b-Mo and 783 cm^{-1} corresponds

to ν_{as} Mo-O_c-Mo (where O_a refers to oxygen atoms bound to 3 Mo atoms and the central P atom; O_b and O_c refer to oxygen atoms bound to adjacent Mo atoms; O_t refers to terminal oxygen atoms) [2]. This Keggin structure was preserved when the HPA was calcined at 380 ^oC (Figure 5.1b). At 400 ^oC calcination temperature, IR peaks (Figure 5.1c) corresponding to MoO_3 were observed (984 and 894 cm^{-1}) [1, 4]. The intensity of the MoO_3 characteristic peaks increased as the samples were calcined at 450 ^oC and 500 ^oC respectively. This means that the Keggin structure was destroyed at 400 ^oC, hence the highest stability temperature of the Keggin 12-molybdophosphoric acid is 380 ^oC.

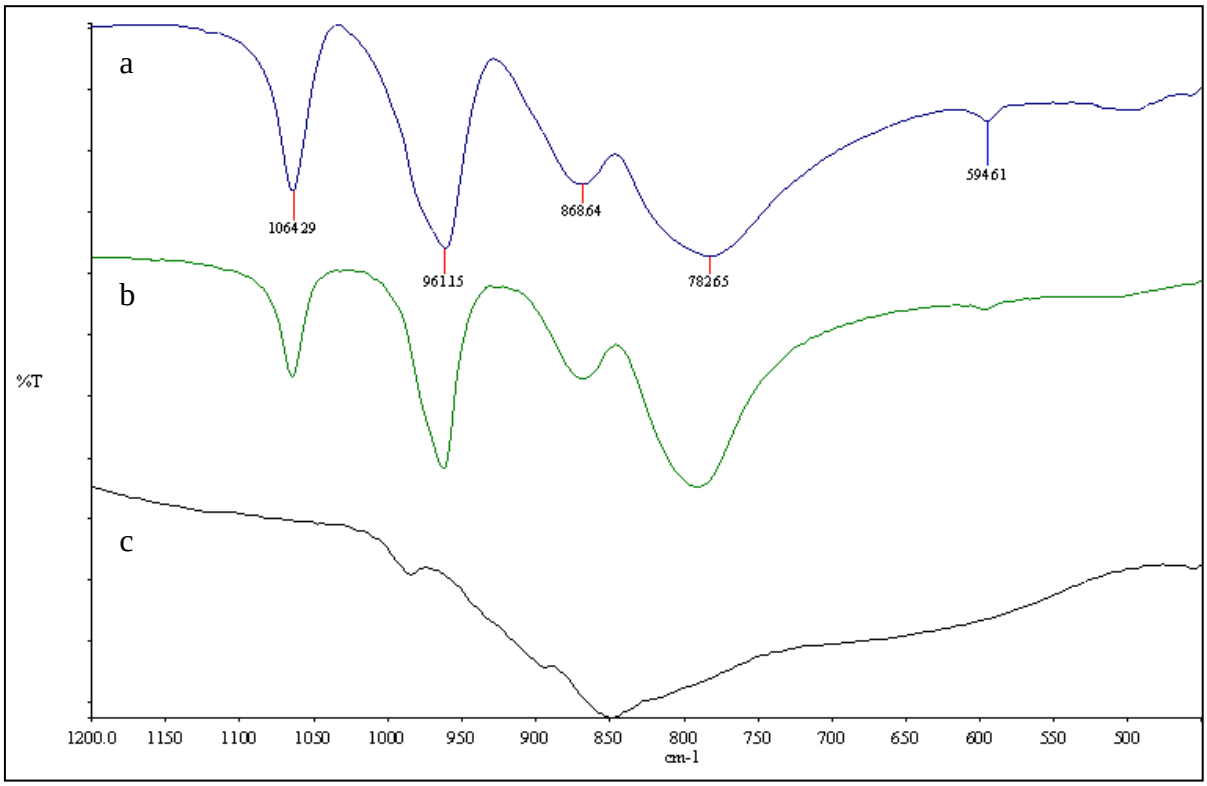

Figure 5.1: IR spectra of the HPA (a) uncalcined (b) 380 ^oC calcined (c) 400 ^oC calcined

In Figure 5.2a Keggin characteristic peaks are observed for the uncalcined iron doped salt of 12-molybdophosphoric acid. This was expected since the substitution of protons with Fe^{3+} does not interfere with the Keggin (primary) structure because it is merely a counter-ion substitution. Furthermore, the Keggin structure of the iron doped salt was also preserved when the salt was calcined a 380 ^oC (Figure 5.2b). Contrary to the protonated (HPA) catalyst, the Keggin structure of the iron doped HPA was only partially decomposed when it was calcined at 400 ^oC (compare Figure 5.1c to Figure 5.2c). It is clear from Figure 5.2c that the Keggin structure is not completely destroyed, since the Keggin IR peaks are observed at 1064, 962, 869 and 786 cm^{-1}. This means that thermal stability of the HPA is improved by the substitution of the protons with Fe^{3+} cations.

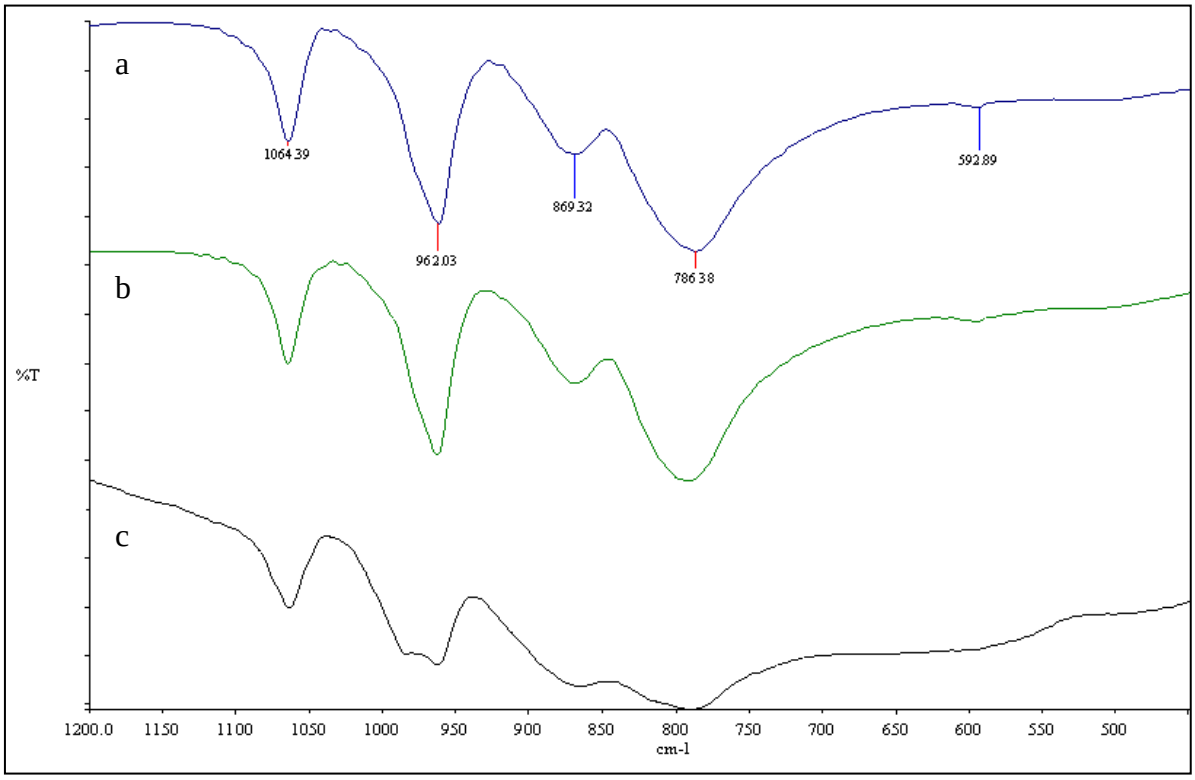

Figure 5.2: IR spectra of the iron doped HPA (a) uncalcined (b) 380 ^{o}C calcined (c) 400 ^{o}C calcined

5.1.3 X-Ray Diffraction (XRD)

The thermal transformation of 12-molybdophosphoric acid from its hydrated form ($H_3PMo_{12}O_{40}\cdot 13H_2O$) through its intermediates (anhydrous acid $H_3PMo_{12}O_{40}$ and anhydride $H_xPMo_{12}O_{38.5\,+\,x}$, where x ~ 0.1) and to the final decomposition products (molybdenum trioxide promoted by molybdenyl pyrophosphate $(MoO_2)_2P_2O_7$ and phosphorus) has been suggested and shown from previous *in-situ* XRD studies [5]. The XRD peaks of the uncalcined 12-molybdophosphoric acid catalyst (Figure 5.3a) are similar to the characteristic peaks of the monoclinic Keggin structure [1, 2, 5], with d-spacings of 11.2, 9.8 and 3.21 Å [1].

A complete change in the XRD pattern was observed when the catalyst was calcined at 380 ^{o}C (Figure 5.3b). This change resulted in a formation of an unidentified phase, which might be amorphous or microcrystalline. The nature of this phase is highly dependent on the level of hydration (water of crystallization makes up part of the secondary structure), hence making it difficult to study the crystallographic nature of this partially dehydrated material. However, electron diffraction patterns in the transmission electron microscopy showed that this material was crystalline, see section 5.1.6. When the catalyst was calcined at 400 ^{o}C, peaks belonging to MoO_3 and an unknown phase [5] were

observed. Calcination at 450 to 500 ^{o}C showed a complete decomposition of the unknown phase and the intensity of the MoO_3 characteristic peaks increased. Figure 5.3c-e clearly show peaks with d-spacings of 6.97, 3.81, 3.47, 3.27, 2.70, 2.65, 2.53, 2.31 and 2.27 Å which correspond to the MoO_3 peaks [5]. It was also observed that the solubility in water of this mixture of phases (referring to catalysts calcined at 380 to 500 ^{o}C) had dropped, which was due to the formation of a less soluble, MoO_3, decomposition product. It was also observed from the IR result (above) that the 380 ^{o}C calcined sample had Keggin characteristic peaks, whereas the 400 ^{o}C calcined sample had MoO_3 characteristic peaks (Figure 5.1b and c). This means that the unidentified phase in the XRD of the

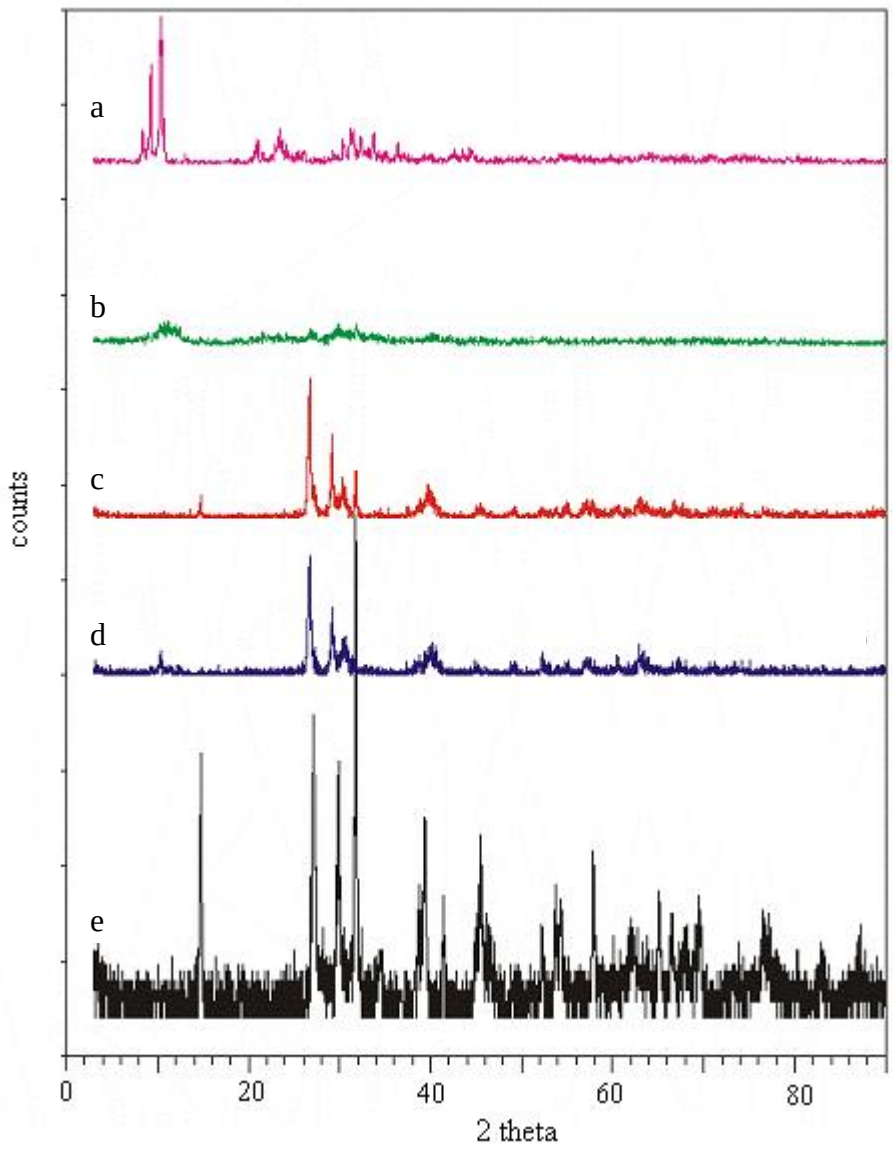

Figure 5.3: XRD patterns of $H_3PMo_{12}O_{40}$ (a) uncalcined (b) 380 ^{o}C calcined (c) 400 ^{o}C calcined (d) 450 ^{o}C calcined (e) 500 ^{o}C calcined

380 ^{o}C calcined sample has a Keggin structure and that this phase dominates at 380 ^{o}C; whereas at 400 ^{o}C MoO_3 dominates.

The XRD pattern (Figure 5.4a) of the iron doped HPA has sharper peaks, which means that the material was more crystalline than the undoped HPA. This change in crystallinity can be due to the fact that the Fe^{3+} cation is larger than H^{+} and so it binds strongly to the adjacent Keggin units and water molecules, hence increases the level of order in the secondary structure. The level of crystallinity dropped or perhaps the particle size changed when the material was calcined at 380 ^{o}C (Figure 5.4b) as a result of dehydration. A completely different pattern was observed at 400 ^{o}C

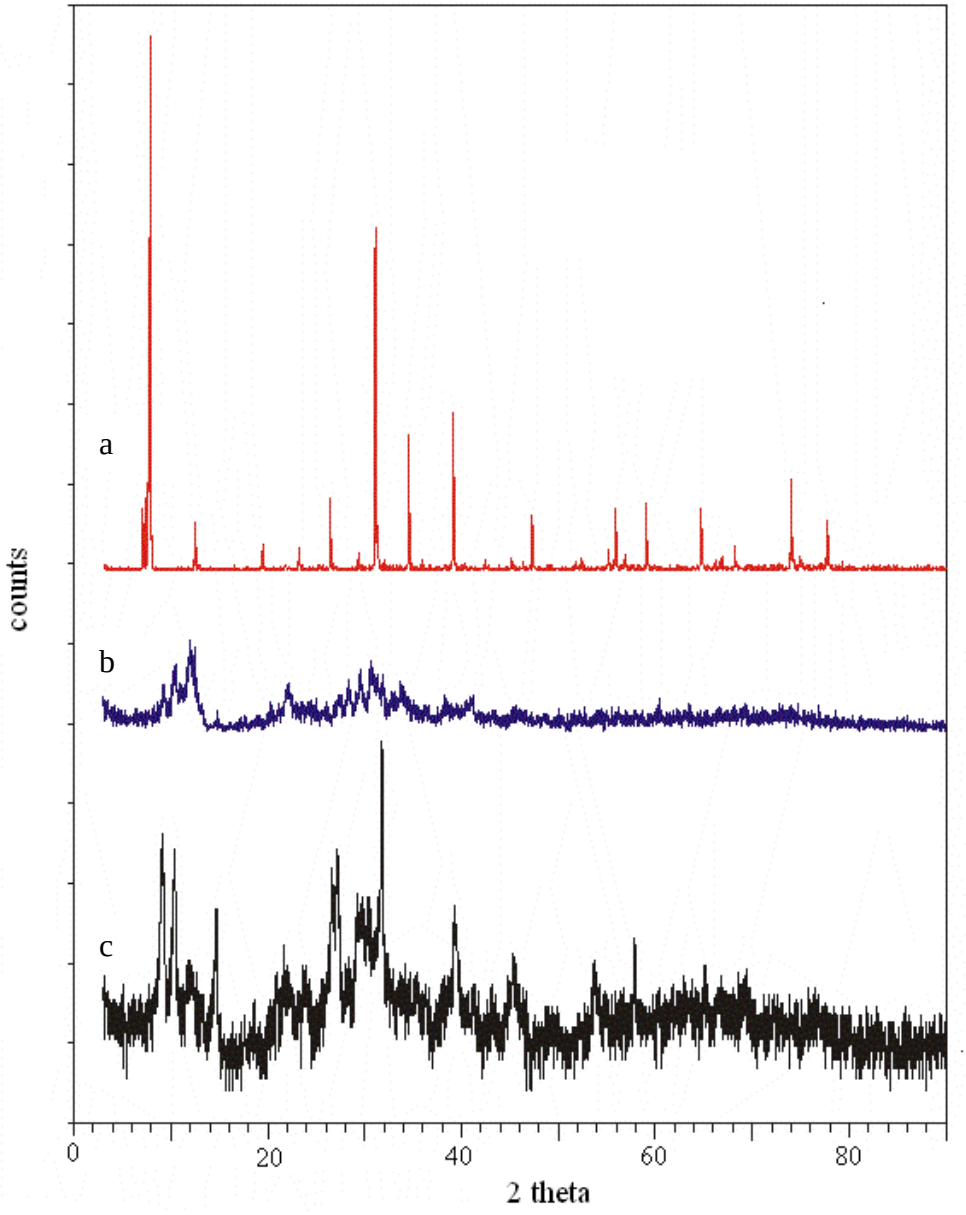

Figure 5.4: XRD patterns of $Fe_{0.69}H_{0.93}PMo_{12}O_{40}$ (a) uncalcined (b) 380 ^{o}C calcined (c) 400 ^{o}C calcined

calcination temperature (Figure 5.4c), which is more crystalline and might be due to the formation of MoO_3.

5.1.4 Nuclear Magnetic Resonance spectroscopy (NMR)

The ^{31}P NMR of the synthesised 12-molybdophosphoric acid shows three peaks (-3.93 ppm, -1.65 ppm and -0.60 ppm), with the peak at -3.93 ppm showing the highest intensity, followed by the peaks at -1.65 and then -0.60 ppm, which has the lowest intensity (Figure 5.5a). The expected chemical shift for the 12-molybdophosphoric acid is -3.9 ppm [6], which corresponds to the high intensity observed peak at -3.93 ppm. The iron doped HPA shows two peaks at -3.93 (most intense) and -1.64 ppm (Figure 5.5b), which are similar to the peaks observed in the pure HPA. The third peak was not observed, possibly due to low intensity, hence it was concluded that the iron dopant did not change the electron environment of the phosphorus atom in the Keggin structure. It also means that there were two forms of phosphorus impurities in the synthesised HPA. To see if these two phosphorus impurity peaks were still present in the materials after calcination, ^{31}P NMR analysis was also done on the 380 ^oC calcined catalysts.

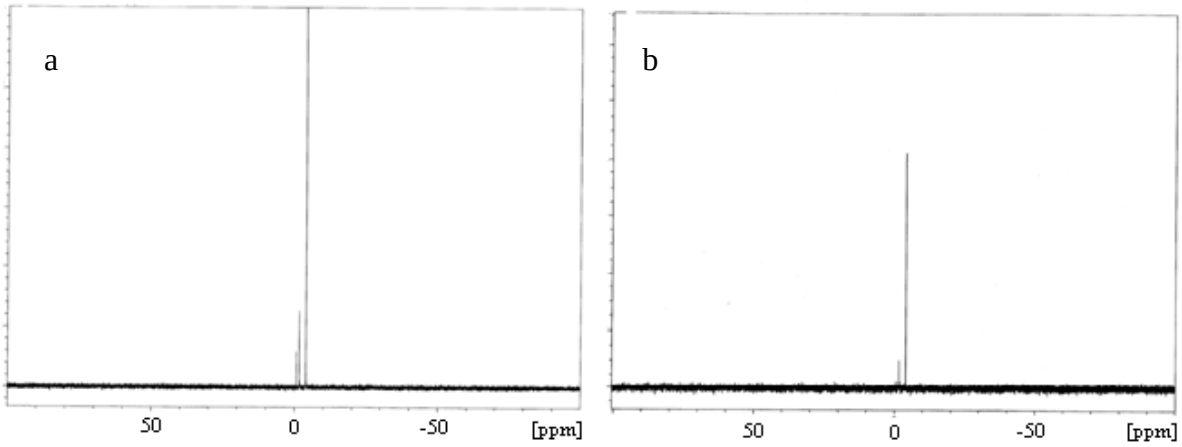

Figure 5.5: ^{31}P NMR of (a) HPA and (b) iron doped HPA dissolved in D_2O solvent

Solid-state NMR was used to analyse the water insoluble calcined HPA. The ^{31}P solid-state NMR of the HPA shows two $[PMo_{12}O_{40}]^{3-}$ characteristic peaks (- 4.65 and – 4.95 ppm) [7]. The iron doped HPA shows three peaks (-3.92; -4.12 and -4.57 ppm) in the ^{31}P solid-state NMR (Figure 5.6a). The major peak is observed at -4.57 ppm and assigned to the Keggin phosphorus atom. The slight shift from the expected value might be due to the Fe^{3+} substituted cations. When the iron doped HPA was calcined at 380 ^oC, a change in chemical shift was observed only for the two small peaks (changes from -3.92 and -4.12 to -2.47 and -3.46 ppm respectively), whereas the major peaks remained

unchanged at -4.56 ppm (compare Figure 5.6b to Figure 5.6a). This means that there was a change in the chemical environment of the non-Keggin phosphorus atoms, whereas the electronic environment of the phosphorus atoms inside the Keggin structure did not change with calcination.

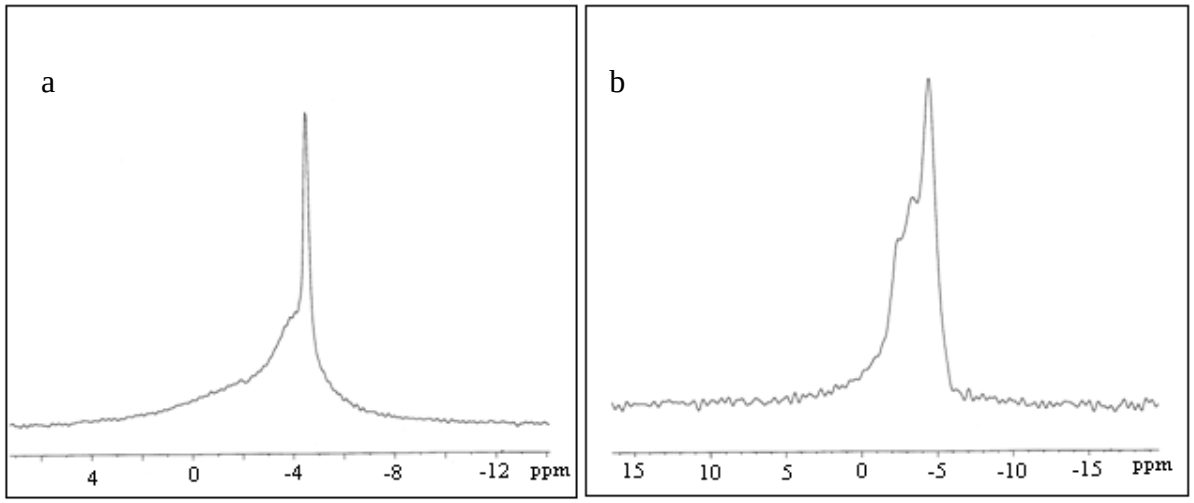

Figure 5.6: ^{31}P solid-state NMR of (a) iron doped HPA and (b) 380 ^{o}C calcined iron doped HPA

5.1.5 Brunauer-Emmett-Teller surface analysis (BET) and Scanning Electron Microscopy (SEM)

The surface area (Figure 5.7) of the uncalcined $H_3PMo_{12}O_{40}$ catalyst (9.5 m^2 g^{-1}) is lower than that of the 380 ^{o}C calcined catalyst (15.9 m^2 g^{-1}), but their respective SEM images are similar (Figure 5.8). This difference in surface area might be due to loss of crystallinity (compare sharp XRD peaks in Figure 5.3a to broad XRD peaks in Figure 5.3b) when moving from the highly hydrated $H_3PMo_{12}O_{40}\cdot 7H_2O$ species to a partially dehydrated $H_3PMo_{12}O_{40}\cdot xH_2O$ species formed after calcination. The surface area of the uncalcined HPA catalyst (9.5 m^2 g^{-1}) is close to the 10 m^2 g^{-1} reported for an uncalcined $H_3PMo_{12}O_{40}$ catalyst [8]. The surface area dropped, from 15.9 to an average of 5.4 m^2 g^{-1} when the catalyst was calcined at 400 - 500 ^{o}C. This trend follows the trend that was observed in the thermal stability of the Keggin structure (refer to IR spectra in Figure 5.1) where a complete phase change was observed at 400 ^{o}C calcination temperature.

The surface area dropped from 9.5 to 4.8 m^2 g^{-1} when the catalyst was doped with Fe^{3+} cations (Figure 5.7). This drop in surface area is explained by the fact that the iron doped catalyst was more crystalline (this was seen in the XRD pattern shown in Figure 5.4a above). The surface area gradually increased from 4.8 to 7.2 m^2 g^{-1} as the calcination temperature increased to 400 ^{o}C. The surface area

dropped (from 7.2 to 3 m^2 g^{-1}) when the iron doped catalyst was calcined at 450 and 500 ^oC, this is also in line with the thermal stability of the Keggin structure. In this case a complete phase change was seen at 450 ^oC.

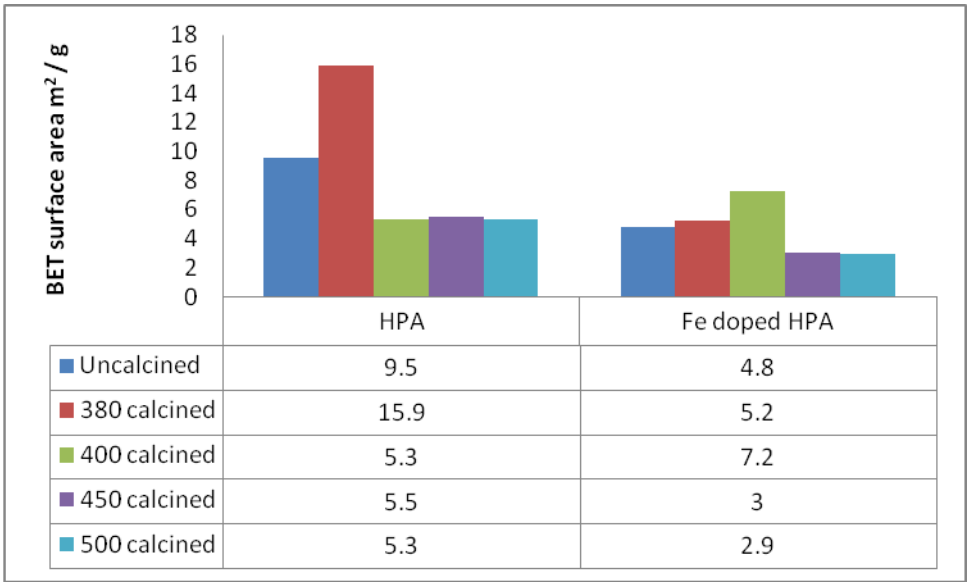

	HPA	Fe doped HPA
Uncalcined	9.5	4.8
380 calcined	15.9	5.2
400 calcined	5.3	7.2
450 calcined	5.5	3
500 calcined	5.3	2.9

Figure 5.7: The BET surface area of the HPA and iron doped HPA catalysts calcined at various temperatures

The SEM images of the uncalcined and the 380 ^oC calcined $H_3PMo_{12}O_{40}$ catalyst were almost similar but the 450 ^oC calcined $H_3PMo_{12}O_{40}$ catalyst (Figure 5.8) was more "fluffy", which meant that calcination caused increased "fluffiness". The same effect of increase in fluffiness with the increase in calcination temperature is observed in the SEM images of the $Fe_{0.64}H_{1.11}PMo_{12}O_{40}$ catalyst in Figure 5.8 (notice the changes from 380 to 400 ^oC calcination temperature). The drop in surface area (from 400 ^oC in the HPA and from 450 ^oC in the Fe doped HPA) with decreasing particles sizes (in the SEM below) may be due to the loss of microporosity during the crystallisation process [9] of MoO_3.

5.1.6 Transmission Electron Microscopy (TEM)

The TEM image of the uncalcined HPA shows hexagonal (six sided) particles of particle size close to 0.5 μm as seen in Figure 5.9 and the corresponding electron diffraction patterns shows discrete spots which are characteristic of a crystalline material [10]. When the HPA was calcined to 380 ^oC, the particle size dropped and the size distribution range increased, but the material remained crystalline as the discrete spots were still observed in the electron diffraction pattern (Figure 5.9). Although the powder XRD (Figure 5.3b) failed to show the crystallinity of this material as a result of small particle size and partial dehydration, the TEM electron diffraction pattern, clearly shows that the 380 ^oC

calcined HPA is crystalline. The drop in particle size with the increases in calcination temperature behaviour was also observed in the SEM results (Figure 5.8).

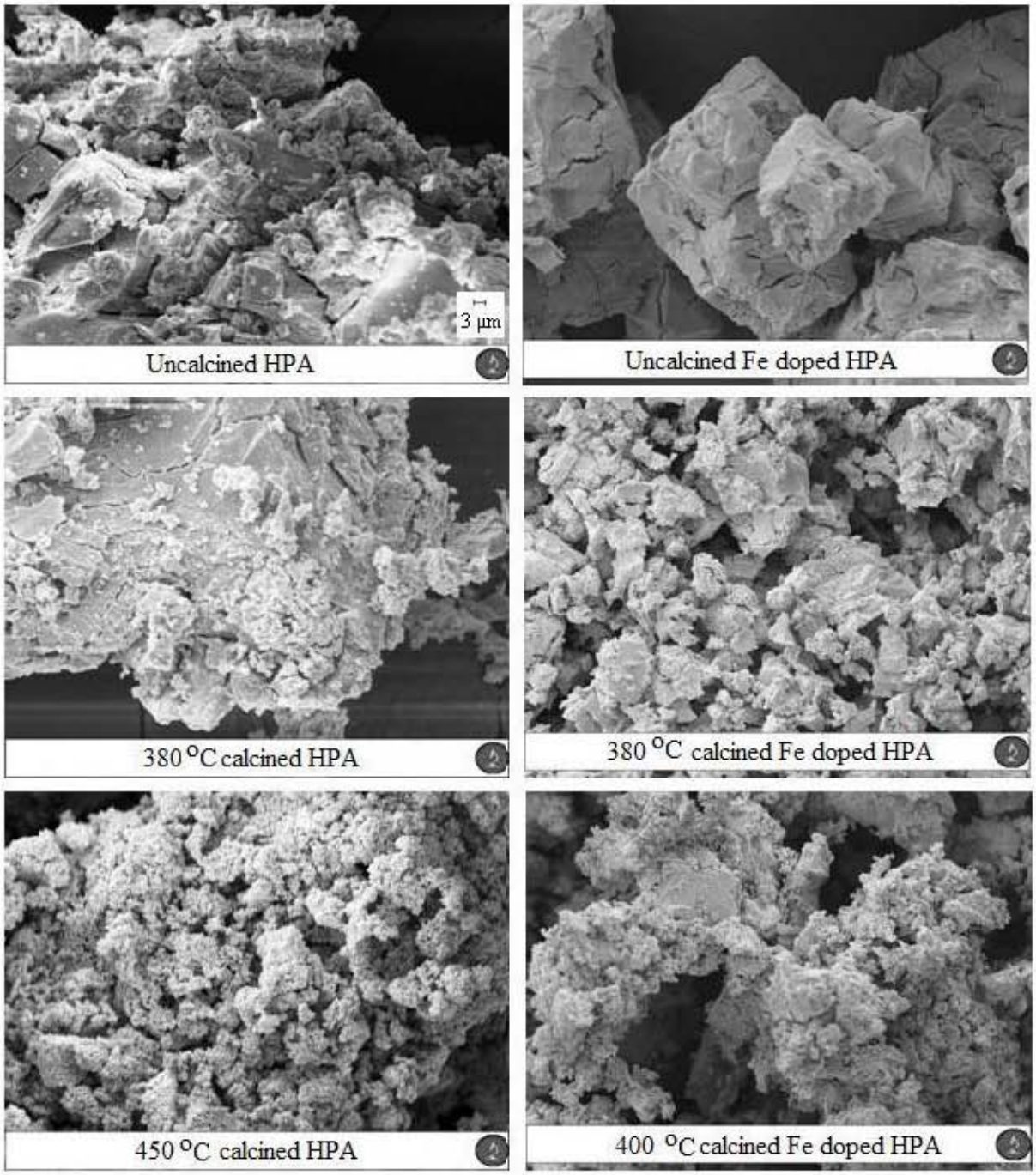

Figure 5.8: SEM images of the HPA and the iron doped HPA catalysts calcined at various temperatures (the scale shown applies to all images)

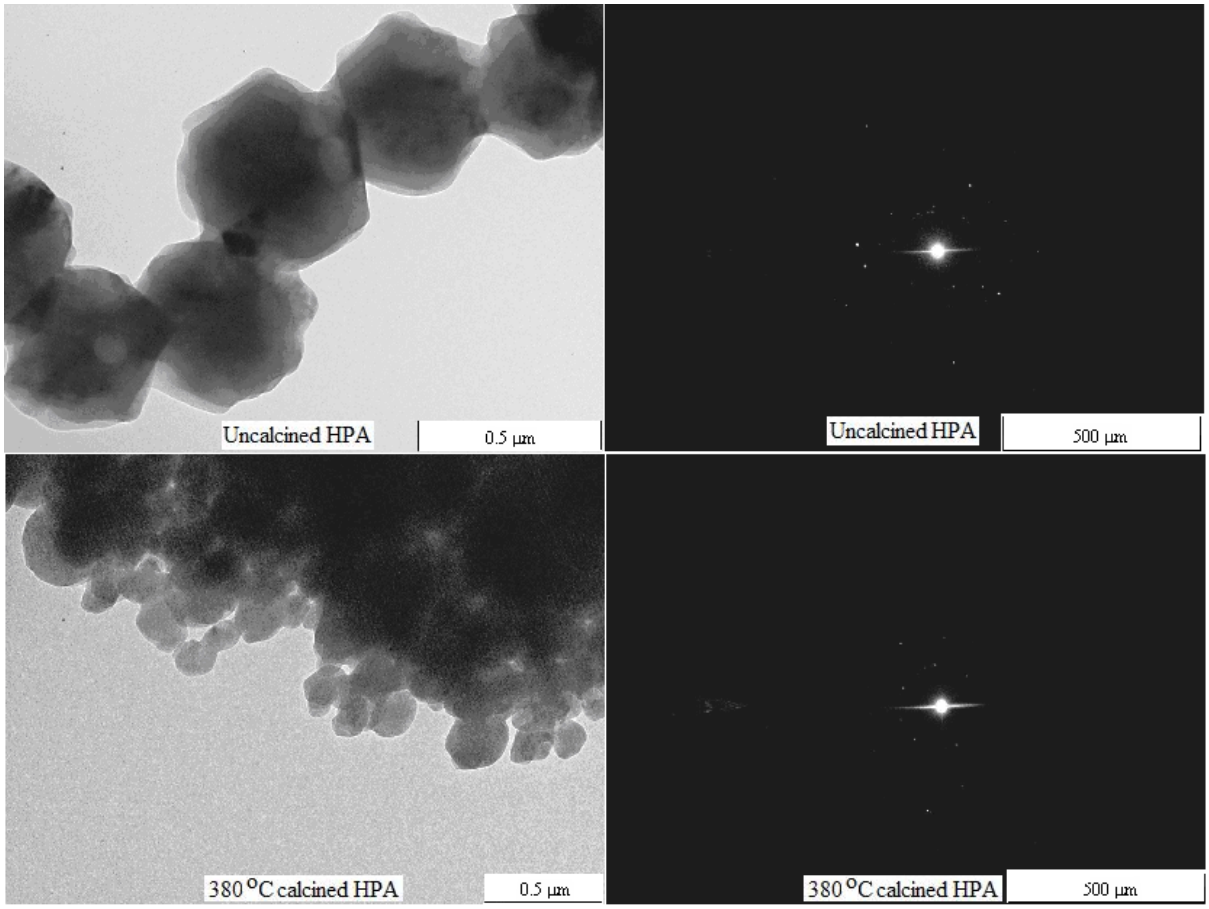

Figure 5.9: TEM images of the 12-molybdophosphoric acid and corresponding electron diffraction patterns

5.1.7 Thermogravimetric Analysis (TGA) and Differential Scanning Calorimeter (DSC)

The TGA of an uncalcined HPA and a 380 ^{o}C calcined HPA showed two weight loss steps due to the loss of water molecules. The weight loss at 136 ^{o}C (Figure 5.10a) corresponds to the loss of 7 water of crystallization molecules per Keggin unit (KU) [11]. This is accompanied by two DSC endothermic peaks at 129 and 140 ^{o}C (Figure 5.10b) for the uncalcined catalyst and one DSC endothermic peak at 146 ^{o}C for the calcined catalyst (Figure 5.10b). A plateau ascribed to the anhydrous acid ($H_3PMo_{12}O_{40}$) is seen between 136 and 237 ^{o}C (HPA in Figure 5.10a) [11]. Further weight loss (2 H_2O molecules per KU) at 403 ^{o}C corresponds to the loss of constitutional water[4] [11, 12]. This gives a total of about 9 water molecules per KU lost (calcined or uncalcined) (Table 5.2 gives full TGA details). Above 403 ^{o}C a plateau is formed and it is ascribed to an anhydride ($PMo_{12}O_{38.5}$), but the nature of this anhydride is controversial [12]. A postulated dehydration pathway is seen in literature

[4] Constitutional water refers to the protons bound to the Keggin polyanion external oxygen

[11].

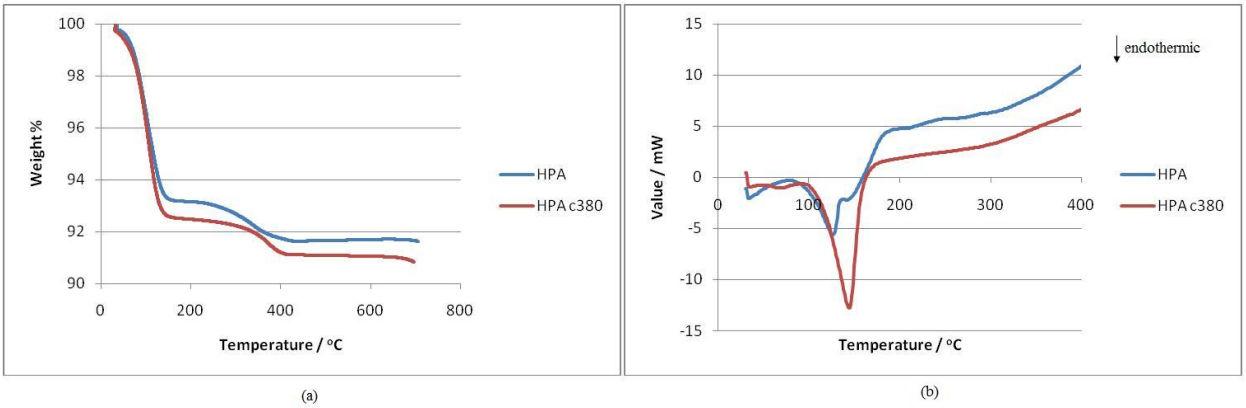

Figure 5.10: (a) TGA plot of the uncalcined HPA and 380 °C calcined HPA catalysts and (b) corresponding DSC graphs

On the other hand, the iron doped HPA behaves differently. The uncalcined iron doped HPA lost 5 H_2O molecules at 94 °C and 5.5 H_2O molecules at 217 °C, giving a total of 10.5 H_2O molecules per KU (Figure 5.11a). The 94 °C water loss is accompanied by four endothermic peaks in the DSC (77, 111, 125 and 143 °C), whereas the 217 °C water loss is accompanied by an endothermic peak at 238 °C (Figure 5.11b). The 5.5 H_2O/KU or 8.8 H_2O/Fe water molecules (Table 5.2) that are lost at 217 °C can be attributed to the $Fe(H_2O)_6^{3+}$ hexa-aqua water which is reported to exist in a bulk iron promoted phosphomolybdic acid [13]. The 380 °C calcined iron doped HPA showed one large water loss step which contributed to a total of about 9 H_2O molecules per KU at 167 °C (Figure 5.11a). The DSC shows about three endothermic peaks at 135, 155 and 200 °C (Figure 5.11b). This could mean that both the crystallization and the hexa-aqua water-loss are overlapping in the TGA or possibly different types of hydration exist.

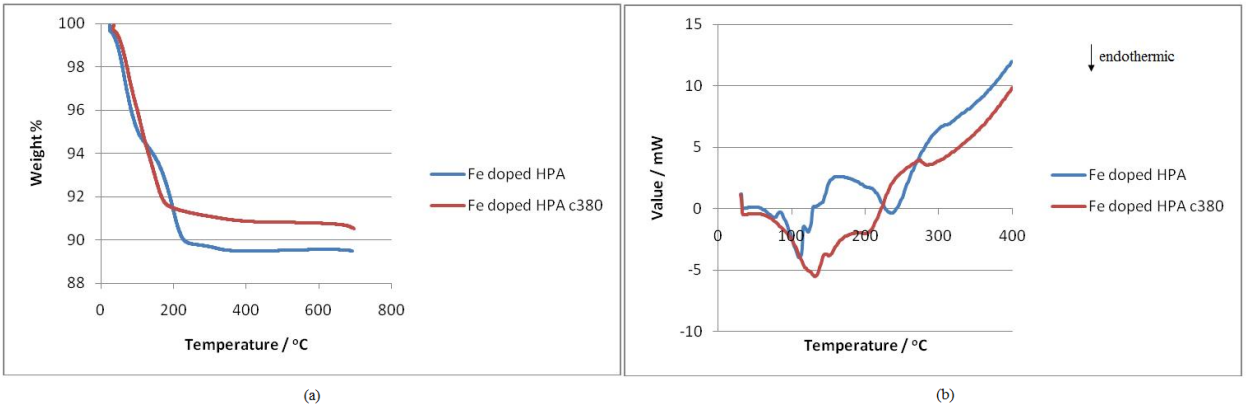

Figure 5.11: (a) TGA plot of the uncalcined iron doped HPA and 380 °C calcined iron doped HPA catalysts and (b) corresponding DSC graphs

Table 5.2: TGA data of the HPA and iron doped HPA obtained from the uncalcined and the 380 ^{o}C calcined samples

Catalyst	First water loss			Second water loss			H_2O/KU
	Temp/ ^{o}C	H_2O /KU*	H_2O/Fe	Temp ^{o}C	H_2O/KU*	H_2O/Fe	
$H_3PMo_{12}O_{40}$ uncalcined	34 - 136	6.93	-	139 - 403	1.96	-	8.89
$H_3PMo_{12}O_{40}$ calcined	33 – 130	7.63	-	130 - 392	1.75	-	9.38
$Fe_{0.63}H_{1.11}PMo_{12}O_{40}$ uncalcined	24 - 94	4.97	7.88	94 - 217	5.55	8.81	10.52
$Fe_{0.64}H_{1.08}PMo_{12}O_{40}$ calcined	36 - 167	8.97	14.02	-	-		8.97

**KU = Keggin unit*

5.1.8 Temperature Programmed Desorption (TPD)

The Temperature Programmed Desorption (TPD) of ammonia of the uncalcined HPA showed one type of weak acid site and three overlapping types of strong acid sites (Figure 5.12). The first peak occurs at 100 ^{o}C with low 0.0059 TPD signal units, which means the concentration of the weak acid sites is low. On the other hand, three overlapping peaks appeared at 392, 428 and 463 ^{o}C with corresponding 0.029, 0.024 and 0.018 TPD signal units, which means there is a higher concentration of strong acid sites than weak acid sites. The ammonia desorption temperature of the strong acid sites occurs above the decomposition temperature of the $H_3PMo_{12}O_{40}$ Keggin structure (decomposes at 400 ^{o}C according to the IR results in Figure 5.1 above), which means that an unknown metal oxide structure is responsible for these strong acid sites.

Although the acid site distribution did not change, a slight increase in the acid strength was observed

when the HPA was calcined at 380 ^{o}C prior to analysis (Figure 5.12); three peaks were observed at 121, 407 and 448 ^{o}C with corresponding 0.011, 0.028 and 0.022 TPD signal units. The fourth peak had disappeared, which suggests that it might have been due to some impurity in the secondary structure, since calcination at 380 ^{o}C resulted in the rearrangement of the secondary structure while retaining the primary structure (refer to the IR and XRD results above).

The iron doped HPA calcined at 380 ^{o}C (Figure 5.12) showed a complete change in the acid site strength and distribution. In this case, four acid sites were observed, but all of them occur below 400 ^{o}C and the high intensity peak is due to the weak acid site, which means that the population of weak acid sites is the highest. These peaks are observed at 166, 225, 257 and 365 ^{o}C with corresponding TPD signal units of 0.018, 0.015, 0.015 and 0.009, respectively. It is also interesting to note that the weakest acid site desorbs NH_3 at 166 ^{o}C (versus 100 ^{o}C for the undoped HPA), which means Fe^{3+} might be responsible for the increased acid strength of the weakest acid sites (a possible contribution may be due to the Fe-O Lewis acidity), but at the same time blocked or destroyed the strong acid sites (Fe^{3+} replaces the strong H^{+} acid sites to form $Fe_xH_{3-3x}PMo_{12}O_{40}$). The increase in the number of weak acid sites may the due to the increase in Brønsted acidity of the polyoxometalate (POM) as a result of the $Fe(HO)_n^{(3-n)}$ cationic species that are formed from the Fe^{3+} cation and water of hydration [14]. This observation can be compared with literature, where the thallium salt of 12-molybdophosphoric acid, which consisted of a deficit or stoichiometric amount of thallium atoms, had a similar NH_3 TPD pattern. In that (literature) case, initially, the major peak appeared at approximately 440 ^{o}C; but when there was excess thallium, the majority of ammonia desorption occurred at 300 ^{o}C. This meant that strong acid sites were lost upon addition of excess thallium [15].

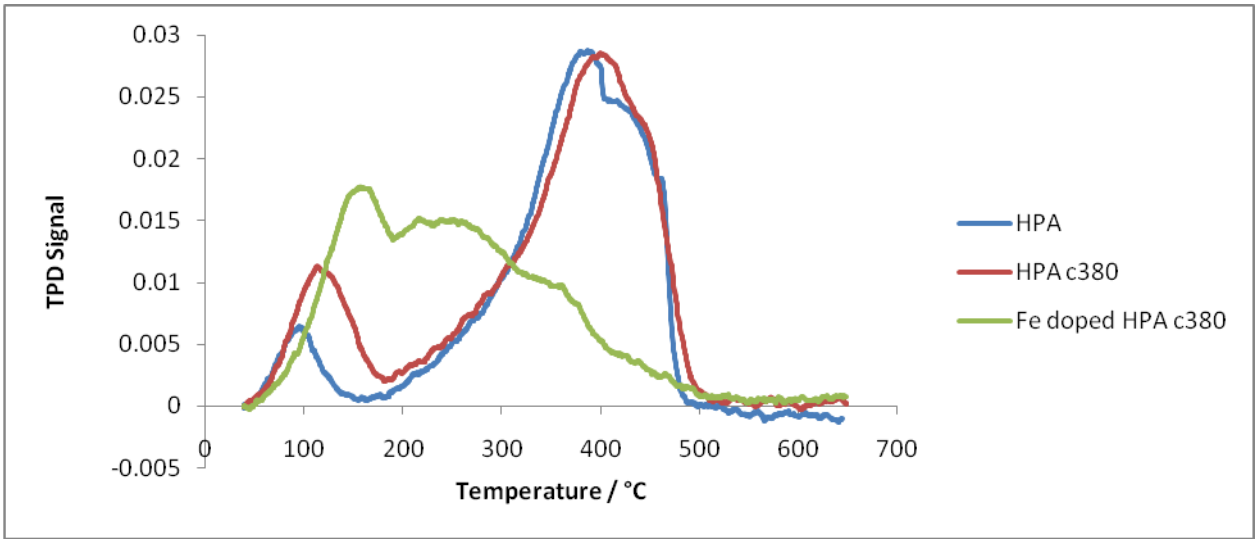

Figure 5.12: TPD of uncalcined $H_3PMo_{12}O_{40,}$ 380 ^{o}C calcined $H_3PMo_{12}O_{40}$ and 380 ^{o}C calcined $Fe_{0.69}H_{0.93}PMo_{12}O_{40}$

5.2 The Iron phosphate catalyst

This section will discuss the characterization results of the iron phosphate catalyst ($FePO_4$) and it focuses on the various phases that were obtained at different calcination temperatures.

5.2.1 Inductively Coupled Plasma-Optical Emission Spectrometer (ICP-OES)

The bulk phosphorus to iron ratio of the iron phosphate calcined at 500 ^oC was obtained in the range of 1.21 to 1.29 (Table 5.3). A P/Fe bulk composition ratio of 1.2 was a targeted since literature has shown that the tridymite-like phase is stabilised when there is excess phosphorus in the iron phosphate catalyst [16, 17]. There was a slight increase in the P/Fe ratio observed when the iron phosphate precursor was calcined at 500 ^oC.

Table 5.3: The P/Fe ratio obtained from the bulk iron phosphate

Name of precursor	P/Fe ratio in the uncalcined iron phosphate	P/Fe ratio in iron phosphate calcined at 500 ^oC
$FePO_4$ 1	1.24	1.29
$FePO_4$ 2	1.20	1.24
$FePO_4$ 3	1.19	1.21
$FePO_4$ 4	1.15	1.22

5.2.2 Infrared Spectroscopy (IR)

A drastic change in the IR spectrum was observed from the uncalcined iron phosphate precursor (Figure 5.13a) to those calcined samples (Figure 5.13b-d). This change may be due to the loss of volatile impurities and also since calcination is regarded as a solid-state reaction (or can be regarded as one of the iron phosphate catalyst preparation steps). The IR spectra of iron phosphate calcined at temperatures ranging from 400 ^oC to 550 ^oC were almost similar to the tridymite-like phase IR

spectrum (Figure 5.13b) [18]. Looking at Figure 5.13b, the peak in the region of 3000 - 3400 cm^{-1} corresponds to the hydroxyl groups from the water molecules [18, 19] and the peak at 1622 cm^{-1} may be due to the OH from H_2O [19]. The absence of the peaks in the 734 and 935 cm^{-1} region ascribed to the symmetrical and asymmetrical vibrations of the P-O-P groups, respectively, [19-21] is consistent with the expectation that $FePO_4$ has alternating Fe-O and P-O tetrahedra and therefore should not have P-O-P groups [20]. The peaks in the region of 550 and 1000 cm^{-1} correspond to the symmetric and asymmetric vibrations of the phosphate groups, where the vibration at 1011 cm^{-1} corresponds to the symmetric vibrations of the PO_3 groups. The peak at 519 cm^{-1} is due to the bending of the PO_3 groups [19].

When the iron phosphate was calcined at 600 ^oC, a slight change in the IR peaks was observed (Figure 5.13d) when compared to the low temperature calcined samples. The two peaks at 635 and 591 cm^{-1} became more intense as the calcinations temperature increased from 550 to 600 ^oC, which possibly means that some bond interactions might be getting stronger as the quartz-like phase becomes more dominant.

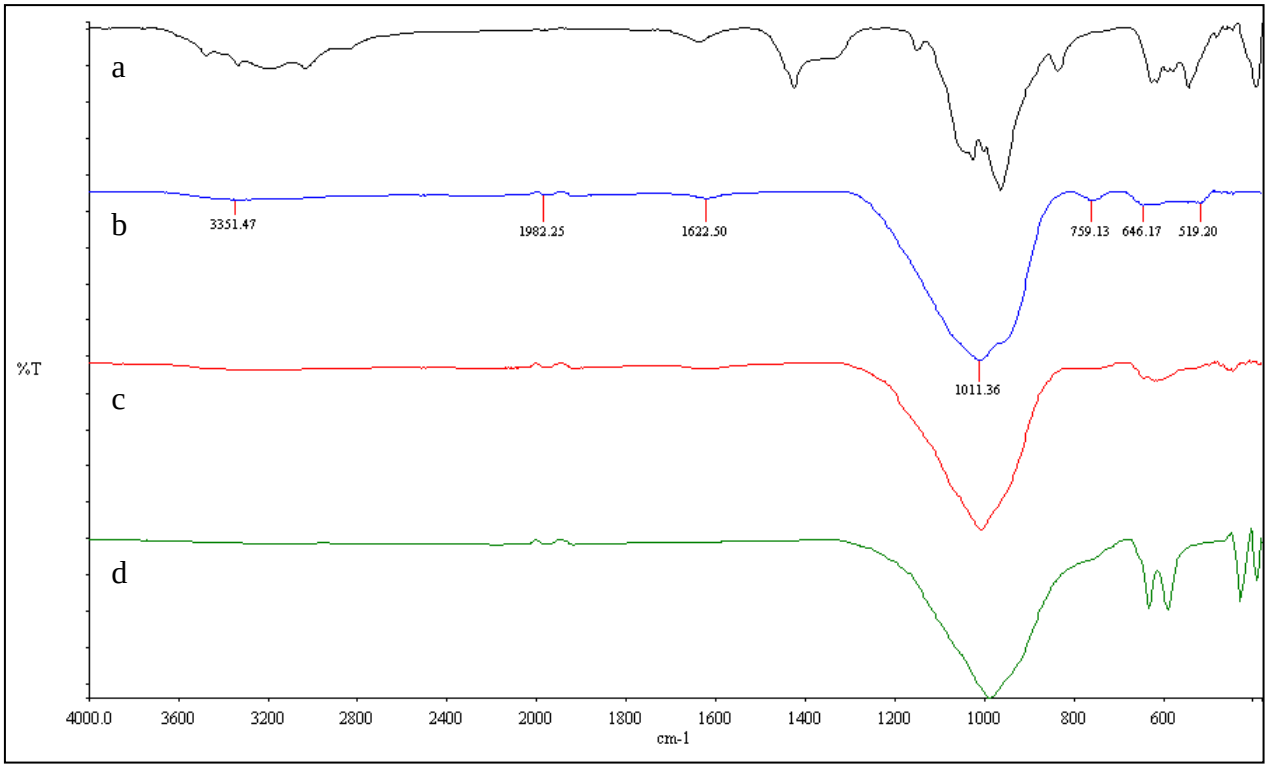

Figure 5.13: IR spectra of (a) uncalcined, (b) 500 ^oC, (c) 550 ^oC and (d) 600 ^oC calcinced iron phosphate catalyst

5.2.2 X-Ray Diffraction (XRD)

The XRD results of the uncalcined iron phosphate (Figure 5.14a) showed some crystallinity in the material. An amorphous material was formed after calcination at 400 ^{o}C (Figure 5.14b). Traces of the tridymite-like phase were observed after calcining the material at 480 ^{o}C. A well define tridymite-like phase pattern is observed for the iron phosphate calcined at 500 ^{o}C (Figure 5.14c) with d-spacings of 4.43, 4.24, 3.93 and 3.04 Å [18, 22]. Calcination at 550 ^{o}C resulted in the gradual loss of the tridymite-like phase, whereas calcination at 600 ^{o}C (Figure 5.14d) resulted in the formation of the quartz-like phase (d-spacing of 4.37 and 3.45 Å) [22]. This means that the tridymite-like phase of the iron phosphate catalyst was selectively prepared by calcining a precursor, with P/Fe composition

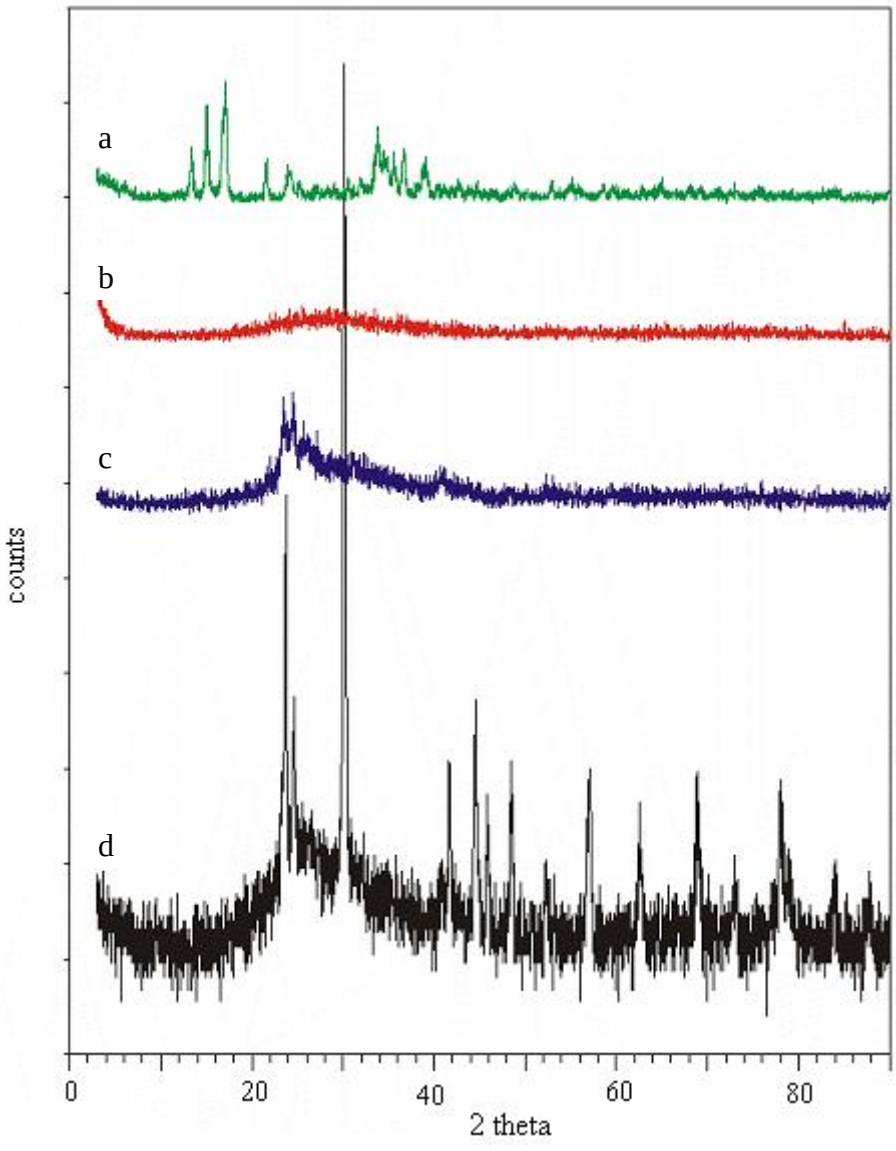

Figure 5.14: XRD patterns of iron phosphate (a) uncalcined (b) 400 ^{o}C calcined (c) 500 ^{o}C calcined (d) 600 ^{o}C calcined

ratio close to 1.2, at 500 ^{o}C in air for 4 hours. Hence the targeted catalyst was obtained.

5.2.4 Brunauer-Emmett-Teller surface analysis (BET), Scanning Electron Microscopy (SEM) and Transmission Electron Microscopy (TEM)

A BET surface area of 9.0 m^2 g^{-1} was obtained for the 500 ^{o}C calcined iron phosphate catalyst with a P/Fe ratio of 1.22 (see Table 5.4), which is below the expected 14.5 m^2 g^{-1} reported for a catalyst with a P/Fe ratio of 1.2 [23, 24]. The surface area dropped from 9.0 to 5.7 m^2 g^{-1} when the catalyst was calcined to 600 ^{o}C as expected [23], as a result of quartz-like phase formation. This drop in surface area is confirmed by the formation of plate-like surfaces when comparing the SEM images of the 500 ^{o}C calcined catalyst to the 600 ^{o}C calcined catalyst (Figure 5.15). The trend of increase in particle size with increase in calcination temperature and the drop in surface area is observed in the BET results, SEM and TEM images (compare Table 5.4 with Figure 5.15). Medium particle sizes (an average of about 22 nm in the TEM) are observed for the 400 ^{o}C calcined catalyst, followed by a slight increase (to 28 nm) when calcined at 500 ^{o}C, whereas a mixture of big and small particles (ranging from 11 to 52 nm) are observed in the 600 ^{o}C calcined sample. The substantial increase in the particles size from 28 nm of the 500 ^{o}C calcined sample to 52 nm of the 600 ^{o}C calcined sample is due to morphological changes; from the tridymite-like phase to the quartz-like phase of the $FePO_4$ catalyst [25].

Table 5.4: The BET surface area with corresponding chemical composition of the iron phosphate catalysts

Catalyst	P/Fe	S_{BET} / m^2g^{-1}
$FePO_4$ ($A^{\$}$) calcined at 400 ^{o}C	1.24	14.8
$FePO_4$ (T*) calcined at 500 ^{o}C	1.22	9.0
FePO4 ($Q^{\#}$) calcined at 600 ^{o}C	1.21	5.7

$^{\$}$ *A = amorphous phase, * T = Tridymite-like phase,* $^{\#}$ *Q = Quartz-like phase*

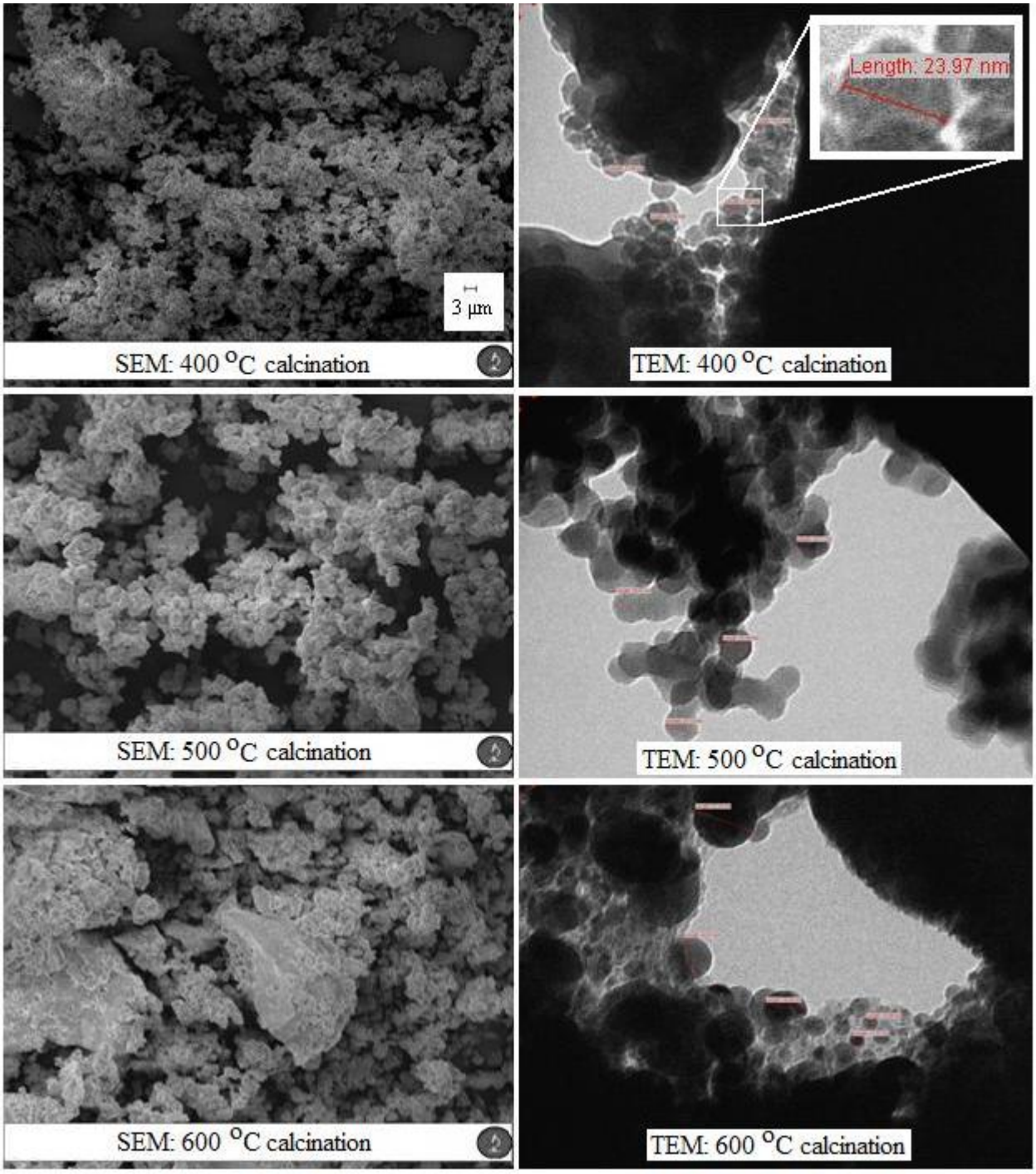

Figure 5.15: The SEM and TEM images of the iron phosphate catalyst calcined at various temperatures (the scale shown applies to all SEM and TEM images, respectively)

5.2.3 Differential Scanning Calorimetry (DSC) and Thermogravimetric Analysis (TGA)

The TGA of the 500 °C calcined iron phosphate catalyst (Figure 5.16a), shows one weight loss step at

163 ^{o}C, which is attributed to the loss of adsorbed water molecules. This is accompanied by an endothermic peak in the DSC (Figure 5.16b) at 174 ^{o}C. The uncalcined catalyst shows four weight loss steps, although they are not clearly visible. According to literature [24, 25], for a catalyst that has a P/Fe ratio greater than one and that was prepared by the ammonia gel method, three weight loss steps are expected. The first weight loss at 137 ^{o}C is due to the loss of adsorbed water molecules and accompanied by an endothermic DSC peak at 185 ^{o}C (Figure 5.16b). The next two overlapping steps at around 329 ^{o}C are due to the loss of crystallization water (in $NH_4FeP_2O_7 \cdot 1.5H_2O$) with DSC peaks appearing at 295 and 341 ^{o}C. The last weight loss at 484 ^{o}C in due to the loss of ammonia, as the $NH_4FeP_2O_7$ decomposes to form $FePO_4$ (tridymite/quartz) and polycondensed phosphate phases, unfortunately the DSC analysis was limited to 400 ^{o}C, hence does not show the expected corresponding endothermic peak [23, 25].

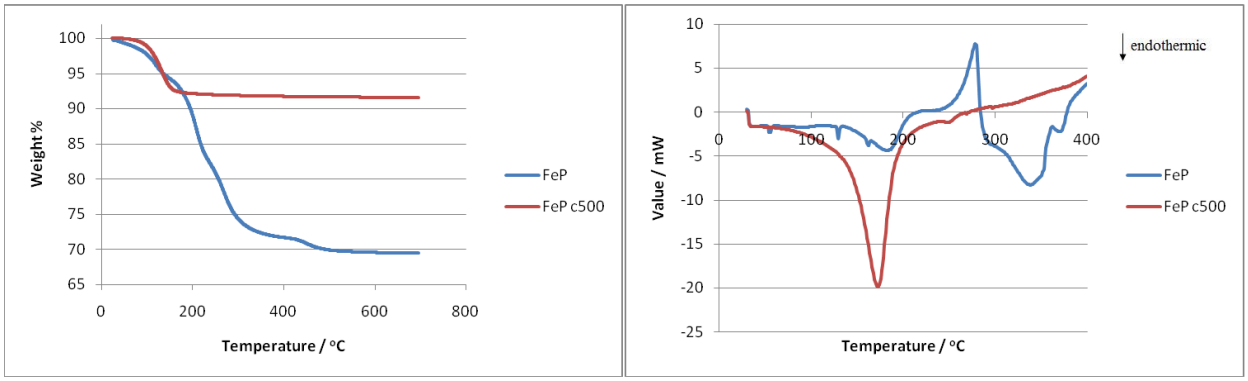

Figure 5.16: (a) TGA and (b) DSC of the uncalcined and 500 ^{o}C calcined iron phosphate catalysts ("FeP" stands for the uncalcined $FePO_4$ catalyst and "FeP c500" stands for a 500 ^{o}C calcined catalyst)

5.3 References

[1] K.N. Rao, N. Lingaiah, I. Suryanarayana, and P.S.S. Prasad, Catal. Lett. 90 (2003) 31-38.

[2] C. Rocchiccioli-Deltcheff, A. Aouissi, M.M. Bettahar, S. Launay, and M. Fournier, J. Catal. 164 (1996) 16-27.

[3] C. Rocchiccioli-Deltcheff, M. Fournier, R. Franck, and R. Thouvent, Inorg. Chem. 22 (1983) 207-216.

[4] K. Song, S.H. Moon, and W.Y. Lee, Korean J. of Chem. Eng. 8 (1991) 33-38.

[5] V.M. Bindareva, T.V. Andrushkevich, R.I. Maksimovskaya, L.M. Plyasova, A.V. Ziborov, G.S. Litvak, and L.G. Detusheva, Kinet. and Catal. 35 (1994) 114-119.

[6] R. Massart, R. Constant, J.-N. Fruchart, J.-P. Ciabrini, and M. Fournier, Inorg. Chem. 16 (1977) 2916 - 2921.

[7] J. Hu, R.C. Burns, and J.-P. Guerbois, J. Mol. Catal. A: Chem 152 (2000) 141 - 155.

[8] M. Sultan, S. Paul, M. Fournier, and D. Vanhove, Appl. Catal. A: Gen. 259 (2004) 141 - 152.

[9] R.A. Shalliker, G.K. Douglas, P.R. Comino, and P.E. Kavanagh, Powder Technol. 91 (1997) 17 -23.

[10] J. Lee, S. Sim, K. Kim, K. Cho, and S. Kim, Mater. Sci. Eng. B 122 (2005) 85 - 89.

[11] M. Fournier, C. Feumi-Jantou, C. Rabia, G. Herve, and S. Launay, J. Mater. Chem. 2 (1992) 971 - 978.

[12] L. Marosi, E.E. Platero, J. Cifre, and C.O. Arean, J. Mater. Chem. 10 (2000) 1949 - 1955.

[13] Q. Huynh, and J.-M.M. Millet, J. Phys. Chem. Solids 66 (2005) 887 - 894.

[14] M. Langpape, and J.-M.M. Millet, Appl. Catal. A: Gen. 200 (2000) 89 – 101.

[15] M.A. Parent, and J.B. Moffat, J. Catal. 177 (1998) 335-342.

[16] M. Ai, and K. Ohdan, Appl. Catal. A: Gen. 165 (1997) 461 - 465.

[17] J.E. Miller, M.M. Gonzales, L. Evans, A.G. Sault, C. Zhang, R. Rao, G. Whitwell, A. Maiti, and D. King-Smith, Appl. Catal. A: Gen. 231 (2002) 281 - 292.

[18] E. Muneyama, A. Kunishige, K. Ohdan, and M. Ai, J. Catal. 158 (1996) 378 - 384.

[19] P. Bonnet, J.-M.M. Millet, C. Leclercq, and J.C. Vedrine, J. Catal. 158 (1996) 128 - 141.

[20] G.O. Alptekin, A.M. Herring, D.L. Williamson, T.R. Ohno, and R.L. McCormick, J. Catal. 181 (1999) 104 - 112.

[21] A.V. Annapragada, and E. Gulari, J. Catal. 123 (1990) 130 - 146.

[22] M. Ai, and K. Ohdan, Appl. Catal. A: Gen. 180 (1999) 47 - 52.

[23] M. Ai, E. Muneyama, A. Kunishige, and K. Ohdan, J. Catal. 144 (1993) 632 - 635.

[24] M. Ai, E. Muneyama, A. Kunishige, and K. Ohdan, Appl. Catal. A: Gen. 109 (1994) 135 - 146.

[25] P. Nagaraju, C. Srilakshmi, N. Pasha, N. Lingaiah, I. Suryanarayana, and P.S.S. Prasad, Appl. Catal. A: Gen. 334 (2008) 10 - 19.

Chapter 6 : CATALYTIC TESTING

This chapter presents and discusses the catalytic results obtained from the activation of *n*-hexane over three catalysts, HPA ($PMo_{12}O_{40}$), iron doped HPA ($Fe_{0.69}H_{0.93}PMo_{12}O_{40}$) and the iron phosphate (P/Fe = 1.22) catalyst. Results from blank studies are also discussed, where carborandum was packed inside the reactor without any catalyst. In the feed composition, a C_6H_{14}/O_2 ratio of two was kept constant for all reactions. The reagent contact time (ct) with the catalyst was varied across 0.5, 1.0 and 1.5 seconds. All calculations were performed on a carbon mole bases. Refer to Appendix 2: Product quantification for calculation details.

6.1 Activation in a carborandum packed reactor

The activation of *n*-hexane in a carborandum packed reactor (no catalyst) shows a maximum conversion at 500 ^oC of 6.5 % at a 0.5 s contact time and 12.5 % at a 1.5 s contact time (Figure 6.1). The product profile is seen in Table 6.1 for the 0.5 s contact time reaction. In Table 6.1, a maximum selectivity of 22.3 % to trans-2-hexene is observed at 302 ^oC, with 6.7 % selectivity to C1-C4 cracked products (compounds having carbon numbers ranging from 1 to 4) and 11.2 % to CO_x (both CO and CO_2). The selectivity to trans-2-hexene drops as the reaction temperature increases. The highest

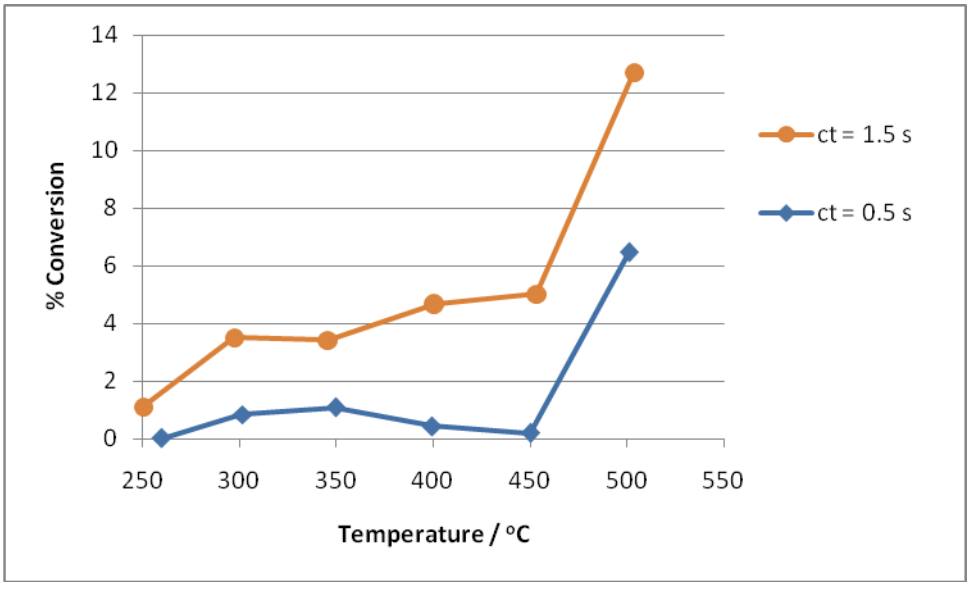

Figure 6.1: *n*-Hexane % conversion in a caborandum packed reactor at various contant times

selectivity of 49.8 % to benzene is observed at 400 ^{o}C and as expected, more CO_x is observed due to combustion at higher temperatures.

Table 6.1: Product profile obtained from a carborandum packed reactor at a contact time of 0.5 s

Temp / ^{o}C	% Conv	% Selec						
		trans-2-hexene	**cis-2-hexene**	**1-hexene**	**benzene**	**C1-C4 products**	**CO**	**CO_2**
260	0	0	0	0	0	0	0	0
302	0.8	22.3	0	0	0	6.7	0	11.2
350	1.1	16.2	0	0	0	4.6	0	46.4
400	0.4	14.8	0.7	0	49.8	2.6	0	23.8
450	3.2	5.0	0.5	0	44.0	1.9	8.8	37.9
501	6.5	2.3	0.4	0	48.6	2.0	9.9	36.0

6.2 Activation over the HPA catalyst

The hexane conversion over the HPA catalyst was much higher than in the carborandum packed reactor at a contact time of 0.5 s (compare Table 6.1 and Table 6.2). This high conversion is due to the high activity of the highly acidic 12-molybdophosphoric acid. This is because the strong Lewis acidity resulting from the presence of the Mo=O double bond (from the Keggin structure) is related to the activity of the catalyst [1]. The TPD results from Chapter 5 also confirmed the strong acidity of the HPA catalyst (although the TPD acidity may be due to Brønsted acidic sites, it does not rule out the contribution from the Lewis acidic sites).

Oxygenated C6 products (2,5-dimethyltetrahydrofuran and 2,5-hexadione) are observed from the HPA catalyst (Table 6.2) and they were not observed in the blank study. This means that these products are catalytically produced and that the HPA promotes oxygen insertion reactions. This

confirms what was reported in literature, namely that the Mo=O double bond plays a vital role during oxygen insertion reactions [2]. At 248 ^{o}C, the selectivity of 11.7 % to trans-2-hexene is the highest and minor cracked (C1-C4) products are observed at a selectivity of 8.0 % (Table 6.2). The oxygenated products were observed at 349 ^{o}C. The selectivity to trans-2-hexene dropped to 1.8 % at 349 ^{o}C, while the selectivity to 2,5-dimethyltetrahydrofuran was at 8.2 % and the selectivity to CO_x was at 41.6 %. This could mean that trans-2-hexene undergoes a catalytic transformation to 2,5-dimethyltetrahydrofuran and/or a non-catalytic combustion reaction to CO_x and water.

A substantial amount of benzene is observed at 349 ^{o}C at a selectivity of 38.1 %. Benzene production might be due to non-catalytic reactions since the carborandum packed reactor (Table 6.1) also produced benzene, but this was only observed at 400 ^{o}C. This could mean that although benzene production is non-catalytic, the reaction is catalytically initiated (carborandum produced benzene at 400 ^{o}C whereas HPA produced benzene at 349 ^{o}C). More CO_x at a selectivity of 68.2 % is observed at 380 ^{o}C, as the selectivities to the other products drop due to combustion. Above 380 ^{o}C, the products started to polymerise and blocked the end of the reactor tube (this was observed by an increased back-pressure in the reactor system). These polymeric products may arise from products like 2,5-dimethyltetrahydrofuran [3].

The IR spectrum of the post reaction catalyst shows, in Figure 6.2, that the Keggin structure of the HPA was still preserved after reaction at 380 ^{o}C. The peaks at 1056 cm^{-1}, 958 cm^{-1}, 873 cm^{-1} and 780 cm^{-1} are characteristic peaks of a Keggin structure [4]. The XRD pattern (Figure 6.3) is undefined since the secondary structure is highly dependent on the level of hydration. But this XRD pattern is not due to MoO_3 (d-spacings of 6.97, 3.81, 3.47, 3.27, 2.70, 2.65, 2.53, 2.31 and 2.27 Å) [5]. MoO_3 would be expected as a decomposition product. This means that the Keggin structure of the HPA catalyst was preserved during the catalytic reaction at 380 ^{o}C.

Table 6.2: Product profile obtained from the HPA catalyst loaded in the hottest spot of the reactor at a contact time of 0.5 s

Temp / ^{o}C	**% Conv**	**% Selec**						
		trans-2-hexene	**2,5-dimethyltetrahydrofuran**	**2,5-hexadione**	**benzene**	**C1-C4 products**	**CO**	**CO_2**
248	3.8	11.7	0	0	0	8.0	0	0
302	4.3	10.6	0	0	0	5.1	0	41.7
349	3.3	1.8	8.2	0.7	38.1	4.7	14.5	27.1
360	4.9	1.9	3.3	0	39.0	5.2	14.9	26.9
383	12	0.6	0	0	21.3	4.6	30.2	38.0

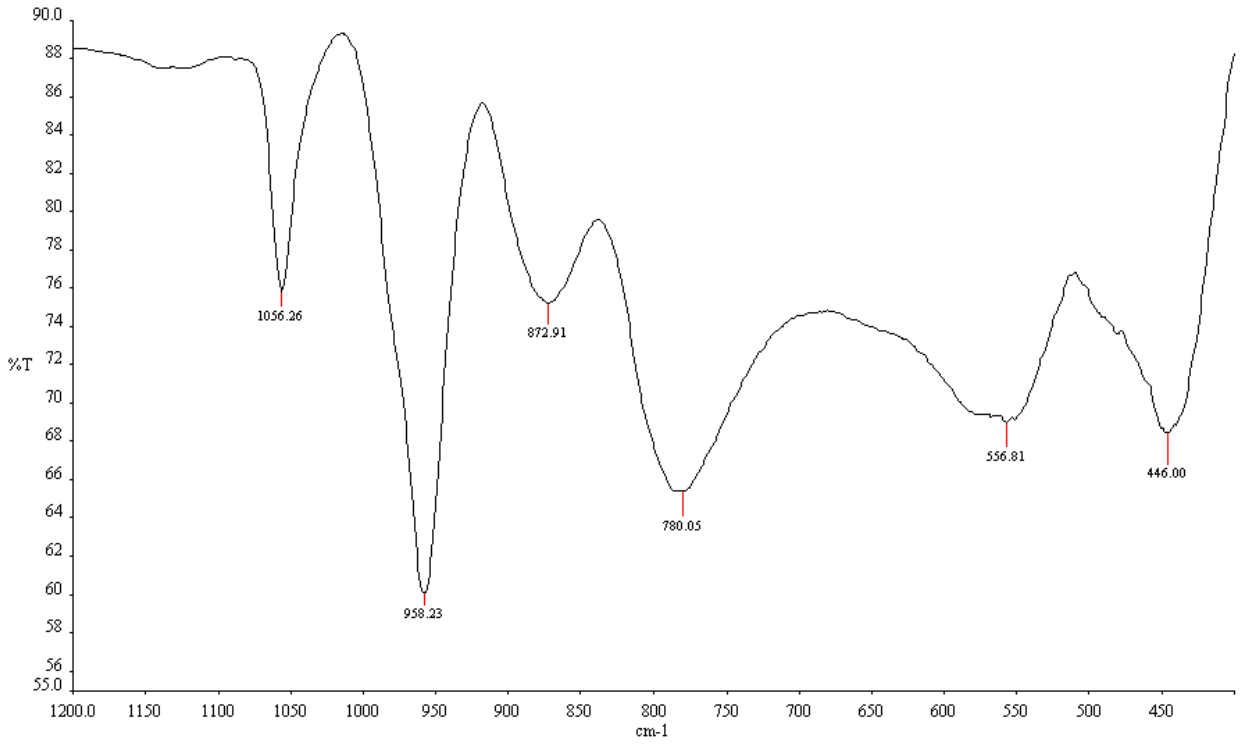

Figure 6.2: IR spectrum of the HPA post reaction catalyst where a reaction was stopped at 380 ^{o}C

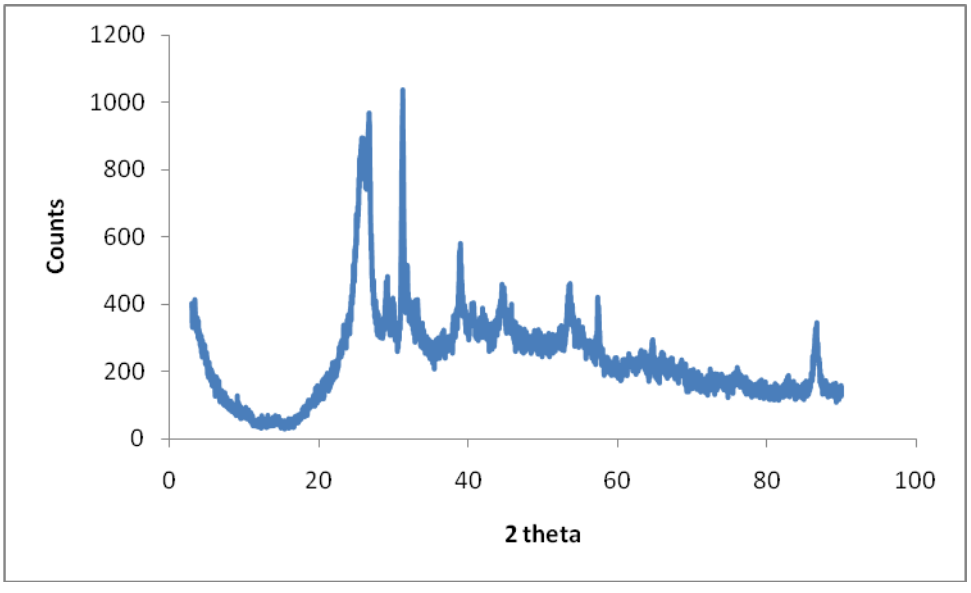

Figure 6.3: XRD pattern of the HPA post reaction catalyst where a reaction was stopped at 380 ^{o}C

Due to polymerisation of products at the end of the reactor tube, it was decided to load the catalyst 6.5 cm below the hottest spot of the reactor tube. The aim was to quench (quick cooling) the reaction products before they polymerise. Table 6.3 shows the product profile obtained after changing the catalyst loading position. It was observed that the conversion of hexane did not change very much when comparing the two reactions (Table 6.2 and Table 6.3) and also that the polymerisation of products did not start until a temperature of 402 ^{o}C was reached. This means that the quench process was effective. It is also interesting to note that the selectivity to trans-2-hexene is higher when the catalyst is loaded close to the end of the tube than when it was loaded on the hottest spot. This implies that trans-2-hexene undergoes a non-catalytic (or gaseous) transformation after being produced inside the reactor.

Table 6.3: Product profile obtained from the HPA catalyst loaded 6.5 cm below the hottest spot of the reactor at a contact time of 0.5 s

Temp / ^{o}C	**% Conv**	**% Selec**						
		trans-2-hexene	**2,5-dimethyltetrahydrofuran**	**2,5-hexadione**	**benzene**	**C1-C4 products**	**CO**	**CO_2**
247	0.3	23.1	0	0	0	2.3	0	0
298	4.7	17.7	0	0	15.2	2.7	0	33.2
348	5.0	4.4	0	0	37.2	2.7	0	50.9
360	5.2	1.5	0	3.4	40.7	2.7	11.4	37.8
370	7.5	1.0	2.8	3.1	40.1	2.8	10.4	37.5
381	8.3	0.9	3.3	2.1	43.7	2.3	9.6	36.5
402	12.5	0.6	4.1	1.0	33.1	2.6	21.9	35.6

In this case, the post reaction catalyst analysis shows (in Figure 6.4) that although the Keggin

structure is not completely destroyed, the intensities of the IR Keggin characteristic peaks have dropped. This could mean partial decomposition of the Keggin structure at 400 ^{o}C. This is in contradiction with the observation made during the calcination process. There, it was observed, in Chapter 5, that the HPA was completely destroyed when calcined at 400 ^{o}C in air for 5 hours. This improved stability of the structure inside the reactor may be assisted by the presence of H_2O by-product (from oxidative dehydrogenation and combustion reactions). The presence of water may have pushed the dehydration equilibrium (refer to Chapter 2) back, hence prolonging the Keggin structure decomposition process. Furthermore, the XRD pattern (Figure 6.5) does not show a MoO_3 pattern.

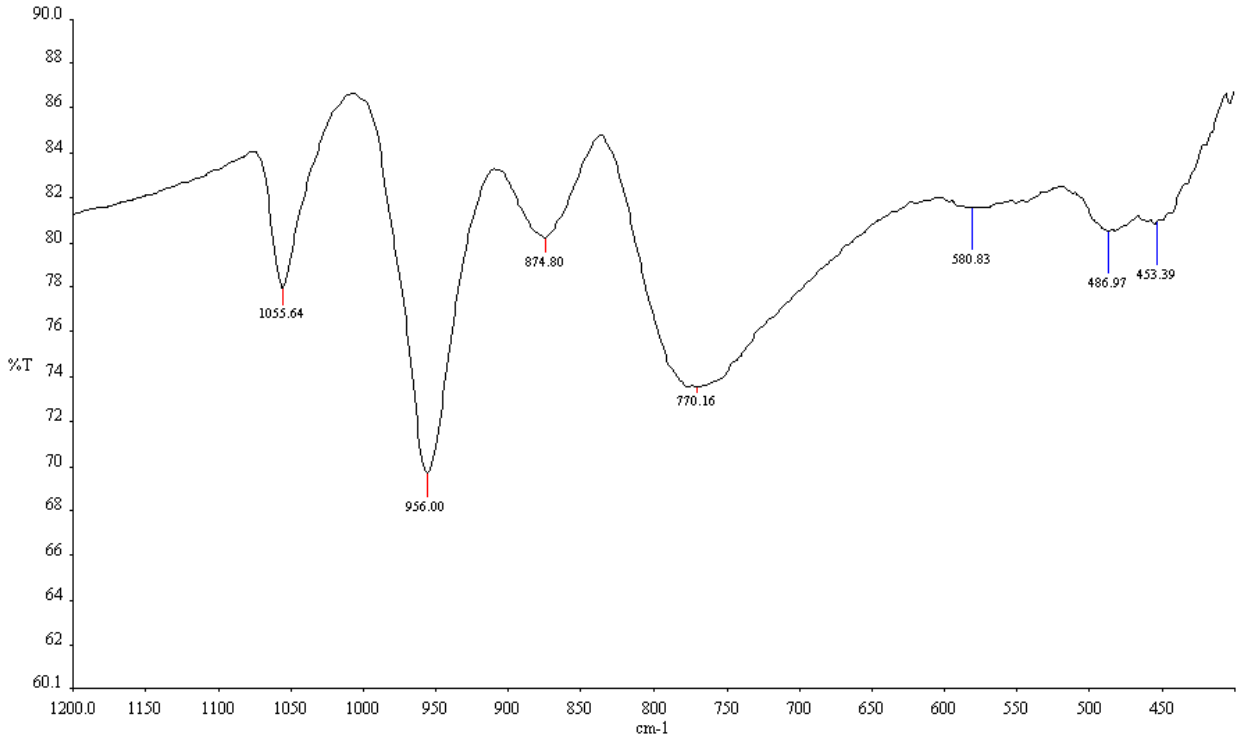

Figure 6.4: IR spectrum of the HPA post reaction catalyst where a reaction was stopped at 400 ^{o}C

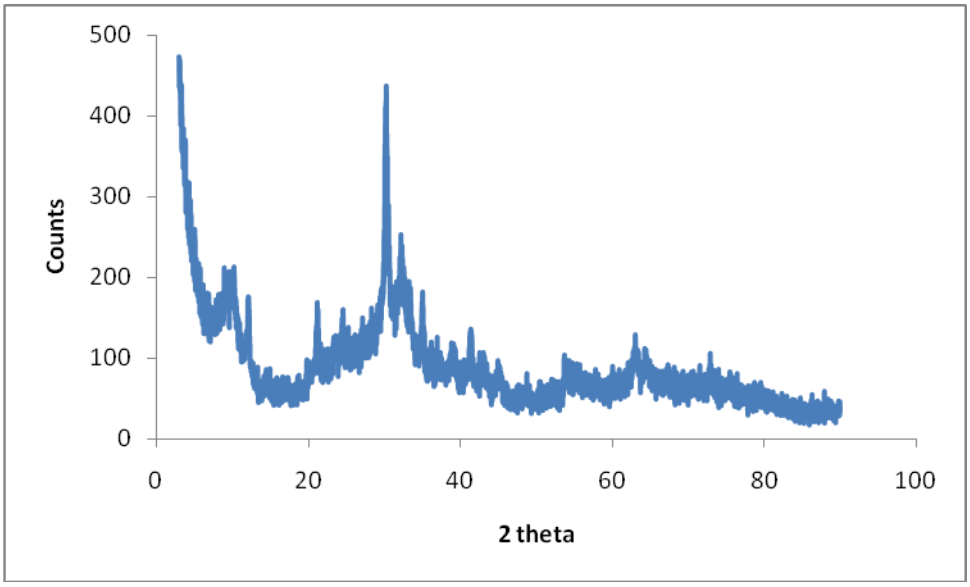

Figure 6.5: XRD pattern of the HPA post reaction catalyst where a reaction was stopped at 400 ^{o}C

6.3 Activation over the iron doped HPA catalyst

The conversion of *n*-hexane over the iron doped HPA ($Fe_{0.69}H_{0.93}PMo_{12}O_{40}$) is lower that the conversion over the HPA under similar reaction conditions (compare Table 6.2 and Table 6.4). The difference is due to the fact that the iron doped HPA catalyst is less acidic than over the HPA catalyst (refer to TPD results in Chapter 5). Hence the iron doped HPA is less active [1]. The total selectivity to 2,5-dimethyltetrahydrofuran and 2,5-hexadione is higher over the iron doped HPA than the HPA catalyst. This means that the iron dopant promotes oxygen insert reactions. It is also observed that the selectivity to CO_x dropped from 60.9 % at 399 ^{o}C to 50.6 % at 449 ^{o}C (Table 6.4) which might result from O_2 deficiency, as more O_2 is used up in the oxygen insertion reactions.

In the case of the iron doped HPA, the post reaction catalyst analysis was done on the reaction that was taken up to 500 ^{o}C. It is interesting to see some IR Keggin characteristic peaks in Figure 6.6 at 1083 cm^{-1} (normally expected to be 1056 cm^{-1}), 975 cm^{-1} and 854 cm^{-1}. The Keggin structure highest stability temperature for the iron doped HPA catalyst was 400 ^{o}C when the catalyst was calcined in air (Chapter 5), which means that the stability was again assisted by the present of H_2O by-product. The XRD pattern (Figure 6.7) on the other hand, clearly shows the MoO_3 pattern , d-spacings of 6.97, 3.81, 3.47, 3.27, 2.70, 2.65, 2.53, 2.31 and 2.27 Å [5], which is an expected decomposition product.

Table 6.4: Product profile obtained from the iron doped HPA catalyst loaded in the hottest spot of the reactor at a contact time of 0.5 s

Temp / ^{o}C	**% Conv**	**% Selec**						
		trans-2-hexene	**2,5-dimethyltetrahydrofuran**	**2,5-hexadione**	**benzene**	**C1-C4 products**	**CO**	**CO_2**
248	0.9	0	0	0	0	0	0	0
301	2.4	10.0	0	0	0	7.8	0	28.1
351	2.5	7.3	0	0	38.6	4.5	0	41.2
360	5.8	4.9	9.8	2.2	27.6	3.2	0	35.4
399	6.0	1.7	8.4	3.9	23.4	5.4	20.3	40.6
449	19.8	1.4	3.6	2.4	28.0	5.3	17.1	33.5

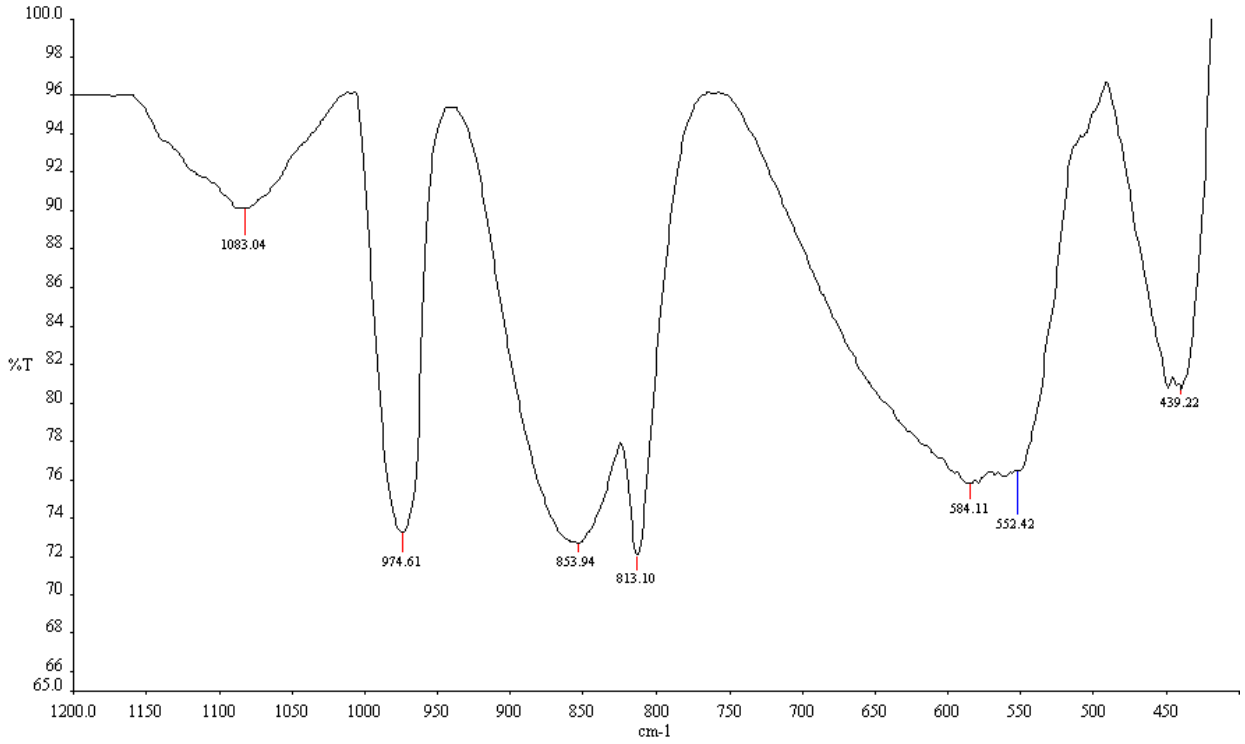

Figure 6.6: IR spectrum of the iron doped HPA post reaction catalyst where a reaction was stopped at 500 ^{o}C

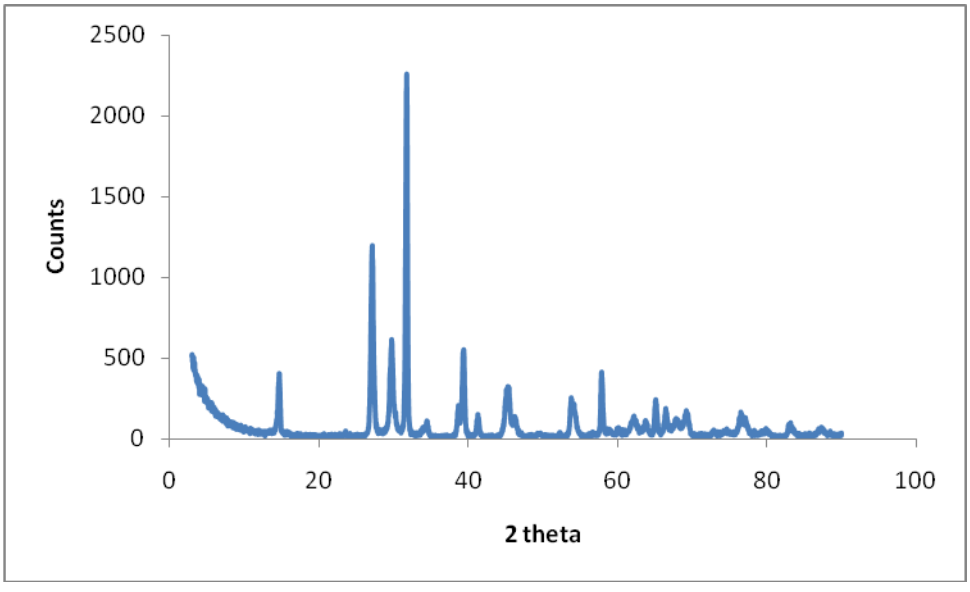

Figure 6.7: XRD pattern of the iron doped HPA post reaction catalyst where a reaction was stopped at 500 ^{o}C

6.4 Activation over the iron phosphate catalyst

The iron phosphate catalyst (P/Fe ratio = 1.22) showed low conversions at a contact time 0.5 s and so the contact time was increased to 1.0 and 1.5 s in order to compare catalytic performances with the highly active HPA and iron doped HPA (heteropoly compound based) catalysts. Figure 6.8 shows the conversion of *n*-hexane over the iron phosphate catalyst at various contact times. The reaction that was run at a contact time of 1.5 s shows conversions which are comparable to those of the heteropoly compound based catalysts and so this contact time was chosen for isoconversion comparison.

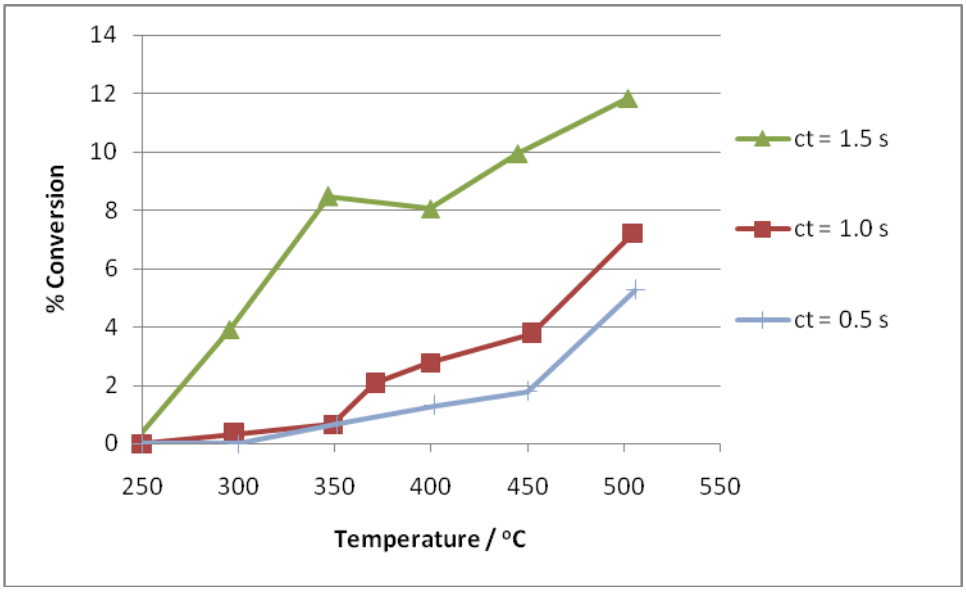

Figure 6.8: *n*-Hexane % conversion in an iron phosphate loaded reactor at various contant times

The product profile obtained from the activation of *n*-hexane over the iron phosphate catalyst at a contact time of 0.5 s (Table 6.5) is different to the profiles obtained from the HPA (Table 6.2) and the iron doped HPA (Table 6.4) under similar reaction conditions. There are no oxygen insertion products like 2,5-dimethyltetrahydrofun or 2,5-hexadione. This supports the argument from literature that iron phosphate promotes oxydehydrogenation reactions, but not oxygen insertion reactions [2]. The iron phosphate catalyst produces similar products to those that were obtained in the carborandum packed reactor (Table 6.1), but at different selectivities. The selectivity to cis-2-hexene (18.9 % at 351 ^{o}C) and 1-hexene (11.7 % at 402 ^{o}C) is higher over the iron phosphate catalyst than over carborandum only (Table 6.1 shows zero selectivities at similar temperatures, respectively). This means that the production of 1-hexene and cis-2-hexene are catalytic, whereas the production of trans-2-hexene could be both catalytic and non-catalytic. It was noticed that the selectivity to benzene had dropped

over the iron phosphate catalyst when compared to carborandum (compare Table 6.1 and Table 6.5). This suggests that the iron phosphate catalyst inhibits the reaction pathway that leads to the formation of benzene.

Table 6.5: Product profile obtained from the iron phosphate catalyst loaded in the hottest spot of the reactor at a contact time of 0.5 s

Temp / ^{o}C	**% Conv**	**% Selec**						
		trans-2-hexene	**cis-2-hexene**	**1-hexene**	**benzene**	**C1-C4 products**	**CO**	**CO_2**
250	0	0	0	0	0	0	0	0
300	0	0	0	0	0	0	0	0
351	0.7	3.5	18.9	8.3	0	2.1	0	31.4
402	1.3	2.8	17.0	11.7	13.0	1.2	0	45.9
450	1.8	1.9	10.4	7.8	24.4	1.3	9.7	42.0
503	5.3	1.3	6.9	5.8	32.0	2.1	6.7	43.9

When the contact time was increased from 0.5 s to 1.0 s, the product profile did not change but the selectivities changed as expected. The selectivity to cis-2-hexene dropped to 16.5 % at 349 ^{o}C and selectivity to 1-hexene dropped to 8.0 % at 400 ^{o}C (Table 6.6). The selectivity to benzene increased from 13.0 % at 402 ^{o}C (Table 6.5) to 25.4 % at 400 ^{o}C (Table 6.6). This implies that the hexenes are transformed to benzene at higher contact time. As expected, the selectivity to CO_x increased at higher contact time (55.6 % at 503 ^{o}C in Table 6.6) than at lower contact time (50.6 % at 505 ^{o}C in Table 6.5) due to combustion.

Table 6.6: Product profile obtained from the iron phosphate catalyst loaded in the hottest spot of the reactor at a contact time of 1.0 s

Temp / °C	% Conv	% Selec						
		trans-2-hexene	**cis-2-hexene**	**1-hexene**	**benzene**	**C1-C4 products**	**CO**	**CO_2**
250	0	0	0	0	0	0	0	0
298	0.3	0	10.8	0	0	3.2	0	0
349	0.7	4.4	16.5	9.1	0	1.3	0	50.3
371	2.1	2.9	13.0	9.8	16.9	2.3	0	46.4
400	2.8	2.8	9.6	8.0	25.4	1.5	0	46.3
452	3.8	1.4	5.0	3.2	38.5	1.1	8.5	40.8
505	7.2	1.9	2.6	1.4	29.1	7.5	9.6	46.0

When the contact time was increased to 1.5 s, significant changes in selectivities were observed. The relationship between cis-2-hexene, 1-hexene and benzene is still observed. The higher the contact time, the lower the selectivities to cis-2-hexene and 1-hexene, but the higher the selectivity to benzene (Table 6.7). On the other hand, the selectivity to trans-2-hexene has drastically increased, showing the highest selectivity of 23.4 % at 300 °C (Table 6.7). At a contact time of 0.5 s, highest selectivity to trans-2-hexene was 3.5 % at 350 °C and it was 4.4 % at 349 °C for the 1.0 s contact time reaction. Furthermore, the selectivity to benzene has also increased significantly, showing a maximum selectivity of 72.1 % at 400 °C. This implies that the converted hexane either forms hexenes (1-hexene and cis-2-hexene catalytically and trans-2-hexene non-catalytically) which get converted to benzene and CO_x; or hexane is directly transformed to benzene in a non-catalytic reaction. There is

also a possibility that benzene may form simultaneously through both catalytical and non-catalytical reactions [6]. Benzene is a very stable product so it does not readily undergo combustion to form CO_x and water under these reaction conditions. According to literature, significant benzene decomposition starts at temperatures >450 ^oC in a carborandum packed reactor, where $C_6H_{14}/O_2 = 0.4$ at a total gas flow of 10 mL min^{-1} [6]. It was also noticed that the selectivity to CO_x at a contact time of 1.5 s was lower (48.7 % at 500 ^oC) than at lower contact times (55.6 % at 503 ^oC in Table 6.6).

Table 6.7: Product profile obtained from the iron phosphate catalyst loaded in the hottest spot of the reactor at a contact time of 1.5 s

Temp / ^oC	**% Conv**	**% Selec**						
		trans-2-hexene	**cis-2-hexene**	**1-hexene**	**benzene**	**C1-C4 products**	**CO**	**CO_2**
250	0	10.4	0	0	5.0	4.4	0	0
300	3.9	23.4	0	0	0	5.3	0	25.9
350	8.5	9.0	4.2	0	39.6	1.9	0	38.7
400	8.1	4.6	0.7	1.7	72.1	0.7	4.1	24.6
450	9.9	3.0	1.0	1.5	59.2	1.9	3.9	22.2
500	11.8	1.1	0.3	0.7	48.0	0.9	37.2	11.5

The post reaction catalyst analysis of the iron phosphate catalyst showed similar IR and XRD patterns in all reactions (refer to Figure 6.9 and Figure 6.10). Both the IR and XRD confirm that the catalyst is made up of the quartz-like phase, since they are similar to the IR and XRD results obtained from the quartz-like phase of the catalyst that was calcined at 600 ^oC (Chapter 5). This means that the activation of *n*-hexane induced the transformation of the tridymite-like phase to the quartz-like phase, a transformation which would otherwise only be expected at 600 ^oC, as was shown by calcining the

catalyst in air (Chapter 5).

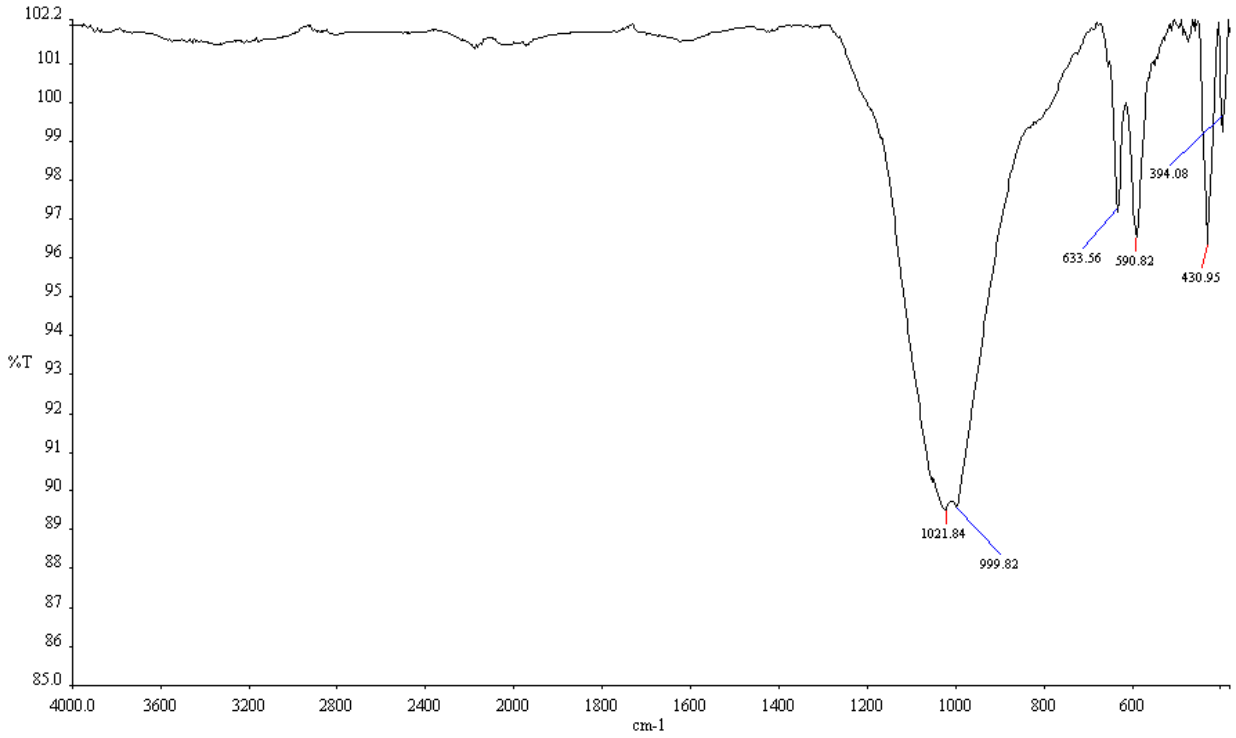

Figure 6.9: IR spectrum of the iron phosphate post reaction catalyst where a reaction was stopped at 500 ^{o}C at a contact time of 1.5 s

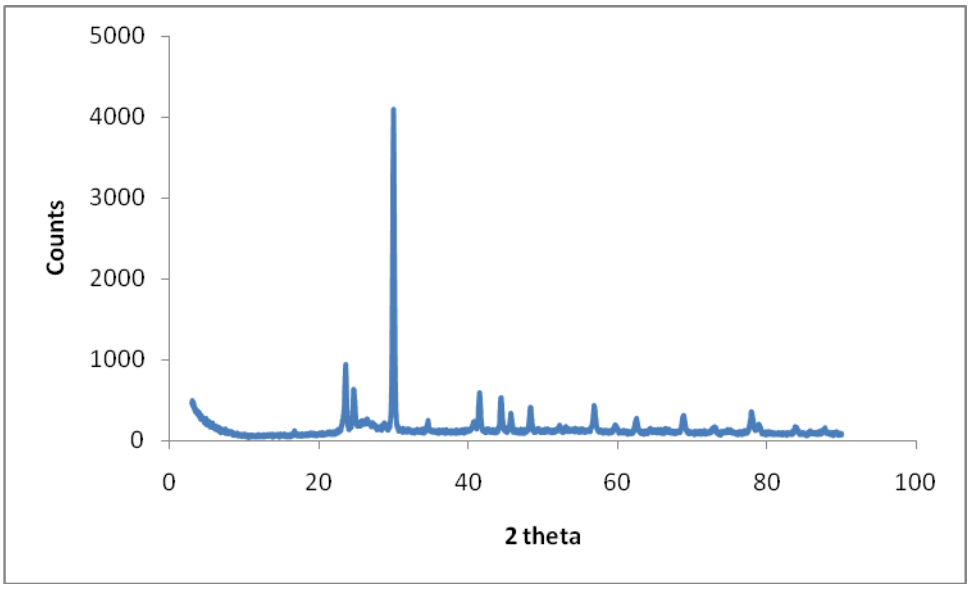

Figure 6.10: IR spectrum of the iron phosphate post reaction catalyst where a reaction was stopped at 500 ^{o}C at a contact time of 1.5 s

6.5 Comparison of the catalysts, including at isoconversion

It is clear from Figure 6.11 that the iron phosphate catalyst produces more benzene (higher yield) and trans-2-hexene than the two heteropoly compound based catalysts (HPA or iron doped HPA) at isoconversion and under almost isothermal conditions (381-400 ^{o}C). Although a substatial amout of benzene is also observed from a carboranum packed reactor, this is only observed at a higher temperature (454 ^{o}C as opposed to 381-400 ^{o}C), which makes this comparison difficult. The iron phosphate catalyst catalytically produced cis-2-hexene and 1-hexene, whereas the heteropoly compound based catalysts produced 2.5-dimethytrahydrofuran and 2.5-hexadione catalytically. The iron doped HPA produced more oxygenated products than the HPA catalyst, which shows that the iron dopant promotes the oxygen insertion reaction. Also noticed was that the benzene production (yield) dropped when the HPA catalyst was doped with iron.

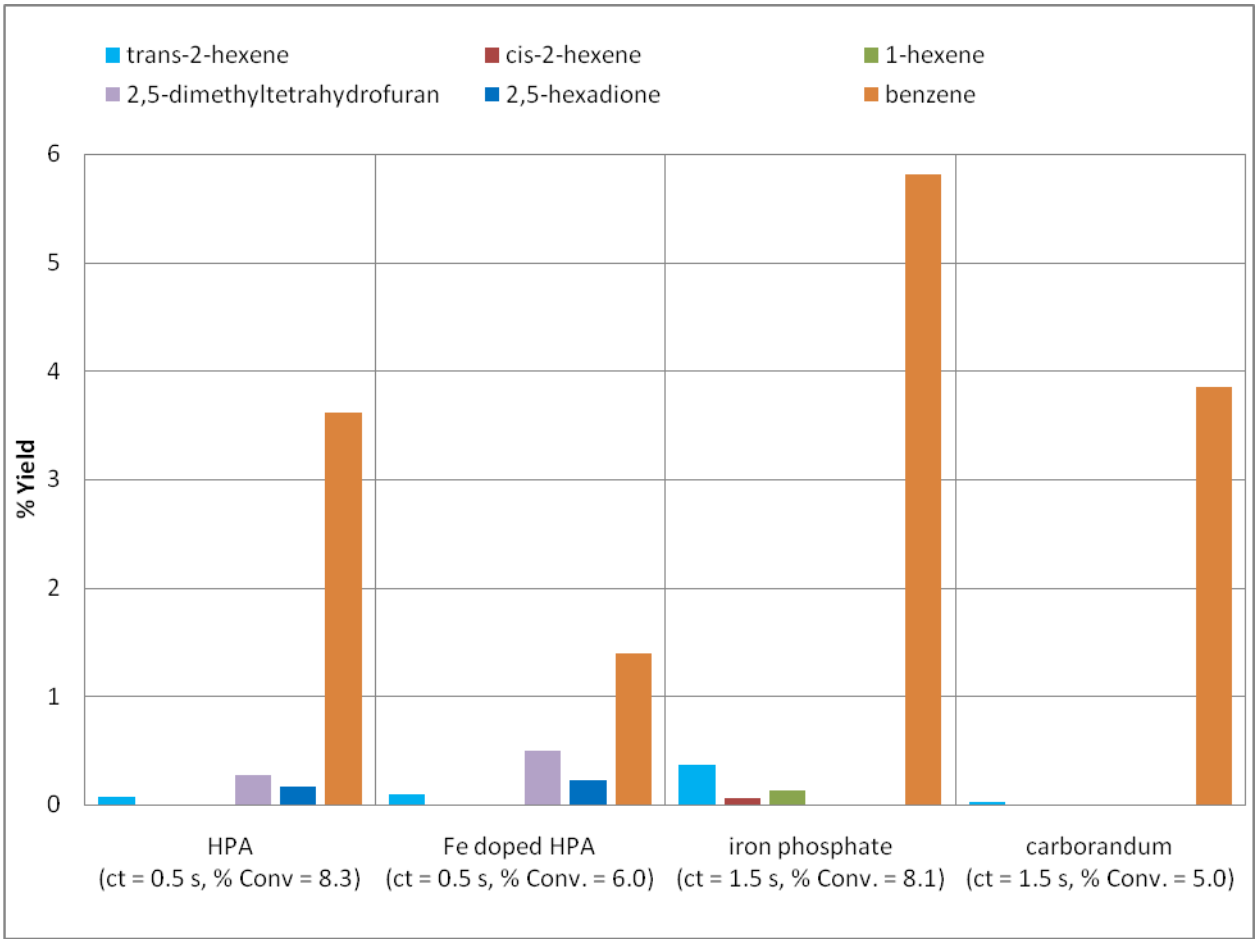

Figure 6.11: The % Yields of products optained at isoconversion and close so isothermal conditions (with HPA at 381 ^{o}C, Fe doped HPA at 399 ^{o}C, iron phosphate at 400 ^{o}C and carborandum at 454 ^{o}C)

It was noticed from Table 6.4 that the Fe doped HPA showed higher selectivity of 12 % to C6

oxygenates at 360 ^{o}C and 5.8 % hexane conversion than the HPA in Table 6.3 showing 3.4 % selectivity to the C6 oxygenats at 360 ^{o}C and 5.2 % hexane conversion. This confirms the observation that the Fe^{3+} dopant promotes the oxygen insertion reactions. Also from Table 6.3 and Table 6.4, it is clear that the HPA catalyst selectively produced more benzene (40.7 % selectivity at 5.2 % hexane conversion) than the Fe doped HPA catalyst (27.6 % selectivity at 5.8 % hexane conversion). Under similar reaction conditions but at different conversions, the HPA initiated the benzene formation reaction at 349 ^{o}C (Table 6.2) as opposed to 400 ^{o}C in a carborandum packed reactor (Table 6.1), whereas iron phosphate inhibited the benzene formation reaction by showing a 13 % selecivity to benzene at 402 ^{o}C (Table 6.5) as opposed to 49.8 % benzene selectivity at 400 ^{o}C in a carborandum packed reactor (Table 6.1). Although the iron phosphate catalyst is shown to play a role in inhibiting benzene formation, Figure 6.11 clearly shows that the highest yields of benzene are obtained with the iron phosphate catalyst at isoconversion. This is expained by the different reaction pathways in which benzene is formed in the reactor. As it was stated earlier, benzene can form from catalytically converted hexenes (1-hexene, cis-2-hexene and trans-2-hexene) or directly from converted hexane.

Traces of 3-hexene (a mixture of the trans-3-hexene and cis-3-hexene isomers) were detected only in the reactions that had a higher contact time (ct = 1.5 s). The separation of 3-hexene and trans-2-hexene was achieved by using a different column, on a different GC. The 3-hexene was produced in the carborandum packed reactor and also in the reactor that was loaded with the iron phosphate catalyst. The 3-hexene was not quantified because it was produced in small quantities, showing an average selectivity of <10 % of the selectivity to trans-2-hexene throughout all the reactions (i.e. the ratio of 3-hexene to 2-hexene was <1:10). Although it might be expected that the 3-hexene would be a dominant isomer over the 2-hexene isomer, it has been reported that thermodynamics favour the following order of selectivities: trans-2-hexene > cis-2-hexene > cis-3-hexene > 1-hexene [7], showing that the 2-hexene isomer dominates over the 3-hexene isomer.

6.6 References

[1] G. Busca, E. Finocchio, G. Ramis, and G. Ricchiardi, Catal. Today 32 (1996) 133 - 143.

[2] M. Ai, Catal. Today 52 (1999) 65 - 69.

[3] R.P. O'Connor, and L.D. Schmidt, Stud. Surf. Sci. Catal. 133 (2001) 289 - 296.

[4] C. Rocchiccioli-Deltcheff, A. Aouissi, M.M. Bettahar, S. Launay, and M. Fournier, J. Catal. 164 (1996) 16-27.

[5] V.M. Bindareva, T.V. Andrushkevich, R.I. Maksimovskaya, L.M. Plyasova, A.V. Ziborov, G.S. Litvak, and L.G. Detusheva, Kinet. and Catal. 35 (1994) 114-119.

[6] H.B. Friedrich, N. Govender, and M.R. Mathebula, Appl. Catal. A: Gen. 297 (2006) 81 - 89.

[7] B. Pillay, M.R. Mathebula, and H.B. Friedrich, Appl. Catal. A: Gen. (2009) in press.

Chapter 7 : SUMMARY AND CONCLUSION

In this project three catalysts were prepared. These catalysts were the 12-molybdophosphoric acid ($H_3PMo_{12}O_{40}$) catalyst, which was then doped with the Fe^{3+} cation to produce the iron doped salt of 12-molybdophosphoric acid ($Fe_xH_{3-3x}PMo_{12}O_{40}$, with x = 0.63 - 0.69) catalyst and the iron phosphate ($FePO_4$) catalyst. These catalysts were characterised and tested for *n*-hexane activation in a continuous gas flow reactor.

The highest stability temperature of the Keggin structure (using IR) of 12-molybdophosphoric acid in air was found to be 380 ^oC, whereas the highest stability temperature of the Keggin structure of the iron doped 12-molybdophosphoric acid was found to be 400 ^oC. This meant that Fe^{3+} improves the thermal stability of the Keggin structure. The decomposition product was MoO_3, which confirmed literature reports. Both the 12-molybdophosphoric acid ($H_3PMo_{12}O_{40}$ or HPA) and the iron doped salt of 12-molybdophosphoric acid ($Fe_{0.69}H_{0.93}PMo_{12}O_{40}$ or iron doped HPA) catalysts were then calcined at 380 ^oC in air before catalytically testing them in the activation of *n*-hexane. It was noted from TPD that the iron doped salt of 12-molybdophosphoric acid was less acidic than the 12-molybdophosphoric acid catalyst.

It was found that the iron phosphate catalyst (prepared by the ammonia gel method) produced various iron phosphate phases upon calcinations at various temperatures. XRD showed that an amorphous phase was obtained at 400^oC, a tridymite-like phase at 500 ^oC and a quartz-like phase at 600 ^oC. Since the target catalyst was the tridymite-like phase, the iron phosphate precursor was calcined at 500 ^oC to prepare the catalyst for the activation of *n*-hexane. The catalytic testing was done on a catalyst that had a P/Fe ratio of 1.22 (bulk composition obtained from ICP-OES).

The catalytic testing results for the activation of *n*-hexane showed that the HPA and the iron doped HPA were much more reactive than the iron phosphate catalyst. Isoconversion and isothermal comparison were made when the contact time over the HPA and iron doped HPA was at 0.5 s, whereas the contact time over iron phosphate was at 1.5 s. The iron phosphate catalyst catalytically produced oxidative dehydrogenation products (cis-2-hexene and 1-hexene), whereas the HPA and iron doped HPA (heteropoly compound based) catalysts produced oxygen insertion products (2.5-dimethytrahydrofuran and 2.5-hexadione).

It was observed that the products produced over HPA started to polymerise inside the reactor tube at around 380 ^oC and so these products were quenched by loading the catalyst 6.5 cm below the hottest spot of the reactor tube and the polymerisation on-set temperature was shifted to 400 ^oC. While a

substantial selectivity to benzene was obtained in non-catalytic reactions (blank study), the HPA catalyst seemed to play a role in initiating this non-catalytic reaction of benzene formation (carborandum produced benzene at 400 ^{o}C, whereas HPA produced benzene at 349 ^{o}C). The iron doped HPA showed higher yields of oxygenated products and a lower benzene yield than the HPA catalyst at isoconversion and under almost isothermal conditions. The improved oxygen insertion capacity of the iron doped HPA is due to the presence of the iron dopant.

The iron phosphate catalyst showed higher selectivity to 1-hexene and cis-2-hexene, but lower selectivity to benzene than the carborandum packed (blank) reactor at 0.5 s contact time. This meant that the iron phosphate catalysts promotes oxidative dehydrogenation but inhibits the reaction pathway that leads to benzene formation. At isoconversion (ct = 1.5 s) and under almost isothermal conditions, the iron phosphate catalyst showed higher yield of benzene than the heteropoly compound based catalysts. This observation was explained by the argument that benzene is formed through more than one reaction pathway. Benzene can form from catalytically converted hexenes (1-hexene, cis-2-hexene and trans-2-hexene) or hexane is directly transformed to benzene. Traces of 3-hexene were detected only in the carborandum packed and the iron phosphate loaded reactors that were run at ct = 1.5 s.

Post reaction analysis of the catalysts showed that the Keggin structure thermal stability of the HPA (380 ^{o}C in air) and iron doped HPA (400 ^{o}C in air) was improved inside the reactor, which may have been assisted by the presence of the H_2O by-product. Keggin structure IR characteristic peaks were observed at 400 ^{o}C for the HPA and 500 ^{o}C for the iron doped HPA in the post reaction catalyst. These IR results indicate that there was partial decomposition of the Keggin structure rather than the expected complete decomposition. On the other hand, the stability of iron phosphate tridymite-like phase inside the reactor decreased, since a complete transformation to the quartz-like phase was observed at 500 ^{o}C inside the reactor as opposed to the 600 ^{o}C transformation observed in air.

Appendix 1: List of chemicals

REAGENTS

A1.1: Chemicals that were used to prepared the 12-molybdophosphoric acid and its iron salt

Chemical Name	Chemical Formula	Purity	Supplier	Catalogue Number
Sodium molybdate dihydrate	$Na_2MoO_4 \cdot 2H_2O$	≥ 99.5 %	Merck	A780521 710
Perchloric acid	$HClO_4$	70 %	Merck	SAAR 4946120 LC
Hydrochloric acid	HCl	37 %	Merck	SAAR 3063054 LCA
Orthophosphoric acid	H_3PO_4	85 %	Merck	SAAR 4818040 LC
Diethyl ether	$(C_2H_5)O$	98 %	Merck	186 3020 LC
Ferric nitrate	$Fe(NO_3)_3 \cdot 9H_2O$	98 %	univAR	234 05 80

A1.2: Chemicals that were used to prepared the iron phosphate catalyst

Chemical Name	Chemical Formula	Purity	Supplier	Catalogue Number
Orthophosphoric acid	H_3PO_4	85 %	Merck	SAAR 4818040 LC
Ferric nitrate	$Fe(NO_3)_3 \cdot 9H_2O$	98 %	uniVAR	234 05 80
Ammonium Solution	NH_4OH	25 %	Rochelle Chem.	-
LUDOX® AS - 40 Colloidal silica	SiO_2	40 wt% in water	DuPont	42,084-0

A1.3: ICP-OES calibration standards

Chemical Name	Element	Concentration	Supplier
Molybdenum	Mo	1000 ppm	PolyChem
Iron	Fe	1000 ppm	PolyChem
Phosphorus	P	1000 ppm	PolyChem

A1.4: Chemical and gases that were used for catalytic testing

Chemical Name	Chemical Formula	Purity or Composition	Supplier	Catalogue Number
n-Hexane	C_6H_{14}	≥ 99.0 %	Merck	1.04367.2500
Air IG Zero	$O_2 + N_2$	19.0 - 22 % O_2	Afrox	513207-SE C

A1.5: GC liqiud calibration standards

Chemical Name	Chemical Formula	Purity	Supplier	Catalogue Number
1-Hexene	C_6H_{12}	97 %	Acros	21321-0010
Trans-2-hexene	C_6H_{12}	97 %	Aldrich	110892
Cis-2-hexene	C_6H_{12}	95 %	Aldrich	538493
Trans-3-hexene	C_6H_{12}	99+ %	Aldrich	447153
Cis-3-hexene	C_6H_{12}	≥ 95 %	Fluka	52985
Benzene	C_6H_6	99 %	Rochelle Chem.	-
2,5-hexadione	$C_6H_{12}O_2$	≥ 97 %	Merck	8.00105.0100
2,5-dimethyltetrahydrofuran (cis and trans)	$C_6H_{12}O$	96 %	Aldrich	D187208
Acetone	C_3H_6O	99.5 %	Rochelle Chem.	-
Ethanol	C_2H_5OH	99.5 %	Merck	SAAR2233540LP
Acetic acid	$C_2H_4O_2$	99 %	Riedel-de Häen	27222
Methanol	CH_4O	99.9 %	Aldrich	34860

A1.6: GC gaseous calibration standards

Cylinder mixture	Component	Percentage concentration	Supplier	Catalogue Number
1	Ethane	3.0 %	Afrox	1705
	Ethylene	6.0 %		
	Butane	9.2 %		
	Nitrogen	balance		
2	Methane	2.0 %	Afrox	1640
	Propane	4.0 %		
	Propylene	6.0 %		
	Nitrogen	balance		
3	Carbon monoxide	5.0 %	Afrox	1604
	Carbon dioxide	15 %		
	Nitrogen	balance		
4	Butane	11.0 %	Afrox	801942-RC-A
	1-Butene	14.0 %		
	Ethane	5.0 %		
	Ethylene	8.0 %		
	Methane	3.0 %		
	Nitrogen	balance		

Appendix 2: Product quantification

CALCULATIONS

To quantify the liquid products (both the organic layer and the aqueous layer) from the sampling cylinder, Relative Response Factors (RRF) were obtained.

Assuming that the RRF of hexane is one

$$\text{RRF} = \frac{\text{Conc. Hexane} \times \text{Peak Area Compound A}}{\text{Conc. Compound A} \times \text{Peak Area Hexane}}$$

Standards were prepared by using Mass/Volume concentration

A2.1: Mass concentration in prepared standards

	hexane	**1-hexene**	**trans-2-hexene**
Concentration / g L^{-1}	1.5	2.5	2

A2.2: Average peak area from three replicates obtained from the GC-FID chromatogram

	hexane	**1-hexene**	**trans-2-hexene**
Peak area	20421.0	25866.6	20883.9

A2.3: Relative response factors

	hexane	1-hexene	trans-2-hexene
RRF	1.0	0.76	0.767

A2.4: Relative response factors

	2,5-dimethyltetrahydrofuran	2,5-hexadione	benzene
RRF	0.68	0.50	1.16

To quantify the gaseous products (using both GC-FID and GC-TCD), calibration equations were obtained ($y = mx + c$).

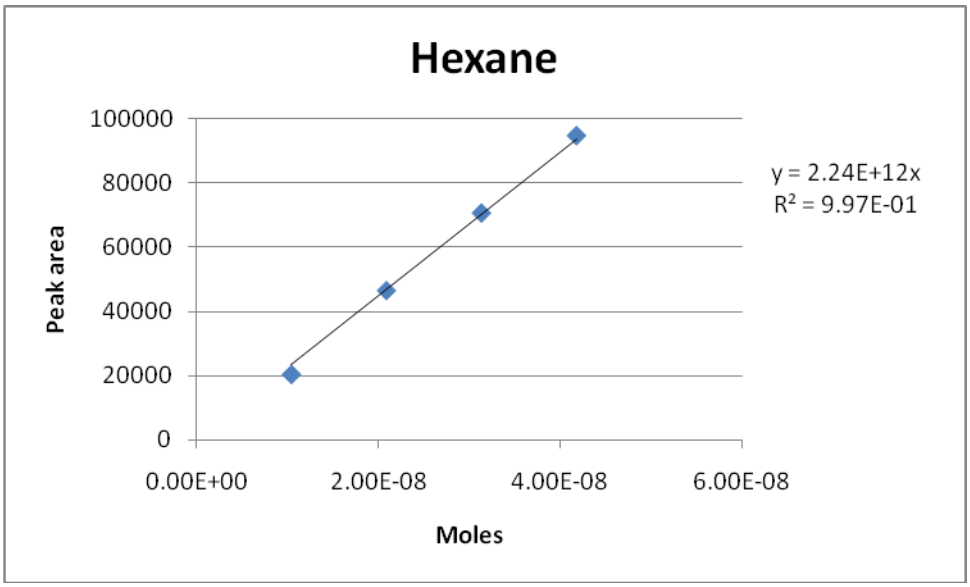

The hexane calibration graph

The carbon balance was calculated on the basis of the number of moles of carbon atoms going into (C_{in}) the reactor and the number of carbon moles going out (C_{out}) of the reactor. The moles of carbon going into the reactor were due the hexane feed and this was quantified by using a calibrated High Performance Liquid Chromatography (HPLC) pump. The moles of carbon going out of the reactor was the sum of carbons obtained from the liquid samples after subtracting the H_2O by-product (Karl Fisher titration was used to determine the water content) and the carbons obtained from the gaseous products (the moles of carbon atoms in a 500 µL gas syringe was multiplied by a factor obtained from the ratio of total gaseous product volume, measured using a Gas-Flow Meter, to 500 µL).

Example:

There were 0.124 moles of hexane going into the reactor at a specific time, and only 0.110 moles of hexane came out, together with 0.00400 moles of 1-hexene and 0.0500 moles of CO_2. The volume of the catalyst used was 0.5 mL and the total flow of feed gas was 60 mL min^{-1} (1 mL s^{-1})

Asked to calculate: Contact time (ct) in seconds, Carbon balance, % Conversion, % Selectivity and % Yield to 1-hexene

$$ct = \frac{\text{Volume of catalyst}}{\text{Total gasflow}}$$
$$= \frac{0.5}{1}$$
$$= 0.5\,s$$

$$\text{Carbon balance} = \frac{\text{Total } C_{out}}{\text{Total } C_{in}} \times 100$$
$$= \frac{(6 \times 0.11) + (6 \times 0.004) + (1 \times 0.05)}{6 \times 0.124} \times 100$$
$$= 98.7\,\%$$

$$\%\,\text{Hexane conversion} = \frac{C_{in} - C_{out}}{C_{in}} \times 100$$
$$= \frac{(6 \times 0.124) - (6 \times 0.11)}{6 \times 0.124} \times 100$$
$$= 11.3\,\%$$

$$\%\,\text{Selec} = \frac{C_{1\text{-hexene}}}{C_{in} - C_{out}} \times 100$$
$$= \frac{6 \times 0.004}{(6 \times 0.124) - (6 \times 0.11)} \times 100$$
$$= 28.6\ \%$$

$$\%\,\text{Yield} = \frac{\%\,\text{Selec} \times \%\,\text{Conv}}{100}$$
$$= \frac{28.6 \times 11.3}{100}$$
$$= 3.23\ \%$$

GC temperature programs

GC-MS:

Injector: 250 ^{o}C

1:75 split

30ml/min flow rate

Intial temperature: 50 ^{o}C; hold 5 min

Ramp: 10 ^{o}C/min to 300 ^{o}C; hold 10 min

GC-TCD

Injector: 220 ^{o}C

1:20 split

50ml/min flow rate

Initial temperature: 46 ^{o}C; hold 4 min

Ramp: 20 ^{o}C/min to 80 ^{o}C; hold 1 min

GC-FID:

Injector: 220 ^{o}C

1:9 split

20cm/min flow rate

Intial temperature: 40 ^{o}C, hold 15 min

Ramp: 10 ^{o}C/min to 120 ^{o}C; hold 2 min

Ramp: 20 ^{o}C/min to 200 ^{o}C; hold 1 min